POLITECNICO DI MILANO

Facoltà di Ingegneria Industriale e dell'Informazione
Corso di Laurea in Ingegneria Biomedica

Developing an Inertial-based System for the Kinematic Analysis of Dogs with Orthosis

Relatore: Prof. Manuela Galli
Correlatori: Dott. Ing. Cecilia Monoli
Dott. Alex Patten Moorhead

Tesi di laurea di:
Boniardi Jacopo 919821
Marzorati Stefano 919730

Anno accademico 2019/2020

TABLE OF CONTENTS

LIST OF FIGURES

LIST OF TABLES

ABSTRACT

In the canine world, orthoses are becoming an increasingly popular alternative to surgery for the treatment of dogs' musculoskeletal dysfunctions. Nevertheless, the reliability and efficacy of these medical devices has not yet been scientifically certified. Since kinematic analysis is widely used in human subjects for the diagnosis of gait-altering diseases and for the optimization and progression of treatment, similar measurement instrumentations and protocols could be adapted to the canine world. This thesis stemmed from the international collaboration between Politecnico di Milano and the Centre for Biorobotics of Tallinn University of Technology to investigate canine kinematics using Inertial Measurement Unit (IMU) sensors. Moreover, the support provided by local realities of the animal orthopaedic sector (Centro Ortopedico Essedi, Fisio4Vet, Maclaren, OrtoPaw) allowed a method for assessing the movement of orthotic dogs to be developed.

Preliminary tests were first performed on human subjects to evaluate the accuracy between the data returned by the IMU sensors and the optoelectronic system. The external knee angles of two healthy subjects were investigated using both measurement systems and results were compared. The Pearson's correlation coefficients prove satisfactory for both subjects, indicating a strong positive relationship between the two methods.

Afterwards, it was possible apply the validated devices to the investigation of animal's motion. The sensors were tested on seven different dogs: five of them were healthy with no previous history of injury, while the remaining two suffered from musculoskeletal disorders and a custom orthosis was designed for each of them. The protocol involved the use of 10 IMUs, 2 for each thoracic limb and 3 for each pelvic limb, which were placed on dogs with paper tape and cohesive bandages. To enforce a constant velocity and a standardized walk during the tests, a specific canine rehabilitation treadmill was used. Since the application of IMU sensors is under development in the canine kinematics evaluation field, a high-speed camera-based system was employed as support in the clinical setting to validate the data acquired during dog tests.

The analysis focused on step detection and the first task involved the identification of universal strategies to detect toe-off and toe-touch of the thoracic and pelvic limbs using the IMUs. After implementing Matlab codes to automate the process (95% average accuracy), the percentages of stance time and swing time were calculated for all subjects and symmetry indices were created to compare healthy dogs with pathological ones. Only for one of the two subjects with motor

dysfunctions an asymmetry was recorded. In this case the application of the orthosis brought improvements reducing the asymmetry between the pathological limb and the contralateral one by 30%.

Furthermore, a preliminary assessment of the joint angles estimated by the sensors was performed. The camera-based system and the IMUs pointed out an acceptable correlation of graph patterns, but the angular range of motion obtained with the sensors was often lower probably due to incorrect positioning of these devices.

In conclusion, the application of IMU sensors could represent an opportunity to obtain a quantitative assessment of the benefits and possible limitations associated with canine orthoses.

SOMMARIO

Nel mondo veterinario, le ortesi canine stanno diventando sempre più una valida alternativa agli interventi chirurgici per il trattamento di cani soggetti a disfunzioni muscoloscheletriche. Tuttavia, l'affidabilità e l'efficacia di questi dispositivi medici non sono ancora state scientificamente certificate. Dal momento che l'analisi cinematica è ampiamente utilizzata su soggetti umani sia per la diagnosi di malattie muscolo-scheletriche che per la valutazione di terapie, strumentazioni e protocolli simili potrebbero essere adattati anche al mondo canino. Questa tesi è nata dalla collaborazione internazionale tra il Politecnico di Milano e il Centro di Biorobotica dell'Università di Tecnologia di Tallinn al fine di condurre uno studio sulla cinematica canina attraverso delle unità di misura inerziale (IMUs). Inoltre, grazie al supporto fornitoci da realtà locali specializzate nel settore dell'ortopedia animale (Centro Ortopedico Essedi, Fisio4Vet, Maclaren, OrtoPaw) è stato possibile sviluppare una metodologia per la valutazione del movimento di cani con ortesi.

Prima di effettuare le prove sui cani, sono stati eseguiti dei test preliminari su soggetti umani per valutare l'accuratezza dei dati restituiti dai sensori IMU rispetto a un sistema optoelettronico. In particolare, con entrambi gli strumenti di misurazione sono stati calcolati e messi a confronto gli angoli esterni del ginocchio di due soggetti sani. I coefficienti di correlazione di Pearson ottenuti sono risultati soddisfacenti per entrambi i soggetti, indicando così una forte relazione positiva tra i due sistemi.

Una volta condotta la validazione, è stato possibile studiare la cinematica dei cani. La ricerca si è basata sull'analisi di sette cani di razze diverse: cinque di loro erano sani, mentre i restanti due presentavano disturbi a livello muscolo-scheletrico per i quali è stata progettata ed applicata un'ortesi su misura. Il protocollo ha previsto l'applicazione di 10 IMU, 2 per ogni arto toracico e 3 per ogni arto pelvico, i quali sono stati posizionati per mezzo di un nastro adesivo ed un sistema di bendaggio. Durante i test, per imporre una velocità costante e una camminata standardizzata, è stato utilizzato un tapis roulant specifico per la riabilitazione canina. Considerato che l'applicazione dei sensori IMU nel campo della valutazione canina non è ancora stata certificata, per convalidare i dati acquisiti durante i test è stato utilizzato come supporto un sistema di telecamere ad alta velocità.

Lo studio si è focalizzato principalmente sull'analisi delle fasi del ciclo del passo. Il primo obiettivo è stato quello di individuare dei metodi universali per identificare tramite i dati restituiti dai sensori

IMU gli istanti di primo appoggio e di stacco dal terreno, sia per gli arti toracici che per gli arti pelvici. Dopo aver implementato codici su Matlab per automatizzare il processo (con un'accuratezza media del 95%), sono state calcolate le percentuali delle fasi di appoggio e di oscillazione e sono stati creati degli indici di simmetria per confrontare i cani sani con quelli patologici. In particolare, solo uno di quest'ultimi ha presentato un'asimmetria tra l'arto patologico e quello controlaterale, la quale si è ridotta del 30% con l'applicazione dell'ortesi.

Infine, è stata eseguita una valutazione preliminare degli angoli articolari attraverso i sensori IMU, i quali, confrontati con la video-analisi, hanno evidenziato una buona correlazione tra gli andamenti dei grafici. Tuttavia, il range angolare ottenuto tramite i sensori è risultato spesso di valore inferiore rispetto a quello ricavato con la telecamera e ciò può essere ricondotto ad un errato posizionamento degli IMU sull'animale in studio.

In conclusione, l'utilizzo dei sensori IMU potrebbe rappresentare un'ottima opportunità per studiare i benefici e i possibili limiti legati all'applicazione dell'ortesi, al fine di ottimizzarne la progettazione e migliorare il benessere degli animali.

CHAPTER 1. INTRODUCTION

Human and animal worlds have always been linked to each other, but something has changed in recent years. The origin of the first veterinary schools in Europe is almost exclusively due to the spread of numerous epizootic diseases, which during the XVIII century caused great damage both to the animal heritage and to the growth of agriculture [1]. From this point forward the role and skills required by veterinarians have changed over time. Veterinarians must be able to indicate the correct therapy, prescribe the respective drugs, and perform surgery [2]. In addition, veterinarians have to provide advice to animal owners regarding nutrition, hygiene and general animal welfare [2]. This development of veterinary medicine, with the constant desire to improve animal health, has led the market for veterinary care to increase over time. According to the Italian Ministry of Economy and Finance, the veterinary expenditure has increased by 130 million euros (+20%) from 2016 to 2018 [3]. In particular, the two primary drivers for owners to invest in the health of their animals are the potential economic gain and the emotional bond.

Owning an animal can be a source of wealth and sustenance since it can provide high economic profit such as in breeding and in racing [4]. In relation to the potential income and to the market demand, the economic price of a single animal can be significant and very variable: the purchase for a cow can range from 500 to 5000 euros [5] and, in the equestrian competitions, horse value can reach up to 20000 euros [6]. The cost of animal maintenance should not be underestimated either: for instance, an average of 4000 euros per year is needed to sustain a horse [7]. Because of the large overall value and yearly cost of animal maintenance, owners are inclined to preserve their "investment" with additional spending on veterinary care.

Economic factors are not the only motivation for animal care. The sentimental role of animals in human society should also be considered. According to the 2019 Eurispes Italy Report [8], 33.6% of Italians have at least one pet. Furthermore, 76.8% of Italians consider their pet a family member, 32.9% as a son and more than 50% consider them a best friend. Therefore, in the event of illness or injury, the owners are willing to do anything to restore the health of their pet. According to the 2018 Assalco-Zoomark Report the pet care market in Italy is worth more than 2 billion euros [8].

A field of veterinary medicine that has been particularly involved in this economic explosion is Veterinary Orthotics and Prosthetics (V-OP). A prosthesis is an artificial device used to replace or augment a missing or impaired part of the body [9]. An orthosis, by contrast, is attached to the

body to assist and improve weak muscles or to support, position, prevent or correct deformities [10]. This medical device provides protected motion within a controlled range, prevents or reduces the severity of an injury, allows lax ligaments and joint capsules to approach normal distensibility and provides functional stability for an unstable limb segment [9]. While a prosthesis is used in case of an amputation surgery, an orthosis can replace medical operations by treating musculoskeletal diseases in which the limb remains present. It can be a good solution for many patients that are not good surgical candidates, because of advanced animal age, perceived increased anesthetic risk or circumstances requiring a delay of surgery [9]. In addition, while the high cost of a surgery is an obstacle for many owners, an orthosis is a viable alternative which may be more affordable. A knee orthosis, which is one of the most popular products, costs between 400 and 600 euros, compared to 2500-4000 euros for the knee operation [11]. Because of these combined factors, orthoses are becoming increasingly widespread.

As these devices are becoming more popular, an objective method to evaluate their efficacy also needs to be developed. The study of body, limb and joint motion, known as kinematic analysis, provides one potential non-invasive option [12]. Gait, as the cyclic act of walking, is the most commonly investigated movement and its analysis allows stance time, swing time and joint angles to be measured in an efficient and quantitative way. Kinematic analysis is widely used in human subjects for the diagnosis of gait-altering diseases [13] and for the optimization and progression of treatment [14]. Camera-based systems, optoelectronic systems and Inertial Measurement Units (IMU) have even been used to accurately assess the gait of human clinical cases, by returning precise kinematic values [15]. These systems have been effectively used in human gait analysis for many years and show potential for the same procedures in animals. However, their adaptation to animals requires the development of new protocols. After this point, these traditional methods could also be used to evaluate the kinematics of healthy and pathological animals with and without an orthosis device. This will return quantitative notion of the kinematics and numerical assessment of the changes that an orthosis brings to a pathological animal movement and can be used in future to improve the manufacture of these devices.

CHAPTER 2. STATE OF THE ART

2.1 Animal selection

When deciding which animals to use as investigation subject, it was important to consider how the outcomes of the study would contribute not only to society but also the forward progress of the scientific community. An animal needed to be chosen which was easily accessible and could provide precise, reproducible data. Dogs are an opportune subject not only because of their great sentimental value to humans but also due to how common they are in society. Recently, the bond between dogs and humans has become so important, that they are no longer simply considered a pet, but rather, a member of the owner's family [16]. This was reflected in the legislative area with an Italian bill presented by a group of parliaments to allow the inclusion of dogs in the family status [17]. Moreover, dogs are the most common pet in our society. In Italy alone, there are estimated to be more than 25 million dogs [18]. As dogs become continually more numerous and their sentimental role also grows in society, canine treatment has become more innovative. Since orthoses were used in human orthopaedics, it was decided to also adapt and use them on dogs with musculoskeletal diseases such as osteoarthritis or hyperextension. From the first company OrthoCare founded by Derrick Campana in 2005, in North America there are now 41 companies that produce and sell canine orthoses [19]. This trend can also be observed in European countries such as Italy, where companies Essedi and OrtoPaw offer the possibility of producing customized external prostheses and orthoses for animals of all sizes and breeds, but especially for dogs [20] [21].

Since this study is focused on the evaluation of canine kinematics, it is important to have some knowledge of the canine anatomy and gait. The dog has more than 300 joints, which are classified into immobile, semi-mobile and mobile. Orthoses are mainly focused on mobile joints and particularly on those of the limbs (Figure 1). In the thoracic limb there are the shoulder, elbow, carpal and digital joints, while in the pelvic limb there are the hip, knee (stifle), tarsal and digital joints [22].

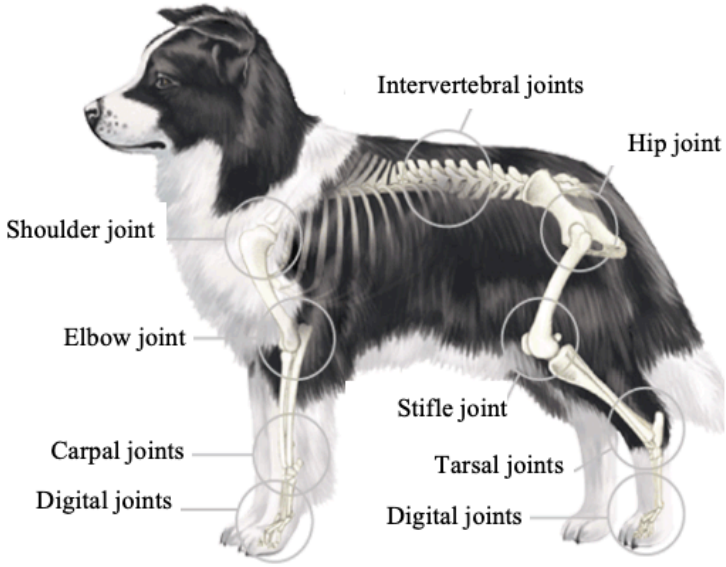

Figure 1. Joints of the thoracic and pelvic limbs of a dog [22].

Considering the general movement of dogs, there are 4 different gaits: walk, trot, canter, and gallop [9]. The walk is the slowest canine gait and is the only one to be addressed in this study. A pelvic limb always makes the first move, followed by the thoracic limb of the same side. The dog places the thoracic paw down on the ground just ahead of the location where the ipsilateral front paw has been located (Figure 2). The walk is the only gait in which there are always three paws on the ground.

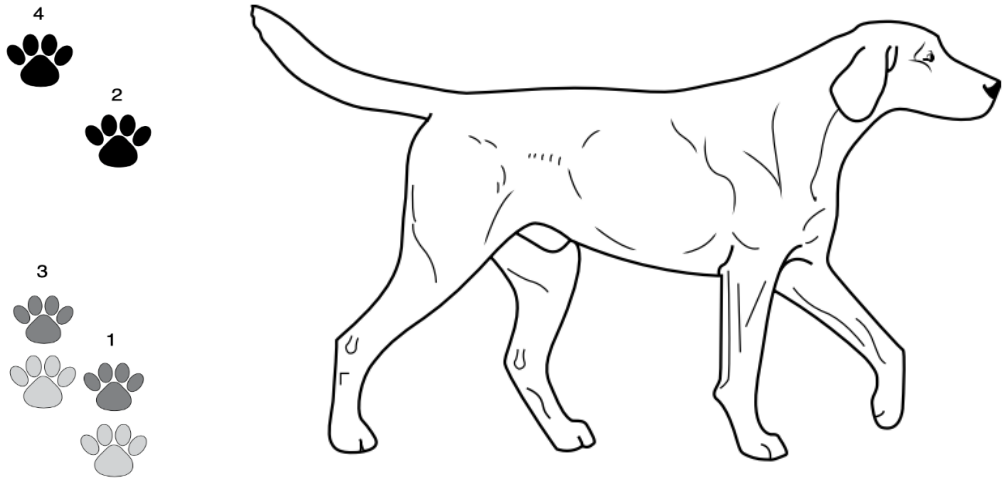

Figure 2. The walk. Diagram of the footprints of a dog walking. The black prints represent the front feet, and the gray prints represent the rear foot. The numbers represent the order of footfall. In this diagram, the light-gray prints represent the prints of the front feet from the previous stride. Illustrated representation of the canine walk [9].

2.2 Is it possible to standardize canine kinematics?

According to the International Dog Federation (IDF), dogs are the most varied species on Earth with more than 400 different breeds [23]. All dogs have the same anatomical components, but their structure and function vary highly between breeds [9]. Because of the specificity required for the design and prescription of a custom orthosis, the development of a standardized testing protocol using the animal's kinematics would be beneficial and efficient. One option for developing such a standard has been considered using reference stature measurements and joint angles in reference to the ground (Figure 3). The reference values are specific to each dog breed and which direction that the limbs are oriented [24]. The link between the reference values of each dog breed and the respective ranges of motion could allow for some parameters, such as joint angles, to be established as standardized the same values which would be representative of healthy stature and movement.

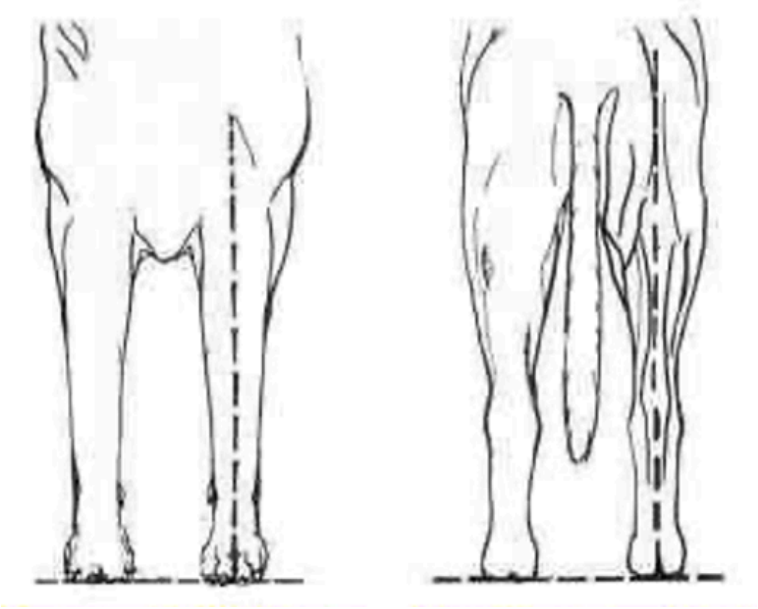

Figure 3. Representation of anterior and posterior reference values of a dog [24].

Reference values are greatly affected by anatomy, age, weight, and sex and for this reason they are not suitable for unequivocally classifying breeds and assessing the health of dogs. The anatomy and the kinematics characteristics of each breed are closely related to the purpose for which the dogs were originally bred. For example, Border Collies were bred to herd sheep, requiring them to be agile, turn sharply and move quickly. Instead, Labrador Retrievers were bred to fetch upland waterfowl and for this reason they tend to run directly to the game and recover it. According to

Zink, Canapp and Carr [25], Border Collies and Labrador Retrievers have quantitatively identifiable differences in gait characteristics, which can potentially be related to the differences in their original purposes. In addition, Channon, Hudson and Webster found that Greyhounds, a dog predisposed to running, and Bull Terriers, a dog dedicated to fighting, developed a completely different muscular structure which result in dissimilarities in kinematics [26]. These differences at the muscular level generate dissimilarities in kinematics. These studies suggest that each breed should have a specific database and reference ranges for gait variables.

This concept of breed-specific database is confirmed by Ocal and Sabanci who examined 135 dogs from 9 different breeds without lameness or history of orthopedic problems [27]. From the measurements of the standing angles of hip, stifle and tarsal joints it is evident that each breed has different physiological range of motion and even dogs belonging to the same breed but of different age, weight or sex can have dissimilar angles or heights.

Based on evidence in current literature which shows the variability of reference angles and stature not only across different breeds, but even within the same breed, analyzing a dog's health profile cannot currently be done based on a universal standard.

2.3 Classifications

Since it was not possible to use a universal standard, other strategies such as generalizing breeds through cluster classification were hypothesized. It could be possible to obtain comparable data considering dogs of different breeds but belonging to the same group. A first classification [9] is based on weight and the relationship between the distance from the ground to the olecranon process (Dgo) and the distance from the olecranon process to the dorsal rim of the scapula (Dod). The *ectomorphic* breeds have a smaller bone structure, are lightweight relative to their height and the Dgo is greater than Dod. These dogs are characterized by long stride length, ease in jumping and low agility at turning. Some examples of ectomorphic breeds are the Sighthounds, Weimaraners, German Short-Haired Pointers, Belgian Tervuren. The *endomorphic* breeds carry more weight on their frame and Dgo and Dod lengths are typically equal. These dogs have disadvantages in performance events requiring speed and agility. Some typical endomorphic breeds include Clumber Spaniels and Newfoundlands. Lastly, *mesomorphic* breeds are of moderate build with Dgo equal to Dod. Speed and agility are representative characteristics of these breeds. This group includes Golden Retrievers, Labrador Retrievers, Border Collies, Beagles and Border Terriers.

Even if an excellent division of dog breeds is obtained through the weight and specific heights, these are not the only parameters that allow to achieve similar results.

A second classification [27] was obtained by analysing 135 dogs belonging to 9 different breeds. Using the percentage of the patellar height with respect to the iliac crest height and the stifle and tarsal joint angles as discriminant variables, it was possible to divide the dogs into three different groups. In *group 1* all and only the German Shepherds were included: they had a different posture from that of other comprised breeds. *Group 2* included Anatolian Shepherds, 89% of the Dobermann Pinschers, 25% of the Berner Sennenhunds, 20% of the Boxers, 17% of the Labrador Retrievers and 5% of the Belgian Malinois. *Group 3* comprised the Golden Retrievers, the Rottweilers, 95% of the Belgian Malinois, 83% of the Labrador Retrievers, 80% of the Boxers and 75% of the Berner Sennenhunds. The fact that dogs belonging to the same breed were classified into different groups could be attributed to several factors as age, weight or sex. Moreover, the small sample sizes and the environmental factors may have increased statistical error. However, the breeds were assigned to one of the groups with a 75% minimal success rate.

Finally, a third classification [28] used the body length ratio (BLR) as discriminating variable. The BLR is given by the ratio between withers height (WH) and body length (BL). In particular, WH is the distance from the ground to the dorsal scapular rim and BL is the distance from the cranial aspect of the shoulder joint to the caudal aspect of the ischiatic tuberosity. A high BLR ratio means longer limbs and a more proximal centre of mass: in this way less force is required to overcome the inertia of the appendicular structure. *Group 1* is characterized by a BLR of 1 and describes dogs with a perfectly square body build. *Group 2* is described by a BLR smaller than 1 and indicates dogs with a long body or short limbs. Some examples of breeds belonging to this cluster are Beagles (BLR=0.8), Belgian Shepherds (BLR=0.89) and German Shepherds (BLR=0.91). *Group 3* is characterized by a BLR larger than 1 and indicates dogs with a short body or long limbs. A typical breed included in this group is the Canarian Warren Hound (BLR=1.17).

In all classifications a specific height is used to divide dog breeds. Even if this height is not calculated on the same anatomical component and is linked to different parameters, the classifications maintain a very similar guideline. This increases the probability that two dog breeds are in the same group in all classifications. However, this does not necessarily happen because even dogs belonging to the same breed could be in different groups due to age, weight or sex.

2.4 Instrumentation

Similar instruments are used to investigate both human and animal kinematics. The main methods are video analysis, optoelectronic and inertial system. Here we briefly explain the use, advantages, and disadvantages of each type.

2.4.1 Video analysis

Video analysis enables movement to be recorded through a single camera or a system of cameras, providing a sampled video as a series of frames [29]. This two-dimensional representation can be analysed manually or through software to obtain specific kinematic parameters. The camera for recording does not require special features, and in some studies a phone was sufficient [30]. However, it is preferable to use a camera with a high resolution and a high sampling frequency in order to obtain precise information.

2.4.2 Optoelectronic system

Optoelectronic systems represent the gold standard of lab-based technologies used in kinematics analysis [31]. It is an optic system, composed of a complex system of cameras which operate in the infrared range and it is equipped with devices for the detection of light and its transduction into an electrical signal. This system of multiple video cameras captures the position of retro-reflective markers, which can be active or passive. In clinic, they are usually passive, not powered by electricity, with smaller size respect to the active one that needs cables or batteries. This set-up offers great flexibility, enabling the visualization of multiple body segments and tracking motions in three-dimensions. However, the set-up is complex, the operation is time-consuming, and it is limited to use only within the laboratory environment, which restricts the variety of clinical applications [32].

2.4.3 IMU

Inertial Measurement Unit (IMU) is an instrumentation based on inertial sensors that allows the dynamics of an object or a body to be monitored. This device is a single unit that includes an accelerometer, a gyroscope or a magnetometer, or a combination of the three sensors.

The *accelerometer* is a sensor that measures the acceleration which the unit undergoes. The acceleration is evaluated by Newton's second law ($F = a \cdot m$), exploiting the force of inertia of a

fixed mass. This sensor is sensitive in three different perpendicular directions (x, y, z). It is important to underline that in a static case it will be measured an acceleration of 9.81 m/s^2, cause by the gravity force.

The *gyroscope* is a transducer capable of measuring the angular velocity of a body. They consist in vibrating masses exploit the accelerations of inertia which arise as a result of the motion of the sensor with respect to a reference non-inertial system, represented by Coriolis force ($a_c = 2\Omega \times V$). Coriolis force is an apparent force that arises in a rotating reference frame and it is proportional to the angular rate of rotation [32].

The *magnetometer* is a sensor that can detect the earth's magnetic field. It is possible to obtain the direction of the device by evaluating the variation of the intensity of the magnetic field in the three spatial directions.

As with the optoelectronic system, it can make mistakes during the measurement, cause by an incorrect positioning of the unit or the presence of soft tissue or hair and the influence on the kinematic that the system may have.

2.4.4 Comparison between the 3 systems

In the choice of the best instrumentation that allows the evaluation of the kinematic of the dog, many aspects must be considered. Video analysis is a simple, economic and portable method to obtain movement representations [33]. It allows movements to be detected in continuous and it does not interfere with the dog's kinematics. Data returned by two-dimensional video analysis can be comparable to those obtained through the gold standard motion capture but only in case of movement assessment in a single plane [33]. The great drawbacks of this system respect to the others are the lower accuracy and the impossibility to return kinematic values without a software or a manual detection. In addition, if the camera is fixed, the volume of acquisition is limited. The use of the video analysis alone may be insufficient to evaluate canine kinematics and it is preferable to use it as a support of the two other systems.

Although the optoelectronic system is nowadays the gold standard in human clinic with numerous protocols established [34][35][36], IMU provides an accurate alternative for a kinematic evaluation as shown in Table 1.

Parameters	Optoelectronic system	IMU	Video analysis
Protocols	+	-	-
Intereference with the gait	+	-	-
Size	-	+	+
Outdoor experiments	-	+	+
Acquisition volume	-	+	-
Continuos acquisition	-	+	+
Wireless transmission	-	+	+
Cost	-	+	+
Sensitivity external parameters	-	+	-

Table 1. Comparison of different methods exploitable for motion analysis. The '+' symbol corresponds to an advantage, while '-' to a disadvantage.

Although IMU systems can interfere with gait and require the development of innovative protocols for dog analysis, they are a single wearable unit, and they do not need a complex and unwieldy camera system as required by the optoelectronic system. This makes it much easier to transport and store them. In addition, the portability of IMU sensors makes it possible to perform experiments outside of a lab. This facilitates the animal experiments by allowing measurements to be conducted in a daily environment. The optical system requires the acquisition volume to be sampled and therefore limited. The gait must be executed within the sampled volume which is difficult to achieve with an animal. While the IMU does not have any limitation in space, allowing to obtain measurements in continuous. Both the IMU sensors and the optoelectronic markers are difficult to attach to the dog especially due to the presents of the hair. However, IMU can obtain values even if is under the hair, while the optoelectronic system requires the hair to be cut around the place of application of the markers. The ability to transmit data wirelessly, lower cost and a better sensitivity to the external parameters make the IMU the best suitable system to evaluate the canine kinematics. In addition to this, studies carry out by Bertocci et al. [37] using both systems on the same dog (Figure 4), showed how the results of the two systems are extremely similar and comparable, as it is shown in Figure 5.

According to all these aspects, IMU can be considered as the most suitable system to measure kinematic values of dogs.

Figure 4. Canine subject fitted both with IMU and optoelectronic markers systems [37].

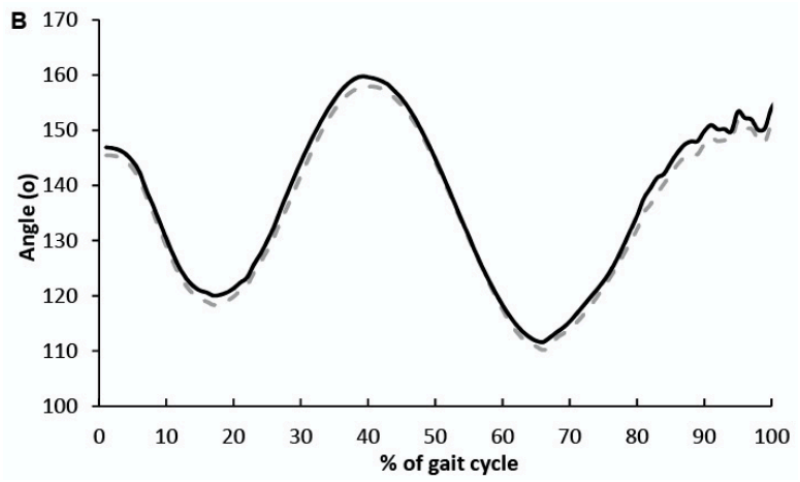

Figure 5. Comparison of sagittal plane angle of the hock during the gait cycle between optoelectronic system and IMU [37].

2.5 Inertial Measurement Units on dogs

There are several kinematic studies on dogs that have already been conducted using IMU. Despite the great benefits connected to this investigation method, a problem that has been highlighted is the correct positioning of these inertial sensors and the validation of IMU system. The use and the positioning directly depend on the final purpose of the tests carried out.

Yam et al. [38] evaluated long-term changes in physical activity and sedimentary behavior in pet dogs already enrolled in a calorie-controlled weight-loss program. In this case, the accelerometers

were attached to the dorsal aspect of each dog's collar for three consecutive weekdays, 24 hours per day, and once every month during the program.

In another study, Beraud et al. [39] evaluated the agreement of the kinetic data provided by the Walkabout Portable Gait Monitor (WPGM), a triaxial accelerometer, compared to the reference standard of the force platform analysis. The sensor and hardware, mounted in a pack and powered by an alkaline battery, were dorsally mounted over the thoracic or lumbar area, and secured by a Velcro strap (Figure 6). However, this solution was not optimal as the accelerometer systematically measured higher peak vertical forces than the force platform. This could be justified by the fact that the accelerometer was placed over the lumbar spine of the dog and therefore measures the whole body as it accelerates and decelerates in a vertical direction. When a dog trots, the force platform measures forces from one individual limb at a time, while the accelerometer placed on the trunk measures the force when two contralateral limbs strike the ground simultaneously.

Figure 6. WPGM positioned over the mid-lumbar spine of a dog [39].

2.5.1 Step detection

Some studies concerning the gait analysis and the calculation of joint angles have also been carried out. A team research of the Newcastle University [30] designed and tested GaitKeeper, an IMU sensor that provides step detection and gait analysis on dogs. The measurements units were attached to each leg of a group of 19 healthy dogs of various breeds. A cohesive bandage wrapped twice was used to ensure a correct attachment of the sensors (Figure 7), even if the authors suggested to find a better solution to fix the sensors in a correct and same position for each

experiment. The tests were carried out on a 15 m long linear track by imposing a gait of walking and trotting. It was possible to detect and calculate many parameters such as step time, stance time and swing time, by knowing the initial and final contact. The results demonstrated good sensitivity and repeatability that it could be sufficient to identify gait abnormalities in dogs.

Figure 7. Attachment of the IMU on each limb [30].

Jenkins et al. [40] showed that to evaluate the step detection of a gait cycle the presence of a single IMU might be sufficient. In fact, it was possible to detect the stance and the swing time with a single IMU mounted above the carpal joint on the lateral side of the left forelimb, using a cohesive bandage (Figure 8). In addition to this a mock sensor was attached to the right forelimb to equalize weight distribution. The tests were conducted on 5 dogs walking on a treadmill. Since the dogs tested belonged to different species (Labrador Retriever, Golden Retriever, Beagle, and Welsh Corgi), the speed set for the treadmill was normalized with the height at withers (HW), using values of 1.5, 2.0, 2.5, 3.0, 3.5 and 4.0 s^{-1}. This allowed the reduction of the effect of the height on gait parameters. Considering the z-axis as the midline (medial side) of the dog, the z-axis angular velocity (Rz) represented the primary rotating motion of the forelimb and it was used signal marker to identify the step (Figure 8). In particular, the swinging forward was represented by a broad peak and the touching the ground by a following smaller negative profile. Moreover, the toe-off coincided with a peak in the x-axis acceleration signal (Ax) and the toe-touch occurred immediately before a major peak in the first derivative of Ax (Ax'). The entire system was validated by means of a comparison with a camera-based system. Analysis revealed a mean error ± standard deviation of 0.00 ± 0.02 and -0.01 ± 0.03 s for determining toe-off and toe-touch events respectively, indicating a good correlation between the two measurement techniques.

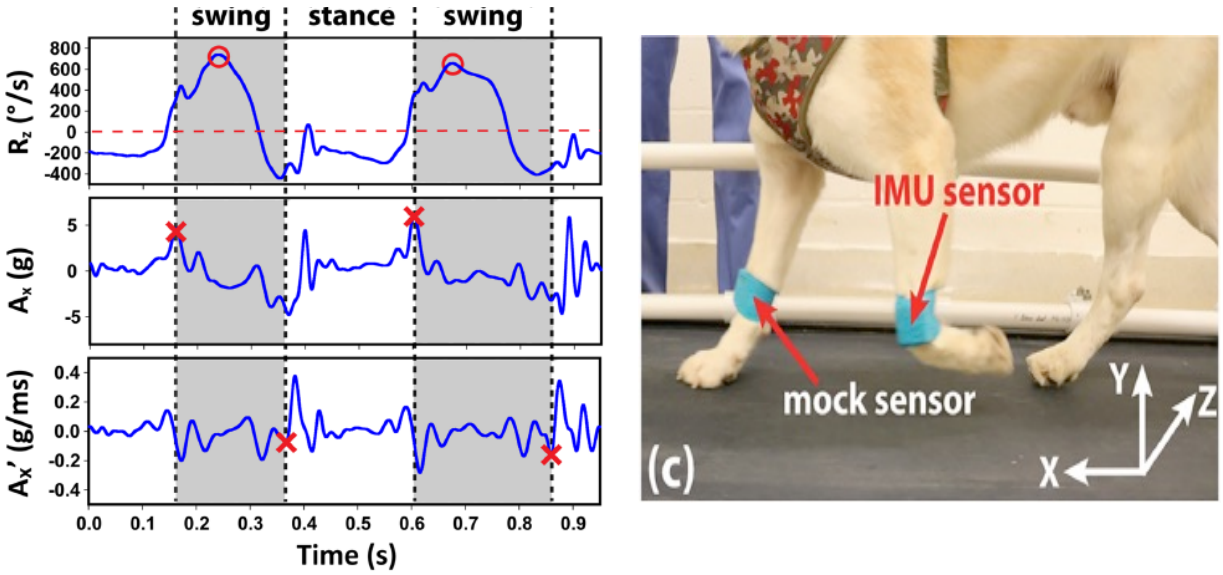

Figure 8. Representative tracing of the kinematic values (Rz, Ax, and Ax'); a photo illustrating sensor positioning and axes orientation [40].

2.5.2 Joint angles

When investigating articular angles of flection and extension, the choice of the number of markers or sensors and their correct position is much more difficult. Many studies using an optoelectronic system were already conducted to evaluate angular measurement of the joints [41] [42] [43] [44]. For instance, El-Warrak et al. [45] used the optoelectronic system to make a comparison between a group of healthy German Shepherd dogs and a group of hip-dysplastic ones. Eleven retroreflective spherical markers were placed on the skin in specific positions. It was possible to evaluate the trend of the graphs of flexion and extension angles and the angular velocity of shoulder, elbow, carpal, hip, stifle, and tarsal joint of both healthy and pathological groups.

Instead, much less studies were conducted using IMU system to determine angular values of the joints. One of the most significant is the study carried out by Bertocci [37], in which 6 IMUs were attached on dogs to calculate the maximum and minimum angles and the joint range of motion of carpus, hock, stifle and hip. In particular, 2 IMU were attached laterally to the thoracic limb at the level of mid-metacarpus and mid-radius and ulna, and 4 IMU were attached laterally at the level of the mid-metatarsus, mid-tibia, mid-femur and back of dogs. A group of 16 clinically health, medium size dogs were trotted at a uniform velocity of 1.8 to 2.5 m/s, monitoring the speed with a series of infrared emitters. Thanks to optical system it was possible to carry out tests with and without the harness system, providing an evaluation of the influence that fixing system and the

higher number of sensors could have. In Table 2 the values of the ranges of motion measured by IMUs are reported.

	Median	Max	Min
Carpus	78.1°	133.8°	44.6°
Hock	57°	98.9°	28.1°
Stifle	65.4°	94.8°	22.6°
Hip	28.1°	43.1°	18°

Table 2. Median, maximum, and minimum angular values of carpus, hock, stifle and hip [37].

2.6 Canine orthoses

Orthoses are defined as any medical device attached to the body to support, align, position, prevent or correct deformity, assist weak muscle or improve function [46]. Orthoses represent a valid alternative to surgery for patients who are poor anesthetic candidates or elderly, subjects with injuries for which there is no surgical correction, and owners with financial limitations. However, these devices should not only be considered as a replacement for surgery. Orthoses can also be used before a surgery to support and protect the limb and after a surgery to provide a safe, effective and dynamic alternative to traditional casting [46].

According to the joint and the pathology for which they are designed, canine orthoses are characterized by specific shapes and mechanical principles. The joints of the paw, carpus, tarsus and knee represent the main areas of interest in the orthotic world [46].

One of the main features that characterized paw orthoses (Figure 9) is the inclusion of the antebrachium (part of the thoracic limb between the elbow and the carpus) or crus (part of the pelvic limb between the knee and the tarsus) within the device for proper suspension. The most common digital pathologies are osteoarthritis, flexor tendon degeneration, supination or pronation and neuropathy causing loss of dorsiflexion.

Figure 9. A custom orthosis with paw insert for digital alignment; sciatic sling orthosis for sciatic neuropathy causing failure of digital dorsiflexion [46].

Carpal joint orthoses (Figure 10) are designed based on a mechanical principle called 3-point correction. Two counter forces and one corrective force are used to support the joint in proper alignment. The further the counter forces are from the corrective force, the longer the lever arm and the greater the mechanical advantage. In this way less force is required and trauma to the soft tissues is minimized. Examples common to carpal joint pathology include osteoarthritis, hyperextension, varus or valgus and supination or pronation.

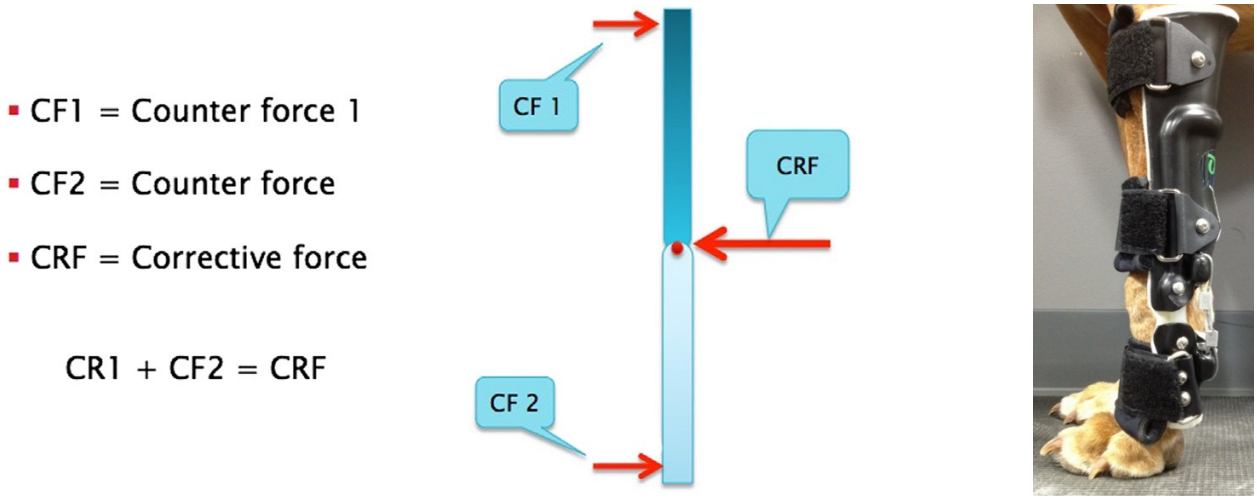

Figure 10. The 3-point corrective system composed of 1 corrective and 2 counter forces; an example of canine carpal orthosis [46].

Tarsal joint orthoses (Figure 11) are similar to those for the carpus and most injuries are managed with the same 3-point corrective mechanism. The classic examples of tarsal joint pathologies are osteoarthritis, hyperextension, varus or valgus and Achilles tendon strain, rapture or avulsion.

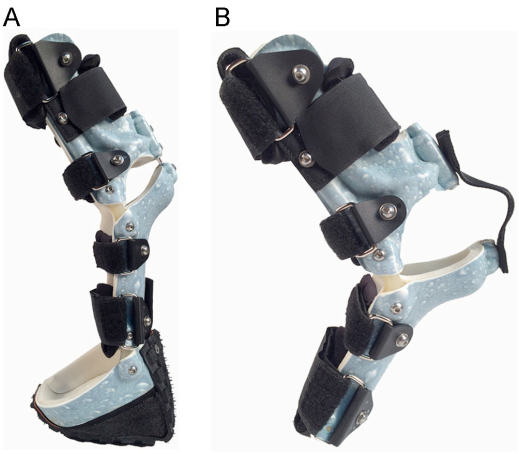

Figure 11. A dynamic Achilles tendon orthosis (A) can be progressed to a sport orthosis (B) [46].

Knee orthoses (Figure 12), on the other hand, are very different from the previous ones. The center of rotation changes during normal range of motion and for this reason the 3-point corrective technique cannot be exploited. In this case the proper mechanical principle is called force coupling. It uses the action of the major muscle groups to couple the femur and the crus while allowing a polycentric hinge to provide articulation and limit shear. The most common stifle joint pathology amenable to orthotic devices is the cranial cruciate ligament rupture.

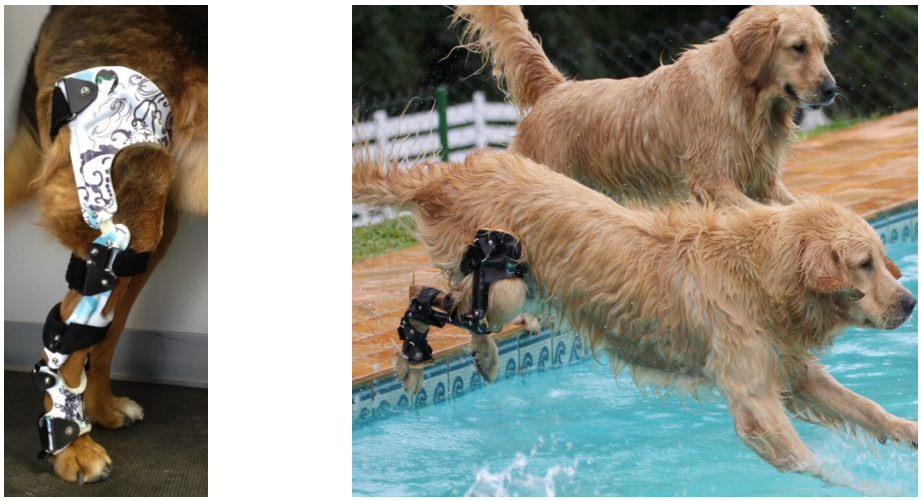

Figure 12. Two examples of stifle orthosis for canine cranial cruciate insufficiency [46].

To the writers' knowledge, a single study was carried out evaluating the effectiveness of canine orthoses and in this case only the optoelectronic system was used. R. Mullis et al. [47] conducted a study on the evaluation of 3-dimentional pelvic limb joint motion in dogs with and without orthosis. Kinematic data were collected from six healthy dogs at walk and trot for hip, stifle, and tarsus, before and after the application of a stifle orthosis. Data were also obtained for the orthosis alone. In Figure 13 it is possible to see the position of the retroreflective markers used to model 3D motion of the orthosis. Markers labelled (A) represent the location of the anatomic markers while markers labelled (T) represent the location of technical marker clusters. The results showed that gait waveforms differed between braced and unbraced limbs for all joints and planes of motion, as well as between the braced stifles and the orthosis alone at both walk and trot. The joint range of motion (ROM) was altered by the presence of the orthosis that limited the extension at the end of the stance, as can be seen in the graphs of Figure 13 in which the black lines represent the stifle alone and the grey lines represent the braced stifle.

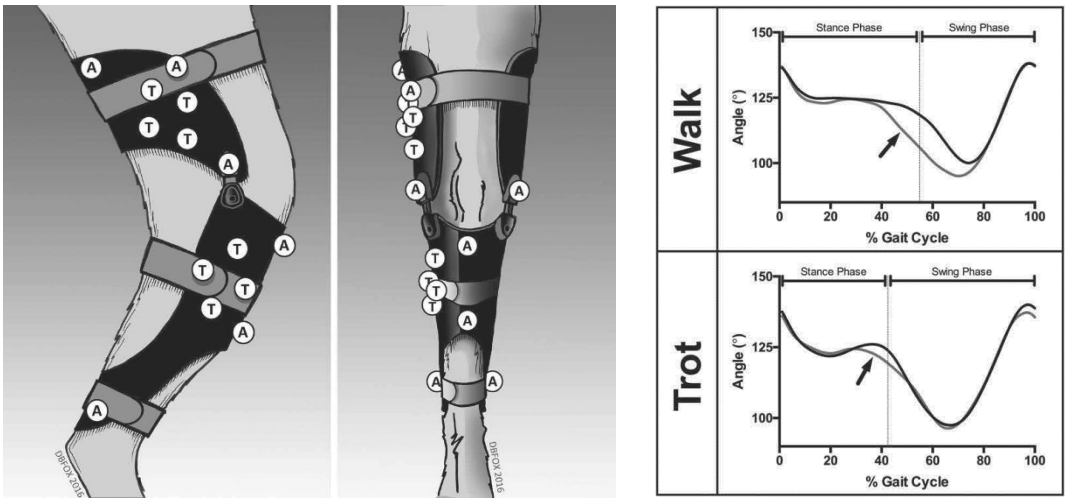

Figure 13. The illustration of the stifle orthosis applied on the pelvic limb with all the retroreflective markers; graphic representation of the mean stifle angles at walk and trot [47].

CHAPTER 3. AIM

The aim of this thesis is to develop and test a universal method for assessing the movement of dogs with and without orthoses. The protocol involves the use of IMU sensors, which will be positioned on the animals' limbs to acquire the parameters of step detection and joint angles. Since this measurement system is not yet experimentally widespread in the canine field, a database obtained from tests on healthy dogs must be firstly created in order to evaluate the correct interpretation of the parameters returned by the IMU sensors. Once this will be sorted out, the collection of these data will be used to provide a comparison with pathological subjects. By testing dogs with motor disfunction with and without orthoses, a preliminary assessment of the quality and advantages of these medical devices can be conducted. Starting from the protocol and the bases afforded by this research, future studies involving a greater number of subjects can be carried out to quantify the efficiency and efficacy of canine orthoses in restoring correct kinematics to the dogs with musculoskeletal pathologies.

CHAPTER 4. MATERIALS AND METHODS

Based on the technological and practical benefits outlined the previous chapter, multiple IMU sensors were chosen for evaluating the effectiveness of canine orthotics on improving pathological gait. While the versatility of a commercial IMU system makes its use convenient, the system utilized in this study needed to be validated first since the sensors are still prototypes. In doing so, the efficacy of their application in animal studies was also evaluated. Since optoelectronic system is currently considered the gold standard for analyzing human or animal kinematics [31], IMU validation was performed against it within a lab.

Preliminary tests were first performed on human subjects to ensure their movements could be accurately repeated and measured for evaluating the affinity between the data returned by the IMU sensors and the optoelectronic system.

Afterwards, it was possible apply the validated devices to the investigation of animal's motion. Since the use of IMU sensors is under development in the canine kinematics evaluation field, a high-speed camera-based system was employed as support in the clinical setting to corroborate the data acquired during dog tests. While an optoelectronic system would have been preferred, it was unavailable in the dog testing facility. However, video analysis is another proven method for motion and kinematic investigation [48].

4.1 Motion tracking systems

4.1.1 IMU

The IMU sensors were designed and manufactured by the Centre for Biorobotics of Tallinn University of Technology (Tallin, Estonia). The dimensions of these devices are small (30 mm x 12 mm x 4 mm) and lightweight (6.9 ± 0.3 g) which permitted the tests to be performed without interfering with the movements of the subjects. Each sensor is composed of a 9-axis, low power, BMX160 IMU sensor (Figure 14), developed by Bosh (Germany) [49]. The IMU provides precise acceleration (m/s^2), angular rate (°/s) and geomagnetic measurement (μT) in each spatial direction. The accelerometer and gyroscope range could be selectable through an interphase respectively between four and five options. In this study, the widest ranges of acceleration and angular velocity were selected. In Table 3 the main characteristics of the BMX160 IMU are reported.

Characteristics IMU BMX160	
Dimensions	2.5 x 3.0 mm^2
Supply voltage	1.71 - 3.6 V
Consumption	1585 µA
Acceleration and gyroscope resolution	16 bits
Acceleration range	±2 - ±16 g
Acceleration resolution range	0.000061g - 0.00049 g
Gyroscope measurements range	125 - 2000 °/s
Gyroscope measurements resolution	0,06 - 0,004 °/s
Magnetic field range	±1150 - ±2500 µT
Magnetic resolution	0.3 µT

Table 3. IMU main characteristics [49].

Figure 14. IMU BMX160 [49].

The sensors (Figure 15) can measure data with a frequency of 100 Hz through an Advanced RISC Machine (ARM) processor which is integrated in the IMU. An external Li-ion battery allows wireless data collection. Data acquired are stored in a micro-SD and later downloaded through a micro-USB connection. The operation of the sensor is guaranteed by a Printed Circuit Board (PCB) that connects all the elements of the unit, also providing for data transfer, battery recharging and programming of the ARM. In addition, a pressure and a temperature sensor are present within the

unit, but they were not used this study. The sensors are turned on and off using a magnet and have a blue light emitting diode (LED) which flash to signify that the sensors are on.

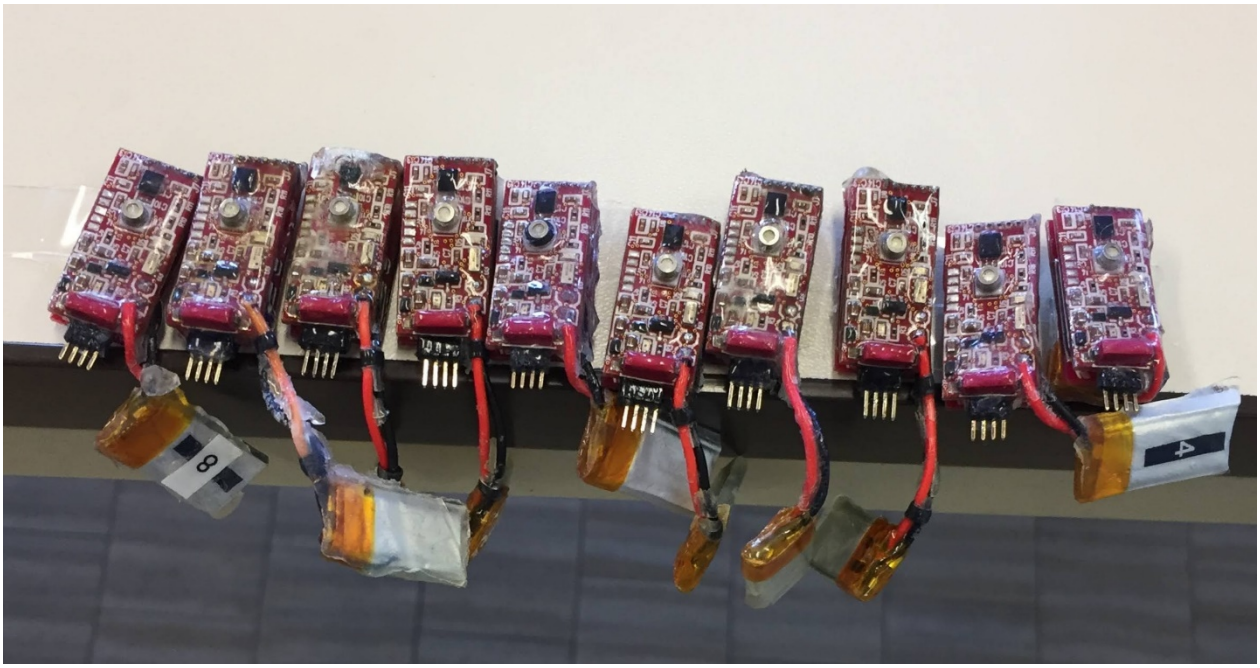

Figure 15. IMU sensors.

4.1.2 Optoelectronic System

The optoelectronic system used in this study is the BTS Smart-DX (BTS, Milan, Italy) available in the "Luigi Divieti Laboratory of Posture and Movement Analysis" of Politecnico di Milano (Milan, Italy). The system consists of 8 cameras equipped with Charge Coupled Device (CCD, Figure 16) sensors, which are sensitive to infrared radiation. The crown of LEDs (IR illuminator), present around each camera lens, emits stroboscopic lighting which the reflects off of passive photo-reflecting markers whose 3D location is detected at less than 100 µm of accuracy [50]. The markers can then be positioned on any subject or object according to the requirements of the experiment.
The infrared cameras identify the position of these markers and track them during the chosen task, recording their coordinates with a sampling frequency of 100 Hz. Each marker must always be framed by at least two cameras with non-parallel optical axis in order to guarantee a continuous three-dimensional reconstruction of it. A schematization of the body segments investigated is then reconstructed starting from the trajectories traced by the markers. The further processing of data through a suitable software and optimization techniques allows the desire kinematic parameters,

such as angles and velocities, to be obtained. The presence of force platforms in the laboratory also allows the ground reaction forces generated by a subject to be measured.

Figure 16. Motion analysis system camera [50].

4.1.3 Camera-based system

A high-speed camera-based system was used to validate the data acquired by the IMU sensors during the tests conducted on dogs in a clinical setting.

The tests were recorded using a GoPro Hero8 Black (Figure 17) mounted on a tripod at the same height as the treadmill to ensure the movement of all four legs was visible. Video was captured at 240 fps and 1080 p resolution and was examined using an image analysis software, Kinovea (0.9.3 version). The main characteristics of this camera are resumed in Table 4.

Characteristics GoPro Hero8 Black	
Video resolution	1080 p
Frame per second (FPS)	240
Field of view (FOV)	Wide

Table 4. Characteristics of GoPro Hero8 Black.

Figure 17. GoPro Hero8 Black.

4.2 Validation trial

For human validation trials, the external knee angles of healthy subjects were investigated using both IMU sensors and the optoelectronic system and results were compared.

4.2.1 Subjects

For the validation trial 2 subjects were considered (Table 5).

Subject	Sex	Age	Pathology
1	Male	25	-
2	Male	24	-

Table 5. Human subjects' characteristics for validation trial.

4.2.2 Test protocol

The validation tests were conducted at "Luigi Divieti Laboratory of Posture and Movement Analysis" (Milan) and consisted of 20 consecutive squats. This trial is one of the most frequently used to evaluate knee movement, since it shows a wide angular range in sagittal plane. Furthermore, the analysis is easily to conduct since the angular knee values are kept constant for a few seconds once the positions of maximum extension and maximum flexion are reached.

Before the start of the experiment, IMU sensors and the optoelectronic system were synchronized through the lifting of the right leg. After synchronization, the trial was performed and approximately 3 seconds were held for each position of maximum extension and maximum flexion.

IMU system

Initially the IMUs were not synchronized with each other, as they were not turned on at the same time. For this reason, the IMUs were first positioned in the same direction on a flat surface to which an impulse was subsequently delivered by the investigator. The impulse recorded by all IMUs was later used to synchronize the sensors during data analysis. After synchronization, 6 IMU sensors were placed on the centers of mass of the shank, thigh and foot [51]. To ensure the sensors remained where they were positioned, a cohesive bandage was used. All sensors were oriented in the same direction, following the main dimension of the body segment to investigate. Additionally, the LEDs always needed to be visible in order to verify that the sensors were still actively acquiring data.

Optoelectronic system

To evaluate kinematic parameters with an optoelectronic system, the global reference frame and a spatial sampled volume must be defined through calibration. A reference frame of three marked sticks corresponding to the three axes (X, Y, Z) was positioned in a specific point of the walking platform and was acquired by the system. Subsequently, one of these sticks was rotated for approximately 5 minutes in the volume dedicated to the trial to allow the system to calibrate the acquisition volume.

To correctly reconstruct human motion and its kinematic, Davis protocol was followed for markers' positioning. Anthropometric measurements were collected (Table 6) and 22 retroreflective markers were placed in specific anatomic positions (Figure 18) [52]. During the test, to collect the spatial position of each marker, Smart Clinic software (BTS S.p.A., Italy) was used.

Subj	Ht	Wt	Leg Ht	Pelvis Wd	Knee Wd	Ankle Wd	Pelvis Ht
1	178 cm	74 kg	97 cm	19,5 cm	9 cm	7 cm	9 cm
2	188 cm	86 kg	105 cm	25 cm	9 cm	8 cm	9 cm

Table 6. Anthropometric measurements of the subjects (Ht=height, Wt=weight, Wd=width).

Figure 18. Positioning of makers and IMU sensors, (a) frontal and (b) lateral view.

4.2.3 Data processing

IMU system

Thigh and shank sensors were used to calculate 3D knee angles. Before starting the data analysis, the IMUs were first synchronized using a custom script written in Matlab (R2020b, Mathworks, USA), exploiting the great acceleration caused by the synchronization impulse. Subsequently, a second code was implemented to calculate the angles. The data returned by the accelerometers and the magnetometers were used to derive the quaternions and then the rotation matrixes, which were exploited to estimate the 3D knee angles. Specifically, the mathematical formula used to extrapolate the angular values is the following:

$$Knee_i(t) = \tan^{-1}(\| V_i^1(t) \times V_i^2(t) \|, V_i^1(t) \cdot V_i^2(t))$$

where $Knee_i(t)$ is the knee angle in the axis of interest i (x, y, z) at each time stamp, t. It is calculated using the four-quadrant inverse tangent ($\tan^{-1}$) between the cross product and the dot product of the rotated vectors of the two sensors along the axis V_i^{α}, where i denotes the body frame axis of interest and α (1 or 2) is the index of the two sensors.

The codes written in Matlab with the respective descriptions are reported in APPENDIX A.

Optoelectronic system

Before conducting data analysis, SMART Tracker software (BTS S.p.A., Italy) was used to assign each marker its specific anatomical position. This software allows the subjects to be represented as stick diagrams, in which the body segments are displayed as lines between two specific markers. The labelling was automatically conducted by using the Davis protocol already available into SMART Tracker (Figure 19). If the name was not assigned to the respective marker or was lost during the task execution, a manual correction was performed.

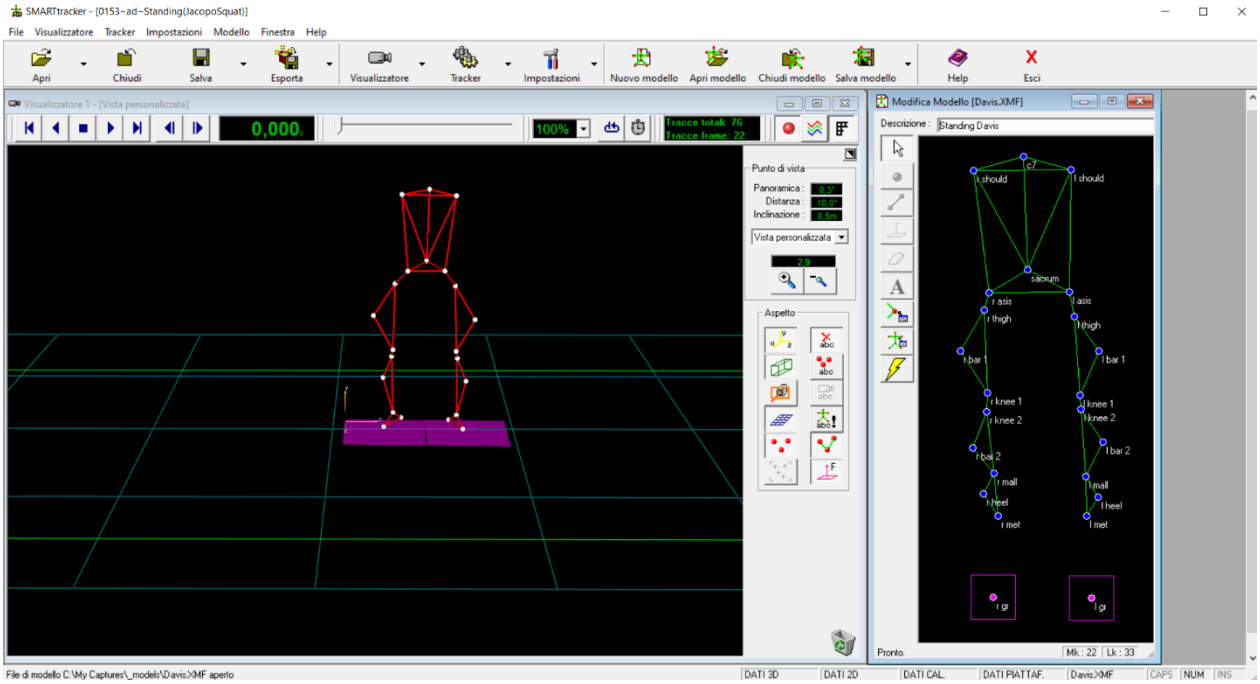

Figure 19. Smart Tracker frontend.

After the labelling of the markers, SMART Analyser software (BTS S.p.A., Italy) was used to evaluate the knee angle. Two different protocols were implemented to evaluate 2D and 3D external knee angles. The three-dimensional coordinates of the markers were interpolated and filtered through a low-pass Butterworth filter with a cut-off frequency of 10 Hz. This allowed a continuous signal to be obtained, reducing signal noise.

4.3 Dog trials

IMU sensors and the camera-based system were used during canine tests to analyze thoracic and pelvic limb step detection. Moreover, a primary investigation on the canine joint angles was performed.

4.3.1 Subjects

IMU sensors were tested on 7 different dogs: five of them were healthy with no previous history of injury. The remaining two suffered from musculoskeletal disorders. The first was born without a phalanx on the right thoracic limb, while the second had partially ruptured the Achilles tendon of the right pelvic limb. The Essedi orthopedic center designed and developed custom-made paw and tarsal joint orthoses for the two subjects (Figure 20). The number and characteristics of the dogs strictly depended on the availability of the owners and it was not possible to impose restrictions on the selection. Table 7 shows the sex, age, breed, and possible pathology of each dog.

Subj	Name	Sex	Age	Breed	Pathology
1	Argo	Male	10 months	Half-breed	-
2	Kira	Female	10 years	Half-breed	-
3	Swiss	Female	8 years	Border Collie	-
4	Joy	Male	6 years	Australian Shepherd	-
5	Siby	Female	4 years	Australian Shepherd	-
6	Mia	Female	11 months	Whippet	Born without a phalanx
7	Uller	Male	11 years	German Shepherd	Partial rupture of the Achilles tendon

Table 7. Characteristics of dogs tested.

Figure 20. (a) Paw and (b) tarsal joint orthoses.

4.3.2 Test protocol

The tests on dogs were conducted at the Fisio4Vet center (Bovisio Masciago, MI) [53], which owns a rehabilitation treadmill designed for canine hydrotherapy (Idrotech 2000 by Maclaren, Figure 21). The rehabilitation treadmill is equipped with a computer that allows to set the duration of the test and the speed of the non-slip mat. Since the rehabilitation aspect was not our focus, the treadmill was not filled with water and the tests were performed dry.

Figure 21. Idrotech 2000 by Maclaren.

To ensure the dogs' safety, a veterinarian guided them on the treadmill by using the harness worn by the animal. Concerning the trials executed, speed was set according to the dogs' height and their experience walking on a treadmill. The duration of each test was variable since the goal was to achieve at least 15 consecutive regular steps. If any time the dogs were observed walking with an abnormal gait, the timing was noted and later removed from the data analysis. At least 2 tests were carried out for all dogs and, if possible, varying treadmill speed to have an extra comparison parameter (Table 8). Pathological dogs were tested with and without orthosis at the same speed for both trials.

Subject	Test 1	Test 2	Test 3
1	1.3 km/h	1.8 km/h	2.3 km/h
2	0.9 km/h	1.1 km/h	-
3	1.5 km/h	1.7 km/h	1.8 km/h
4	1.5 km/h	1.7 km/h	1.8 km/h
5	1.5 km/h	1.7 km/h	1.8 km/h
6	1.1 km/h	1.1 km/h	-
7	1.4 km/h	1.7 km/h	-

Table 8. Speed of each test.

IMU system

The same synchronization method used in the validation trial was performed also for the dog tests. After synchronization, IMUs were placed on dogs with paper tape and cohesive bandages. The protocol adopted in this case involved the use of 10 IMUs, 2 for each thoracic limb and 3 for each pelvic limb. The IMUs were all positioned between two joints on each limb's segment: between shoulder and elbow, elbow and carpus, hip and knee, knee and tarsus, tarsus and posterior digital joints (Table 9 and Figure 22).

IMU number	Upper joint	Lower joint
1	Left shoulder	Left elbow
2	Left elbow	Left carpus
3	Right shoulder	Right elbow
4	Right elbow	Right carpus
5	Left hip	Left knee
6	Left knee	Left tarsus
7	Left tarsus	Left posterior digital joints
8	Right hip	Right knee
9	Right knee	Right tarsus
10	Right tarsus	Right posterior digital joints

Table 9. Protocol adopted for the positioning of the IMUs.

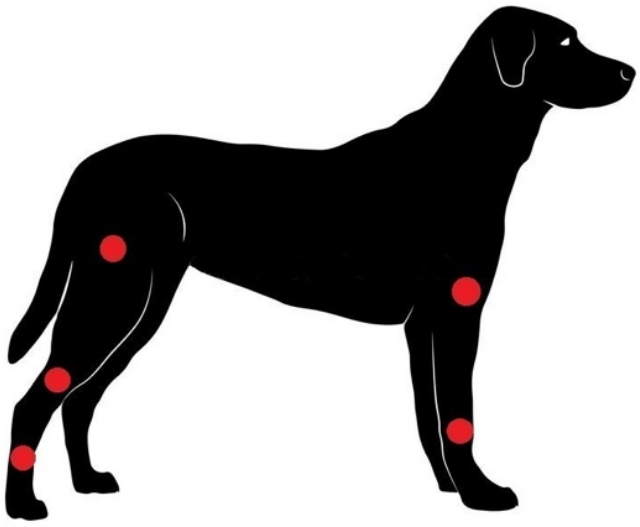

Figure 22. Illustrated representation of the sensors positioning from lateral view.

While with humans the IMUs were positioned at the centers of mass of the body segments, this practice was difficult to implement on dogs since each breed has a different anatomical structure, and the authors could not find any reference tables. Moreover, it was preferred to choose areas which allowed safe and correct mobility of the limb, even if this implied moving away from the estimated centers of mass (Figure 23). As for the validation trial on humans, all the sensors were oriented in the same way, following the bone segments length.

Finally, to verify the symmetry between the right and left side, the distances from the ground of each IMU were measured using a tape measure: in the event of differences between the right and left limb, the IMUs were repositioned before the start of the tests.

Figure 23. Examples of the positioning of IMU units on dog.

Camera-based system

To assure time synchronization between the motion capture system and the IMU sensors, the camera was switched on before turning on the sensors and a chronometer, with a sensitivity of 10 ms, was started and left on for the duration of the test. The camera captured both the sensors' synchronization phase and the chronometer to record the precise time value in which the hand hit the surface. This moment was considered as the time zero of the test. Subsequently the camera was switched off for as long as the positioning of the IMUs on dogs. Once all the sensors were attached, the camera was turned on again, capturing the chronometer in order to synchronize the video with the sensors. The camera was positioned beside the treadmill at the ground level, recording all the tests.

4.3.3 Data processing

IMU system

Step detection protocols followed those originally validated by Jenkins et al. [40]. The sensors used were the ones positioned between elbow and carpus of the thoracic limb and between knee and tarsus of the pelvic limb. After synchronization, the acceleration data were filtered using a 3rd order low-pass Savitzky-Golay filter to reduce signal noise.

Thoracic limbs were the first to be analyzed. Toe-off, which is defined as the instant the paw leaves the ground and initiates swing phase, was identified using a distinguishable peak in the acceleration signal along the axis of the dog's walk (Figure 24).

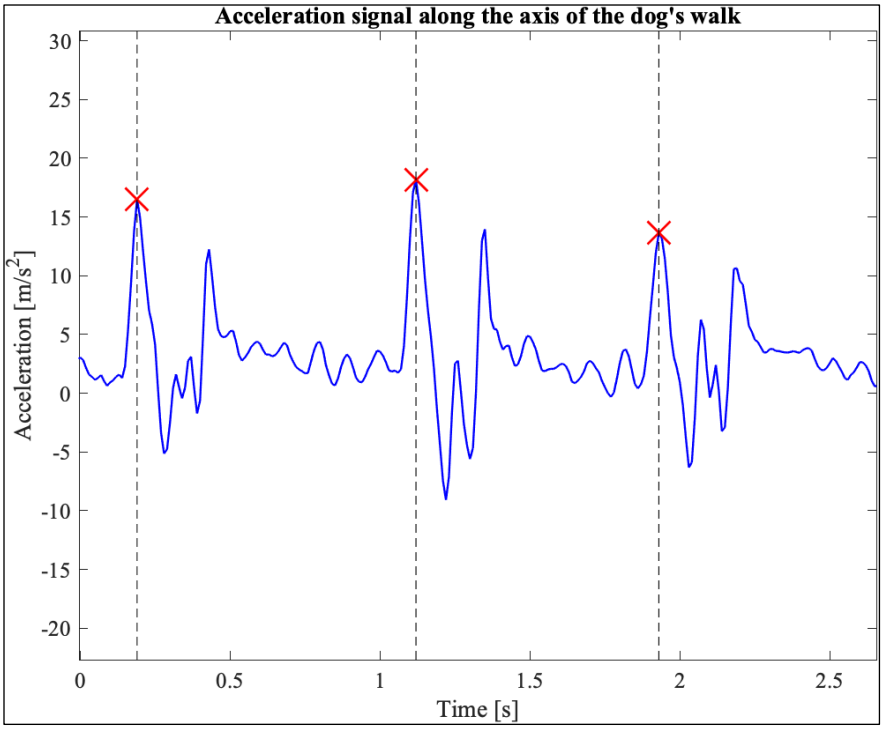

Figure 24. Three toe-off events of the thoracic limb identified with a red cross on the acceleration signal along the axis of the dog's walk.

Toe-touch, which is defined as the instant the paw touches the ground and initiates stance phase, was more complicated to be identified, as the approach offered by Jenkins [40] was not directly applicable to the graphs returned by IMU sensors. Nevertheless, this guideline was used as a starting point to hypothesize five other different methods. The first two procedures identified the initial contact of the paw with the ground as a valley in the graph of the acceleration signal along

the axis of the dog's walk (Figure 25). Since for several steps the valley indicated by Jenkins as the point near to the toe-touch was represented in our graphs by two closely spaced valleys, both were considered as potential points of interest. For the steps where this problem did not occur, the methods localized the same point.

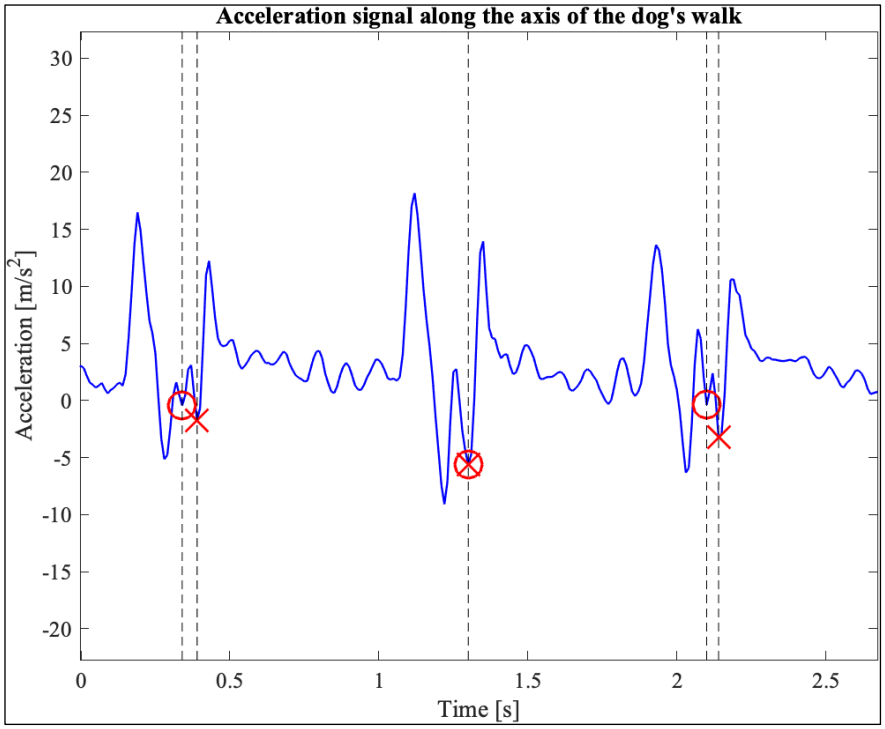

Figure 25. Identification of three toe-touch events of the thoracic limb using the acceleration signal along the axis of the dog's walk. The method identifying the previous valley is displayed by the red circle, the other method by the red cross.

For the third and the fourth method, the first derivative of the acceleration signal (jerk) along the axis of the dog's walk was considered. The valleys recognized with the first two approaches were used as a constraint to detect the new points of interest: going backwards from these instants, the first valleys on the graph of the first derivative of acceleration signal along the axis of the dog's walk were selected (Figure 26).

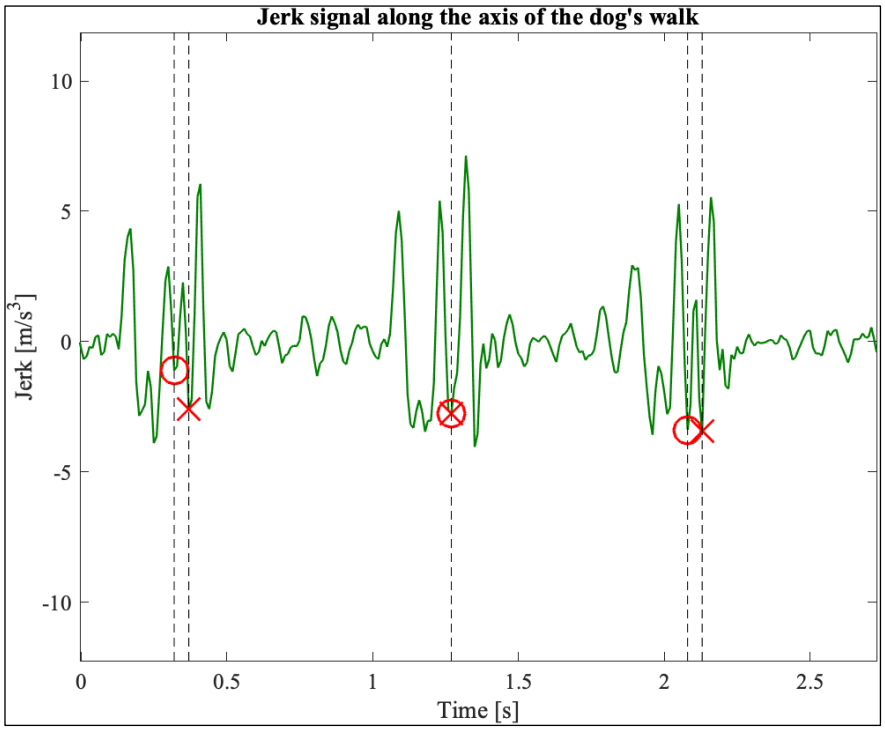

Figure 26. Identification of three toe-touch events of the thoracic limb using the first derivate of the acceleration signal (jerk) along the axis of the dog's walk. The method identifying the previous valley is displayed by the red circle, the other method by the red cross.

Finally, a method for detecting the toe-touch of the thoracic limbs was hypothesized involving the use of acceleration signal along the vertical axis: the highest peak between two toe-off events was selected (Figure 27).

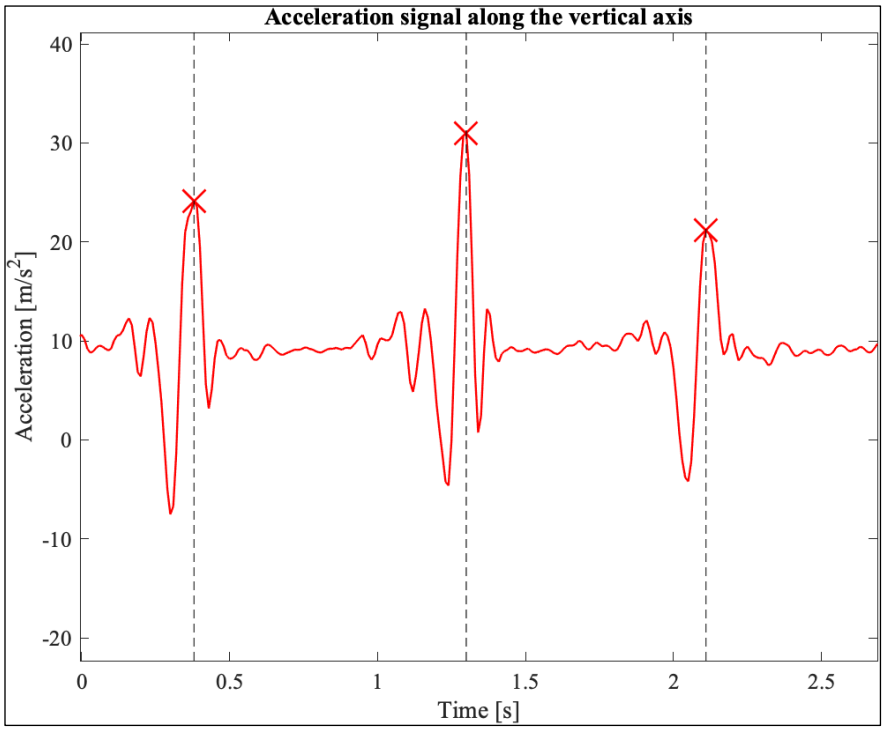

Figure 27. Three toe-touch events of the thoracic limb identified with a red cross on the acceleration signal along vertical axis.

While Jenkins et al. exclusively considered thoracic limbs in their study, we were also interested in developing an alternative method for analyzing the gait patterns of the pelvic limbs. We experimentally noticed that the pelvic limbs movement at the toe-off is quite different from the one of the thoracic limbs: while the second is predominantly in the dog's walk direction, the pelvic paws move firstly upward and then forward. Since it was not initially known in which of the two directions the acceleration occurred most, the peak identifying the toe-off of the pelvic limbs was detected using both the acceleration signal along the vertical axis (Figure 28) and the acceleration signal along the axis of the dog's walk (Figure 29).

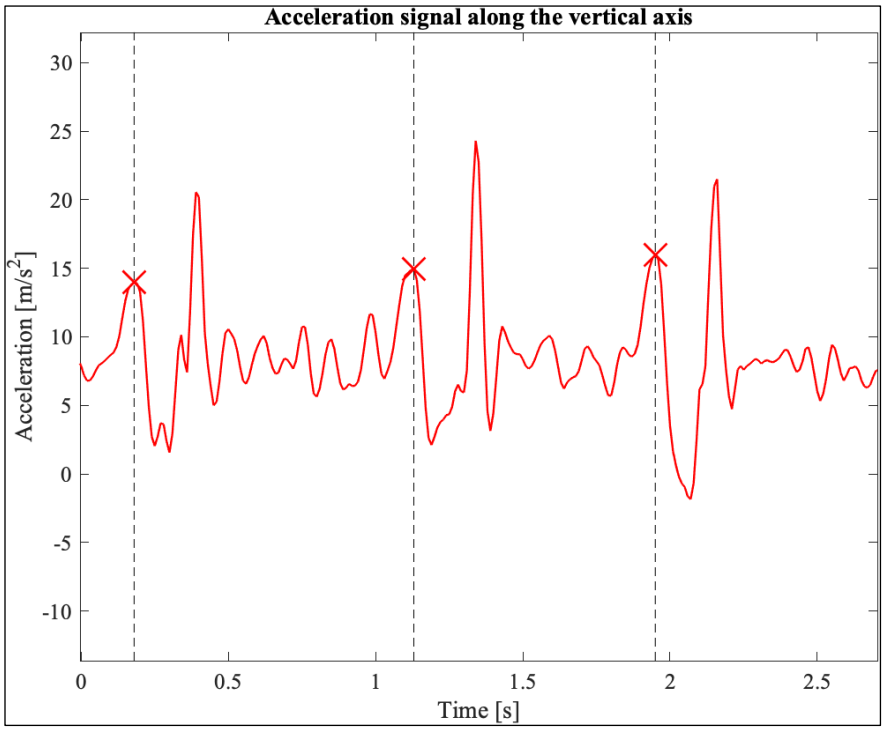

Figure 28. Three toe-off events of the pelvic limb identified with a red cross on the acceleration signal along the vertical axis.

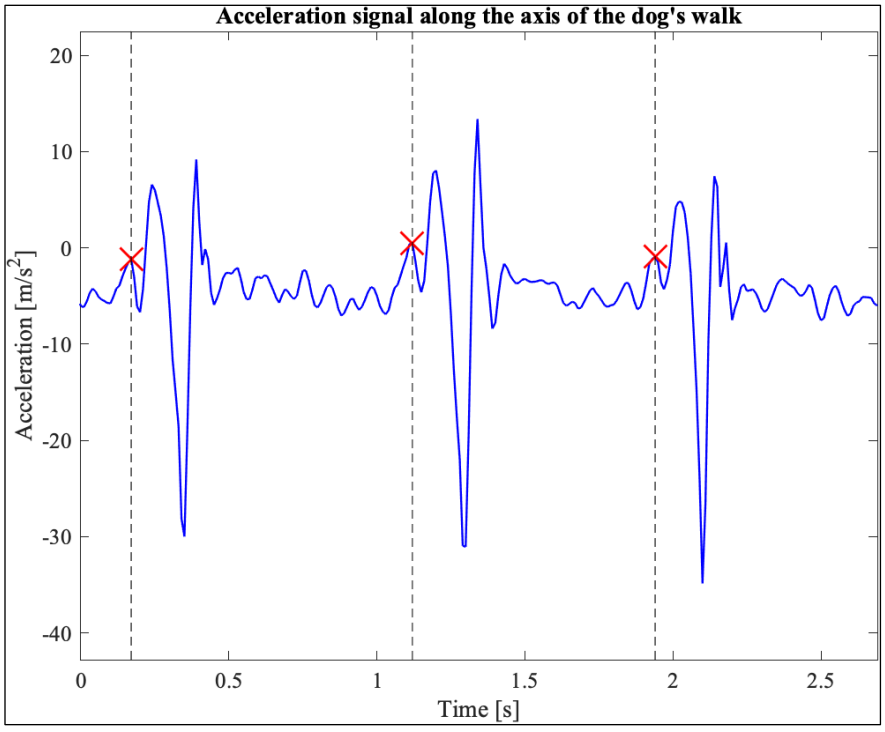

Figure 29. Three toe-off events of the pelvic limb identified with a red cross on the acceleration signal along the axis of the dog's walk.

In contrast, toe-touch of the pelvic limbs was more distinguishable. In the graph of the acceleration signal along the axis of the dog's walk there is a deep valley that should indicate the instant the paw touches the ground (Figure 30). Influenced by what Jenkins hypothesized for the thoracic limbs, this method was compared with a second one that uses the first derivate of acceleration in the same direction. The procedure was the same as for the toe-touch of the thoracic limb: going backwards from the instant identified with the previous method, the first valley on the graph of the first derivative of acceleration was selected (Figure 31).

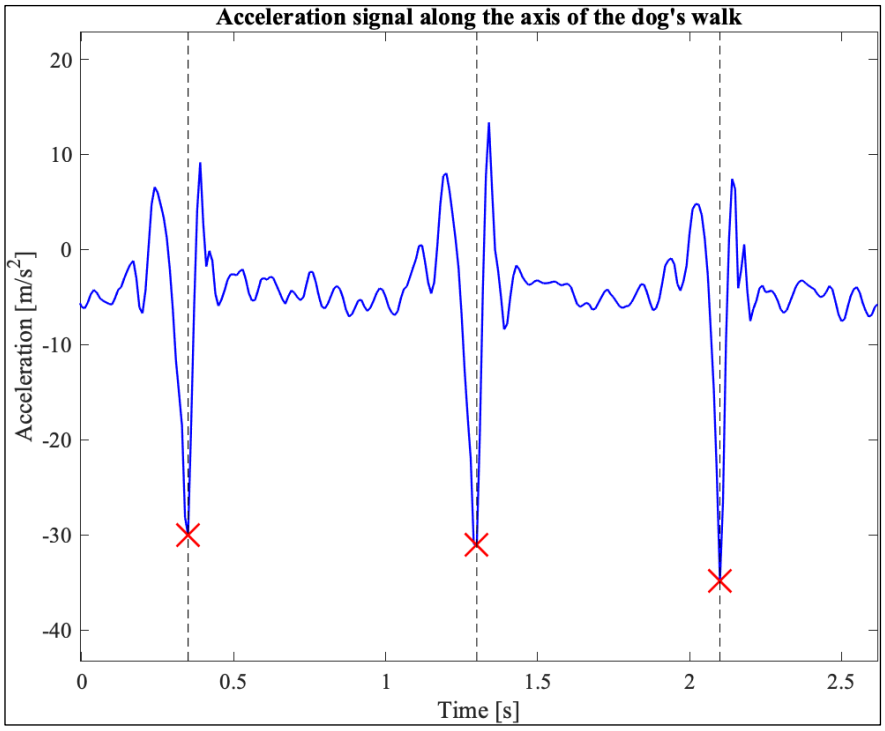

Figure 30. Three toe-touch events of the pelvic limb identified with a red cross on the acceleration signal along the axis of the dog's walk.

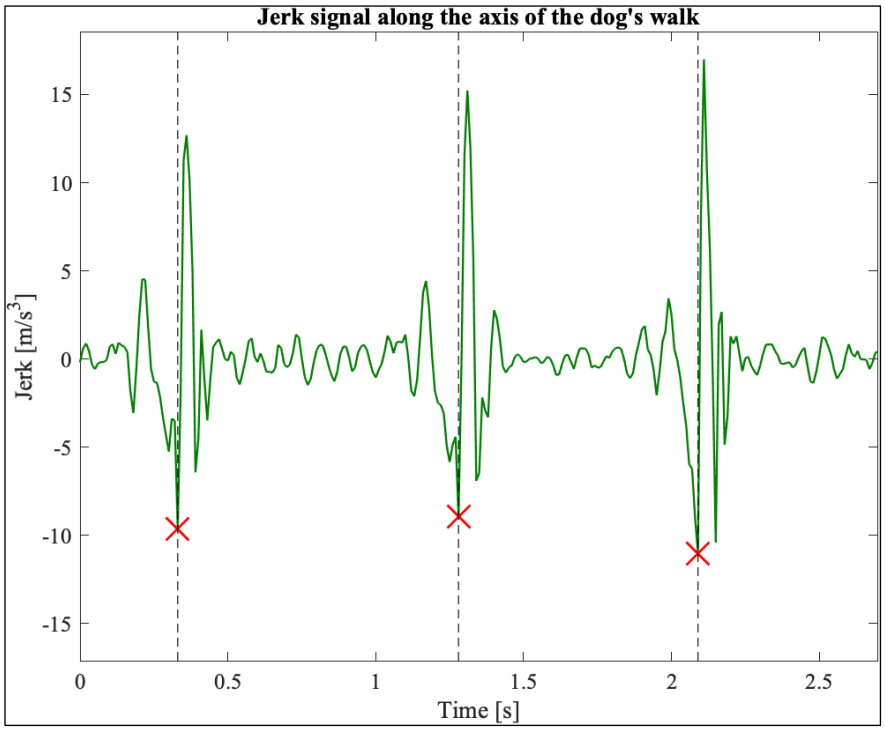

Figure 31. Three toe-touch events of the pelvic limb identified with a red cross on the first derivate of the acceleration signal (jerk) along the axis of the dog's walk.

Table 10 contains a summary of all methods introduced to detect toe-off and toe-touch of the thoracic and pelvic limbs. The results were presented following this table as a reference.

After selecting the most accurate methods, two custom function written in Matlab were developed to automatically locate the toe-off and the toe-touch for both thoracic and pelvic limbs (APPENDIX A).

Method	Limb	Detection	Parameter
1	Thoracic	Toe-off	Acceleration along the axis of the dog's walk
2	Thoracic	Toe-touch	Acceleration along the axis of the dog's walk *
3	Thoracic	Toe-touch	Acceleration along the axis of the dog's walk *
4	Thoracic	Toe-touch	Jerk along the axis of the dog's walk *
5	Thoracic	Toe-touch	Jerk along the axis of the dog's walk *
6	Thoracic	Toe-touch	Acceleration along vertical axis
7	Pelvic	Toe-off	Acceleration along vertical axis
8	Pelvic	Toe-off	Acceleration along the axis of the dog's walk
9	Pelvic	Toe-touch	Acceleration along the axis of the dog's walk
10	Pelvic	Toe-touch	Jerk along the axis of the dog's walk

Table 10. Methods for detecting toe-off and toe-touch of the thoracic and pelvic limbs. The '' highlights procedures that exploit the same graph to detect the same instant. In particular, Method 2 and Method 4 anticipate toe-touch of the thoracic limb compared to Method 3 and Method 5 respectively.*

Data returned by the IMU systems were also used to conduct an initial evaluation of canine joint angles. As for the validation trial on humans, 3D joint angles were calculated through a Matlab script, exploiting the accelerometers and magnetometers values to derive the quaternions and then the rotation matrixes. The positioning protocol of 10 IMU sensors (Table 9) allowed the elbow, knee and tarsal angles to be evaluated for both left and right limbs.

Camera-based system

Kinovea was used to identify the toe-touch and toe-off instants for later comparison against the IMU step detection (Figure 32). The video recordings were manually reviewed frame-by-frame to determine the timing of initial swing and initial stance for the strides of each legs in the selected time range. The initial swing was marked when the paw lost contact with the ground, while the initial stance was marked when the paw clearly regained contact with the ground. The process was independently repeated by both investigators to avoid user bias and ensure accuracy. In the case of any mismatch in the chosen frames for either toe-off or toe-touch, a mean of the two time values was taken.

The synchronization with the sensors was achieved adding to values obtained the temporal subtraction between the restart of the camera and the time zero. The initiation of the swing and

stance phases, as well as the calculated mean and standard deviation of swing, stance and stride times, were later compared to those found using the IMUs.

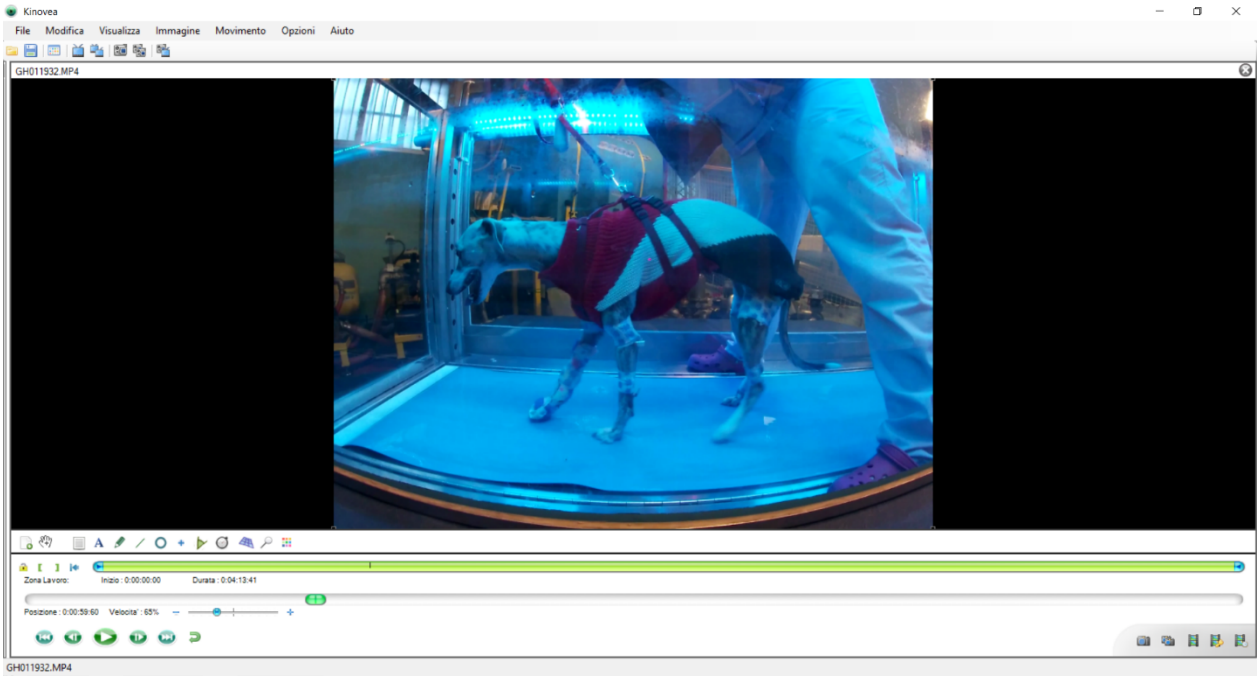

Figure 32. Graphical frontend of Kinovea.

Kinovea software was also used to compare the flexion-extension angular data obtained using IMU sensors. Two-dimensional angle was created on a single frame using the identification of 3 points: the first on the joint centre, the second and the third on the upper and lower body segments (Figure 33). These points can be tracked by the software to obtain the angular values of subsequent frames. The point-location was maintained automatically, but a manual correction was requested as the absence of reference markers caused software errors.

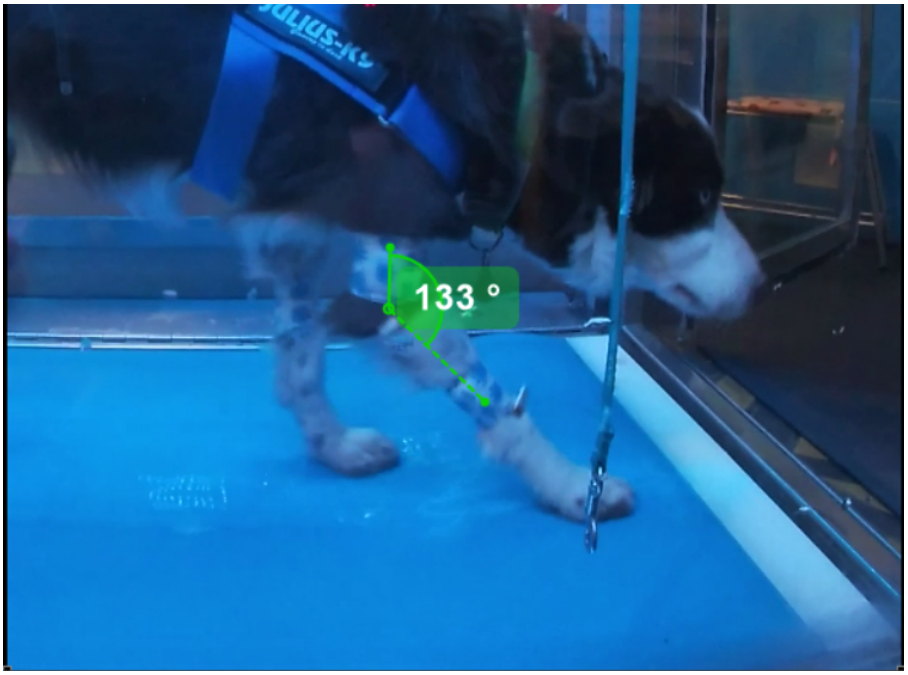

Figure 33. Angular evaluation on Kinovea.

4.4 Statistical analysis

The following statistical tools were used to evaluate the agreement between the various systems and methods for kinematic movement analysis.

4.4.1 Pearson's correlation coefficient

Person's correlation coefficient (r) evaluates the strength of the linear association between two continuous variables [54]. It gives information about the magnitude of the association as well as the direction of the correlation [55] by returning coefficient values between +1 to -1. A value of +1 indicates a perfect positive relationship, -1 reveals a perfect negative relationship and 0 implies no relationship. In Table 11 the Person's correlation coefficient values defining a strong, weak, or medium correlation are reported.

	Lower limit	Upper limit
Weak correlation	0	±0.29
Medium correlation	±0.30	±0.49
Strong correlation	±0.50	±1

Table 11. Pearson's correlation coefficient values defining a weak, medium, or strong correlation.

4.4.2 Bland-Altman plot

The Bland-Altman analysis visually and quantitatively evaluates the agreement between two methods assessing the same measurement to compare the reliability of a newly propped measurement method or system with the established gold standard [56].

Bland and Altman proposed a scatterplot in which the X-axis represented the average $\left(\frac{x_1-x_2}{2}\right)$ and the Y-axis represented the difference $(x_1 - x_2)$ of two measurements. The graph displays the average of the differences, also called bias $\left(\overline{b} = \sum_{i=1}^{n} \frac{d_i}{n}\right)$, and the 95% confidence interval ($CI = bias \pm 1.96\sigma$, where σ is the standard deviation of the differences). If the bias is significant and 0 is not included in its confidence interval, the innovative system commits measurement errors.

The Bland-Altman analysis does not only evaluate the ability of two systems to provide the same result, but also allows to understand if the differences between measurements are random or resulting from a systematic error. In fact, it can be assessed if the innovative system underestimates or overestimates the measurements.

4.4.3 Boxplots

Boxplots are a standardized way of displaying the distribution of data based on a five-number summary: median, first quartile (Q1), third quartile (Q3), minimum and the maximum (Figure 34) [57]. The median marks the mid-point of the data and is shown by the line that divides the box into two parts. While the first quartile is the middle number between the smallest number and the median of the dataset, the third quartile is the middle value between the median and the highest value. The interquartile range (IQR) is the boxplot showing the middle 50% of scores, while the upper and lower whiskers represent scores outside it. The minimum is calculated as $Q1 - 1.5\ IQR$, the maximum as $Q3 + 1.5\ IQR$.

Boxplots are useful as they provide a visual summary of the data enabling researchers to quickly identify average values, dispersion of the data set and signs of skewness.

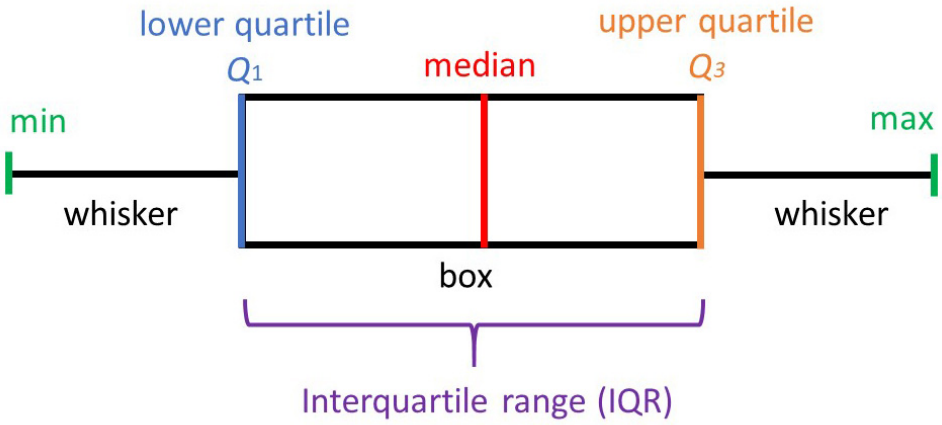

Figure 34. Different parts of a boxplot.

CHAPTER 5. RESULTS

The results obtained from this study and the statistical analysis conducted on them are provided in this chapter by first presenting the validation trials followed by the dog trials.

5.1 Validation trial

Reliability and accuracy of the proposed IMUs have been evaluated comparing their estimation of the knee angle with the one provided by the gold standard optoelectronic during squat execution (Figure 35 and Figure 36).

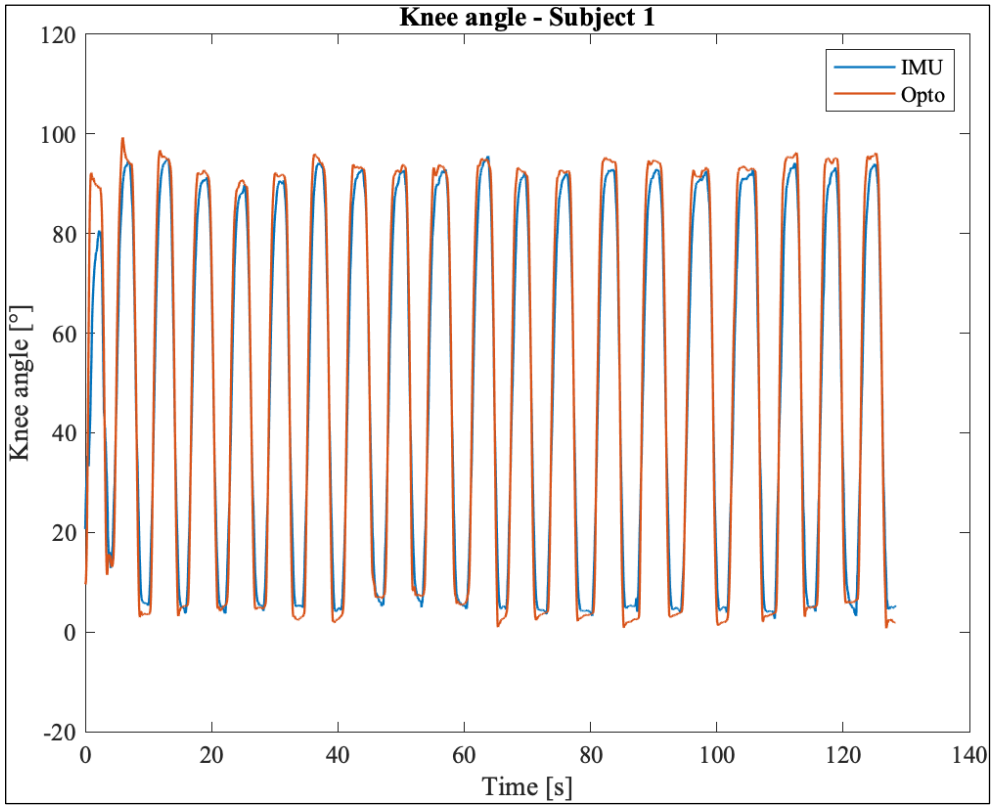

Figure 35. Knee angle (Subject 1). The red line indicates the angle obtained using the optoelectronic system, while the blue line using IMU sensors.

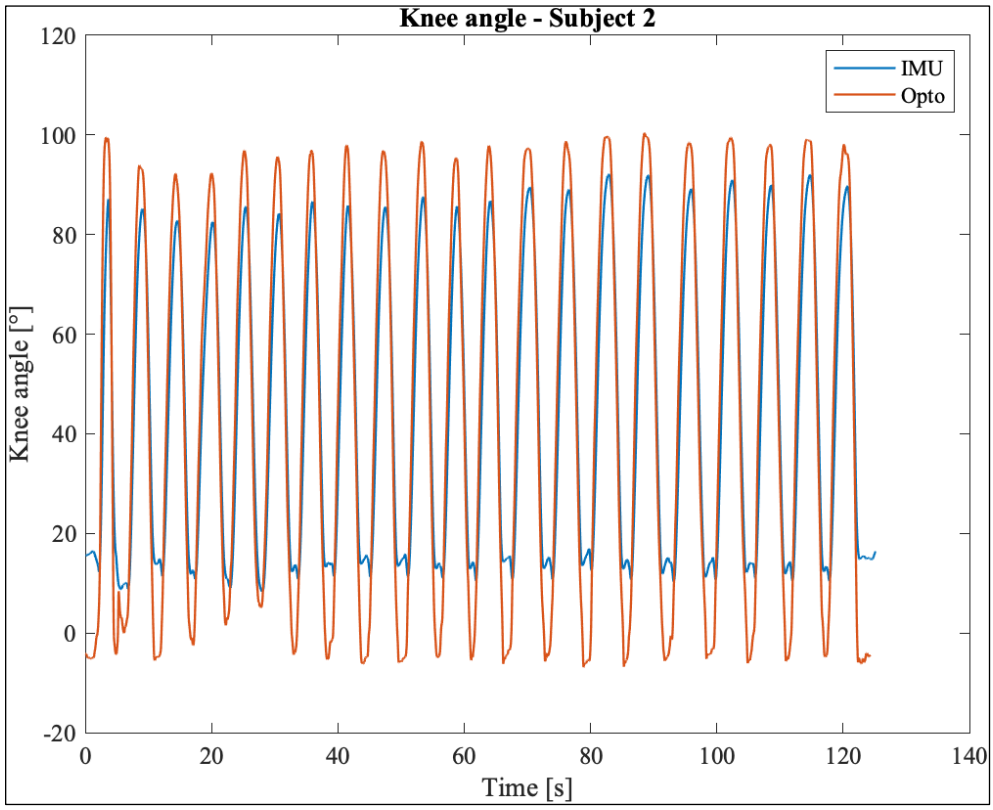

Figure 36. Knee angle (Subject 2). The red line indicates the angle obtained using the optoelectronic system, while the blue line using IMU sensors.

The first statistical tool used to evaluate the performance and trustworthiness of IMU sensors was the Pearson's correlation coefficient. Coefficient values calculated for the two tested subjects are shown in Table 12.

Subject	Pearson's correlation coefficient
1	0.989
2	0.947

Table 12. Pearson's correlation coefficient values of the tested subjects.

The comparison between the results obtained with the IMU sensors and the optoelectronic system was also investigated using the Bland-Altman plot. In Table 13 the values of bias, standard deviation and 95% confidence interval of the two tested subjects are reported, while Figure 37 and Figure 38 display the graphs.

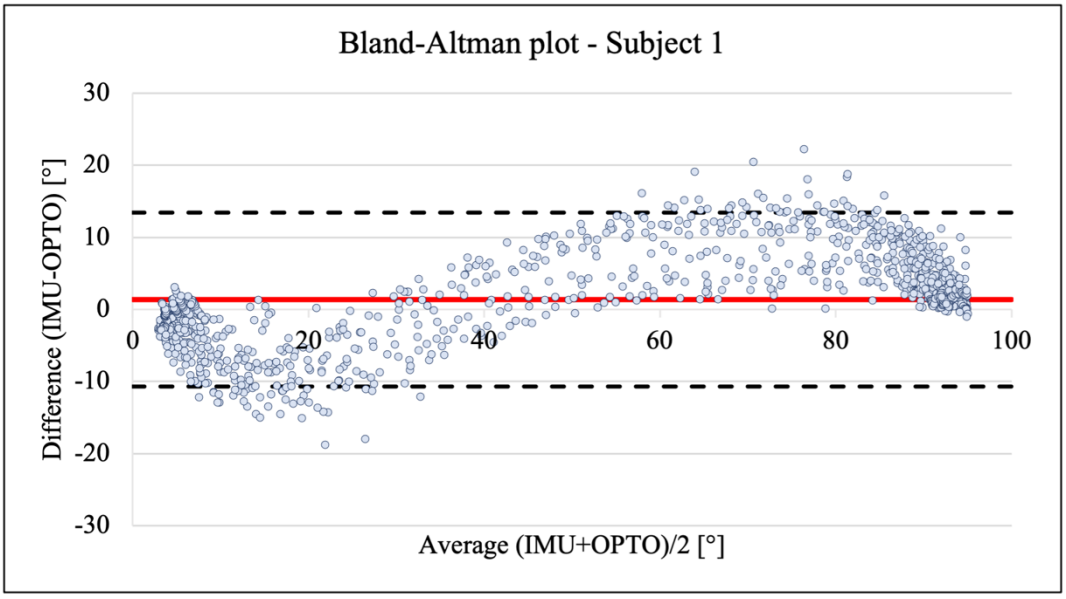

Figure 37. Bland-Altman plot (Subject 1). The X-axis indicates the average of the measurement (IMUi+OPTOi)/2, while the Y-axis their difference (IMUi-OPTOi). Red line: average bias. Black dotted lines: confidence interval.

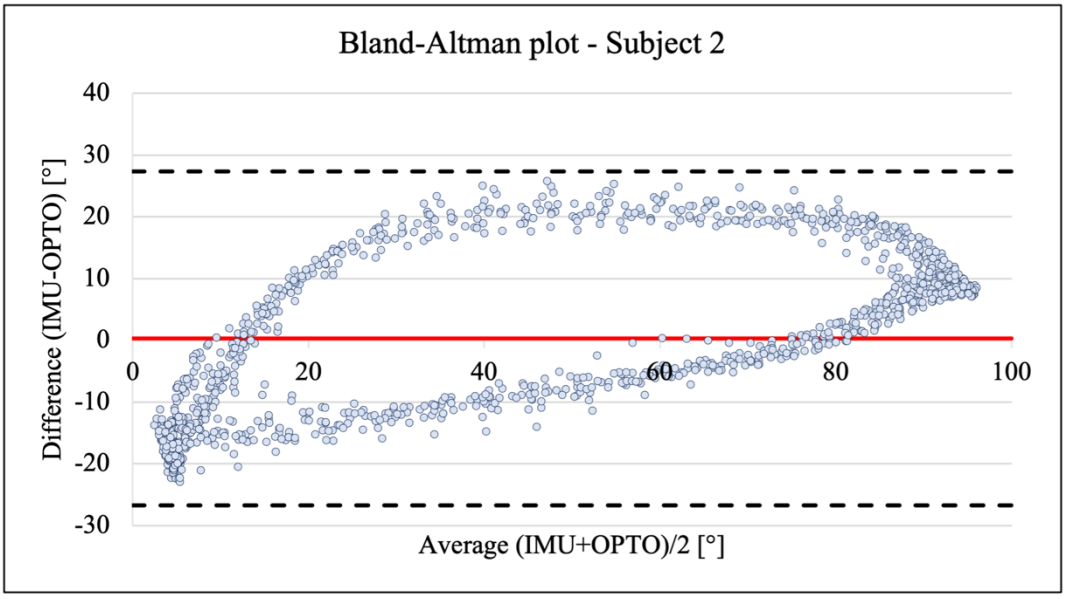

Figure 38. Bland-Altman plot (Subject 2). The X-axis indicates the average of the measurement (IMUi+OPTOi)/2, while the Y-axis their difference (IMUi-OPTOi). Red line: average bias. Black dotted lines: confidence interval.

Subject	Bias	σ	Lower 95% CI	Upper 95% CI
1	1.39°	6.15°	-10.67°	13.45°
2	0.29°	13.79°	-26.73°	27.31°

Table 13. Values of bias, standard deviation and 95% confidence interval of the two tested subjects.

5.2 Dog trials: step detection

A total of 1.232 strides were manually detected thought the video-analysis and each interpretation method of the IMU data. The multiple investigations are reported in the following sub-chapters.

5.2.1 Data interpretation

The first task involved the identification of two universal data interpretation strategies for the thoracic limbs and the pelvic limbs respectively. Boxplots were created to show the time differences between step values obtained with the camera-based system and the methods hypothesized for interpreting the data returned by the IMU sensors (from Figure 39 to Figure 42).

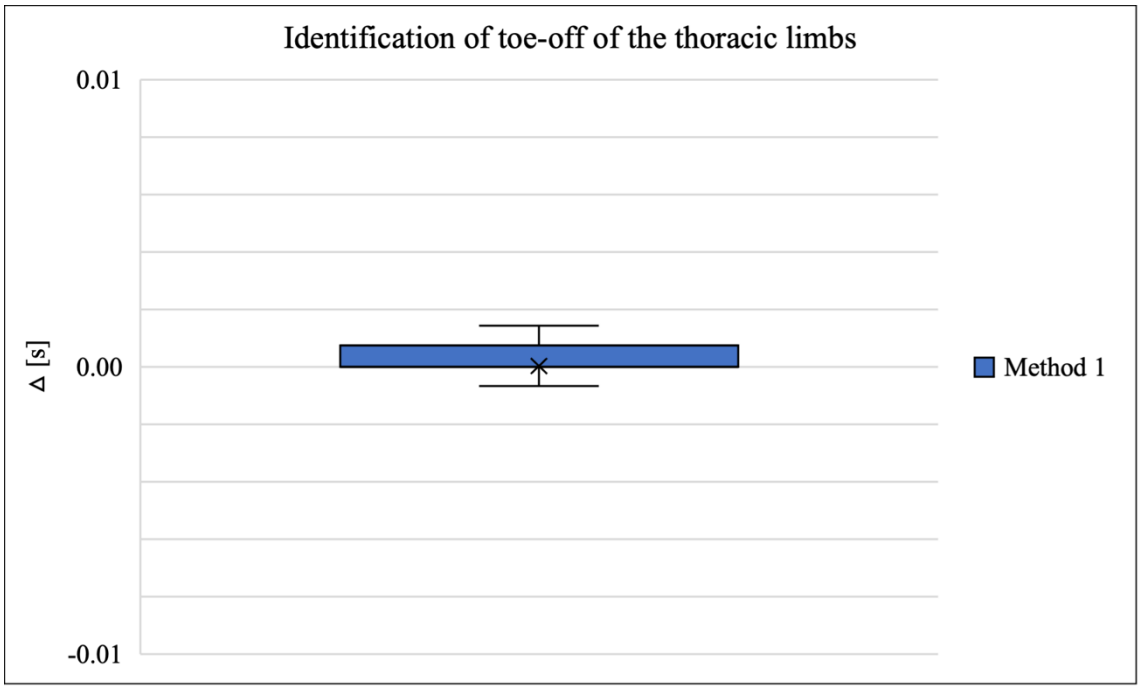

Figure 39. Identification of toe-off of the thoracic limbs. Method 1 detects toe-off using the graph of the acceleration signal along the axis of the dog's walk. The Y-axis indicates the difference between the time values obtained with the two measurement systems.

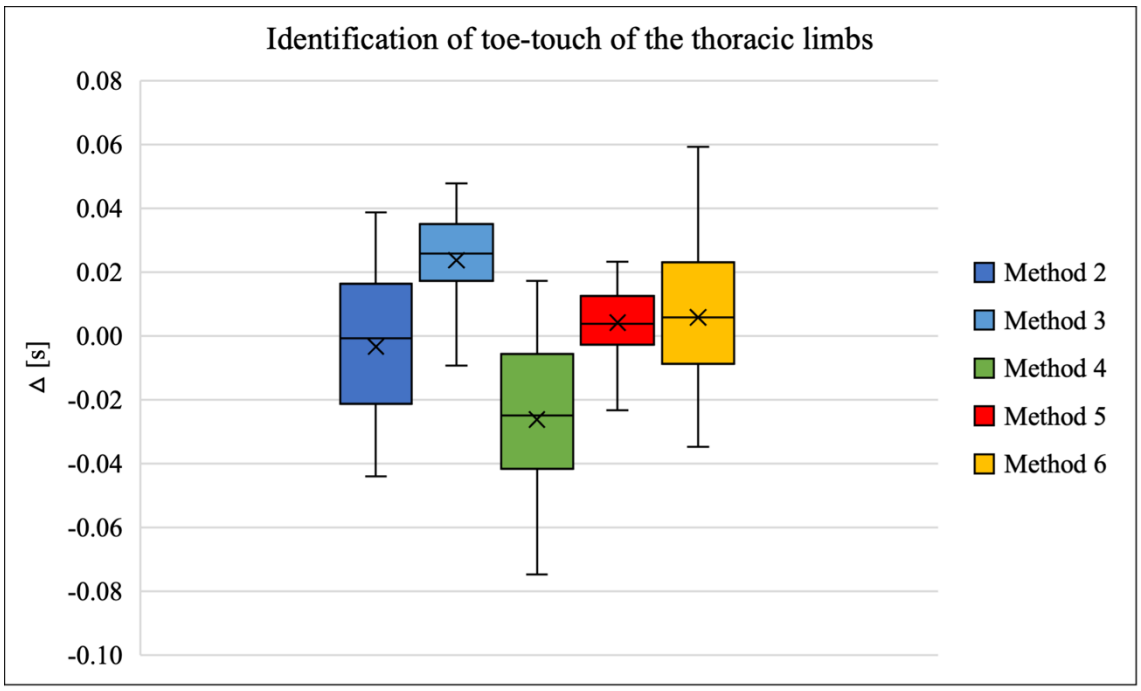

Figure 40. Identification of toe-touch of the thoracic limbs. Methods 2 and 3 detect toe-touch using the graph of the acceleration signal along the axis of the dog's walk, while methods 4 and 5 use the graph of the jerk in the same direction. In contrast, method 6 uses the graph of the acceleration along the vertical axis. The Y-axis indicates the difference between the time values obtained with the two measurement systems.

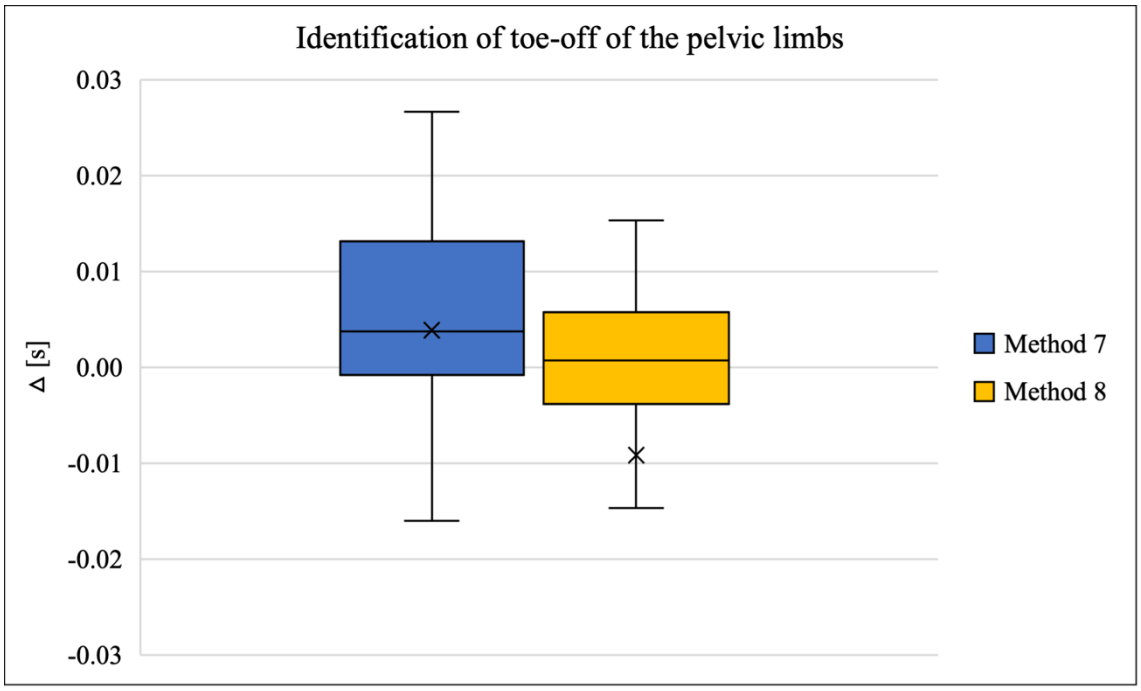

Figure 41. Identification of toe-off of the pelvic limbs. Method 7 detects toe-off using the graph of the acceleration along the vertical axis, while method 8 uses the graph of the acceleration signal along the axis of the dog's walk. Method 8 was not used for subjects 3, 4, and 5, as the points of interest were not clearly visible. The Y-axis indicates the difference between the time values obtained with the two measurement systems.

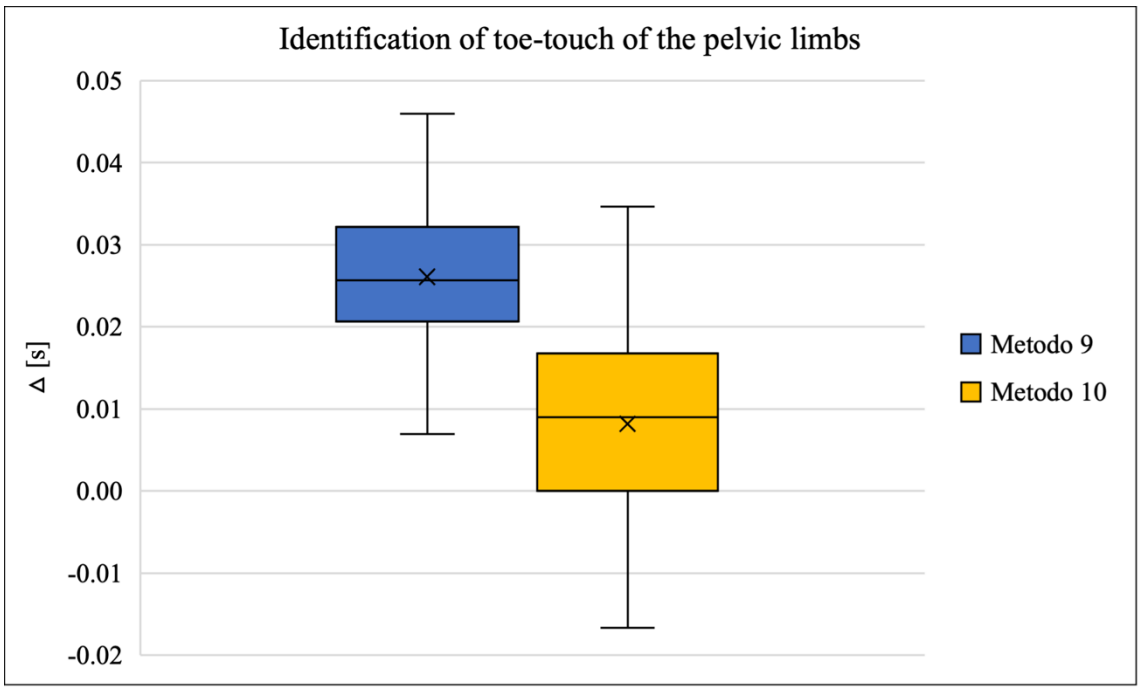

Figure 42. Identification of toe-touch of the pelvic limbs. Method 9 detects toe-touch using the graph of the acceleration signal along the axis of the dog's walk, while method 10 uses the graph of the jerk in the same direction. The Y-axis indicates the difference between the time values obtained with the two measurement systems.

5.2.2 Error distributions

The different methods selected for detecting toe-off and toe-touch of the thoracic and pelvic limbs were specifically investigated for each dog. From Figure 43 to Figure 51 the error distributions of the proposed approaches are reported for each subject both with and without orthosis for the pathological dogs. Error is measured as the difference between the time values obtained with IMU sensors and the camera-based system.

The analysis of the histograms was conducted by investigating three parameters: the most recurring error value (E_{max}), the percentage of the zero error ($\%E_0$) and the sum between the percentages of the most recurring error and errors indicated by the histograms on its sides ($\%E_{max\pm0.01}$). The last parameter allows the variability occurring between the two measurement systems to be established.

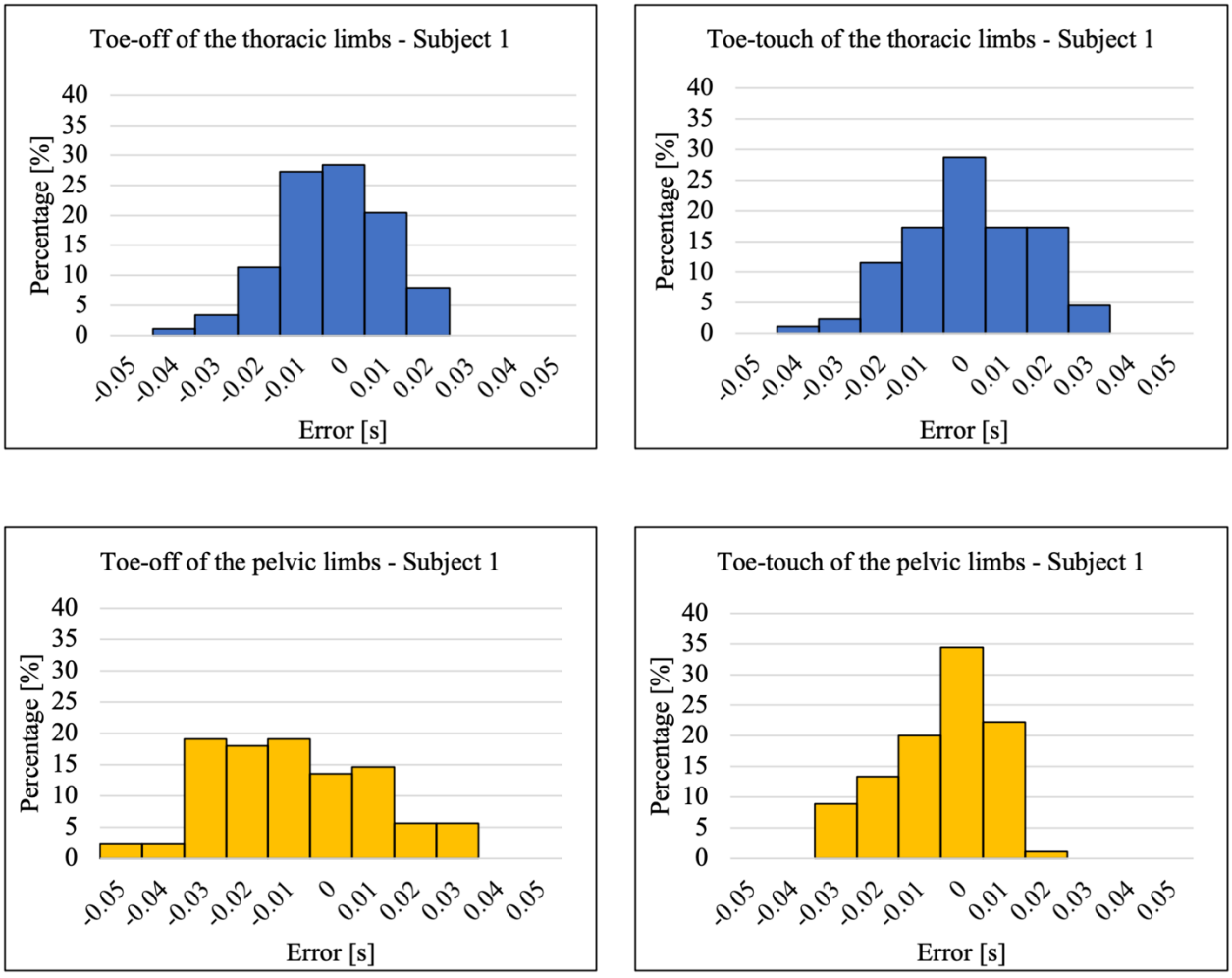

Figure 43. Error distributions (Subject 1). The X-axis indicates the difference between the time values obtained with the two measurement systems.

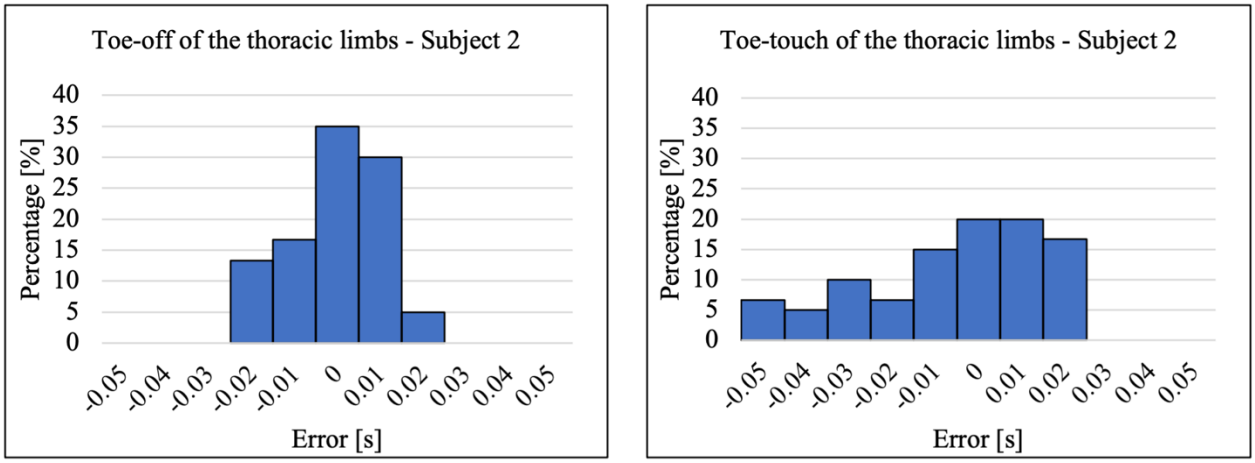

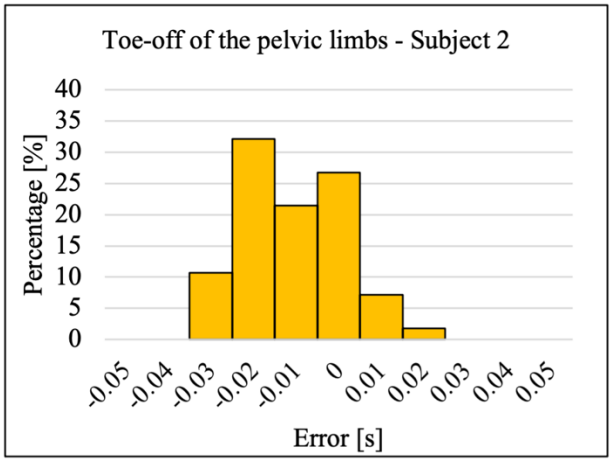

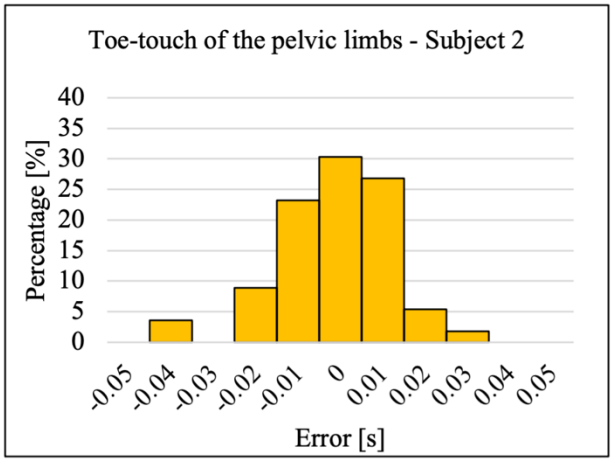

Figure 44. Error distributions (Subject 2). The X-axis indicates the difference between the time values obtained with the two measurement systems.

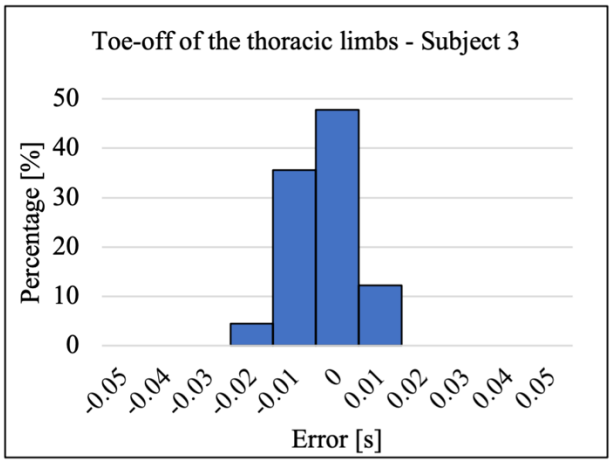

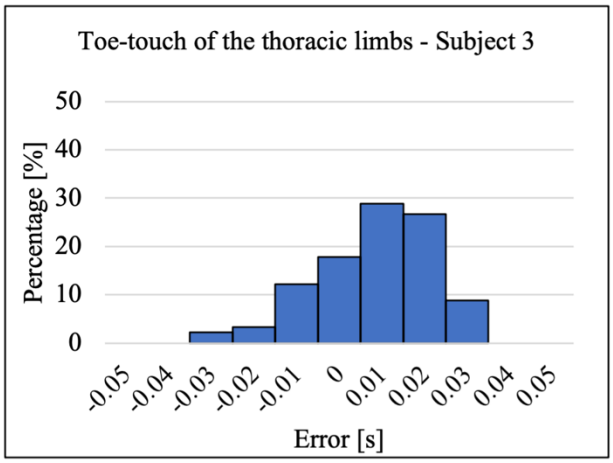

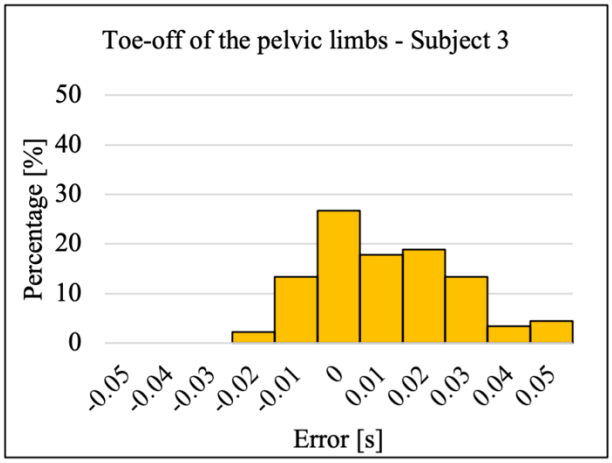

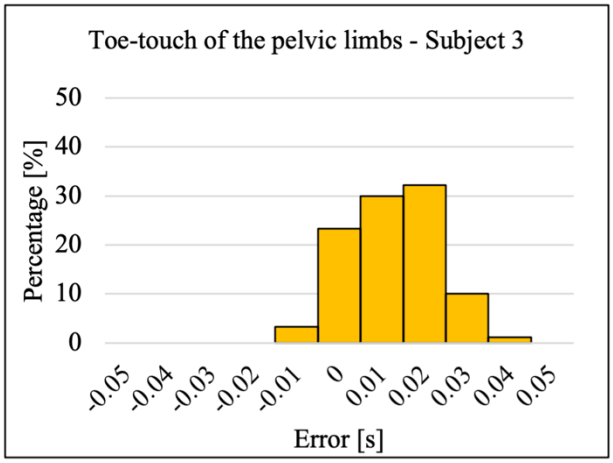

Figure 45. Error distributions (Subject 3). The X-axis indicates the difference between the time values obtained with the two measurement systems.

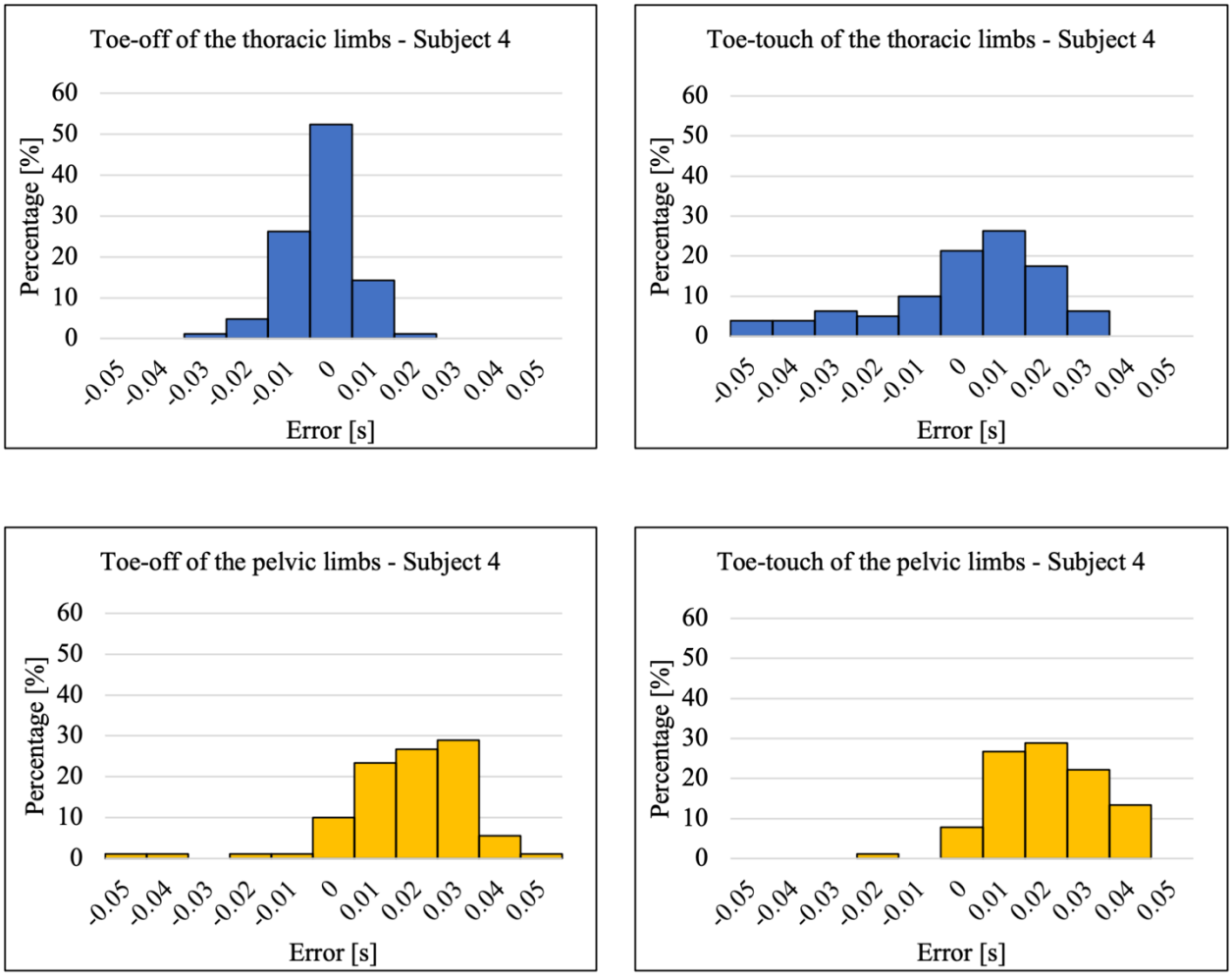

Figure 46. Error distributions (Subject 4). The X-axis indicates the difference between the time values obtained with the two measurement systems.

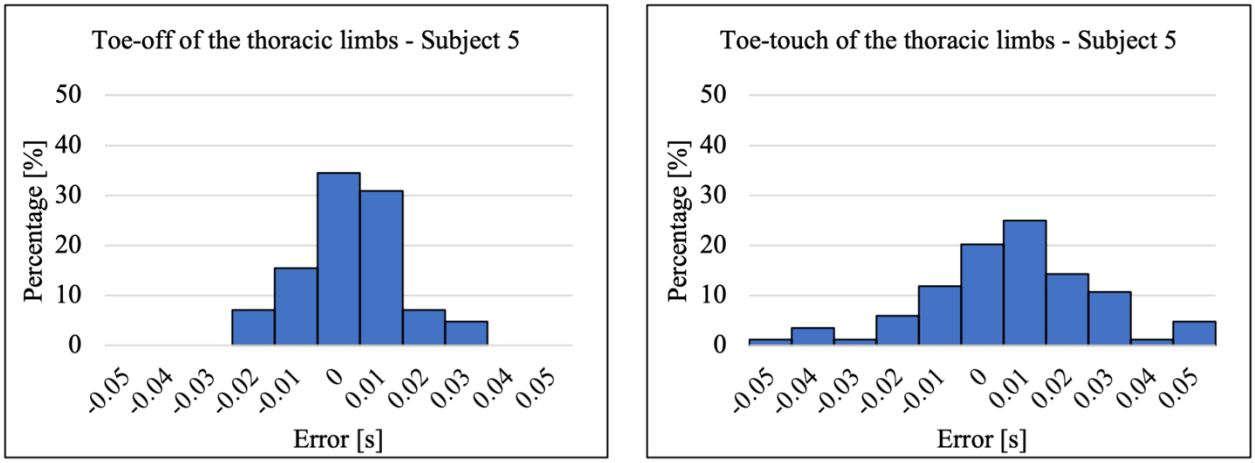

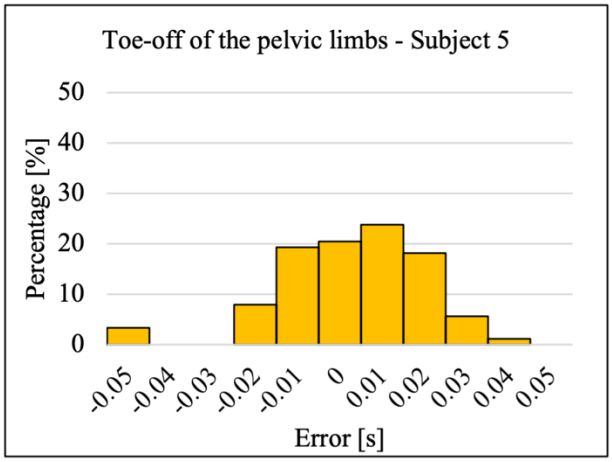

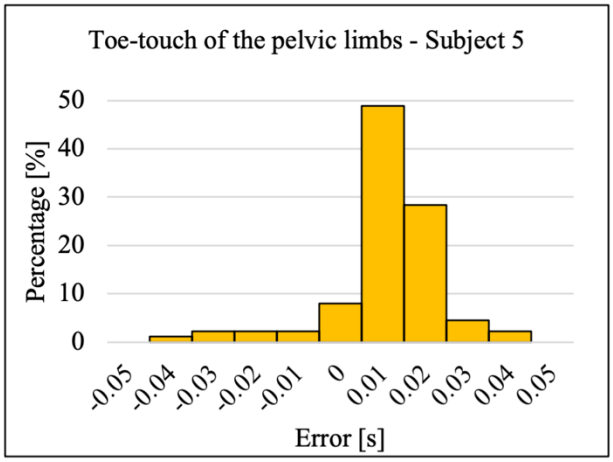

Figure 47. Error distributions (Subject 5). The X-axis indicates the difference between the time values obtained with the two measurement systems.

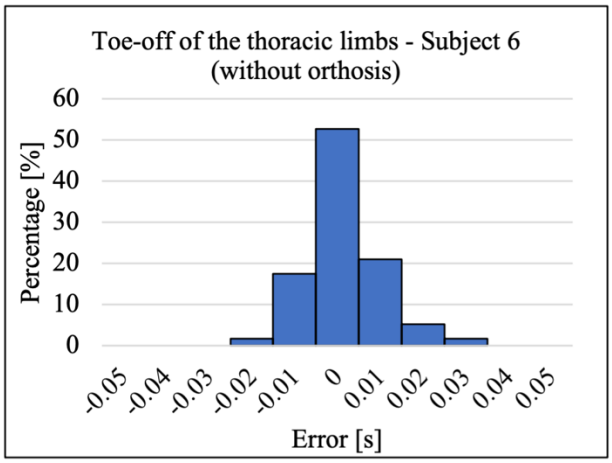

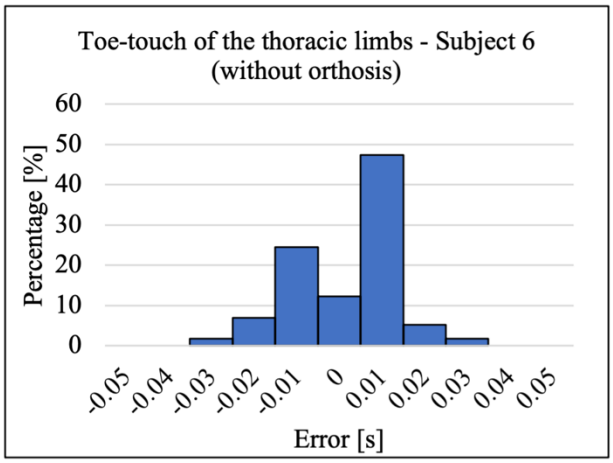

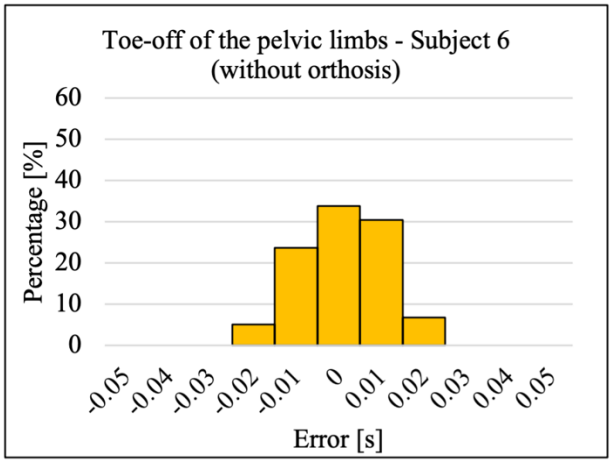

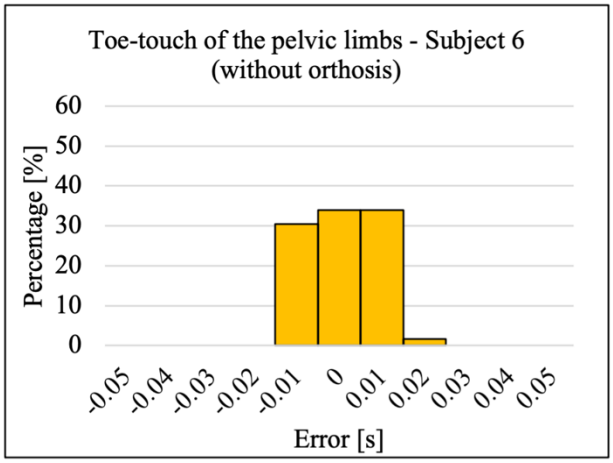

Figure 48. Error distributions (Subject 6 without orthosis). The X-axis indicates the difference between the time values obtained with the two measurement systems.

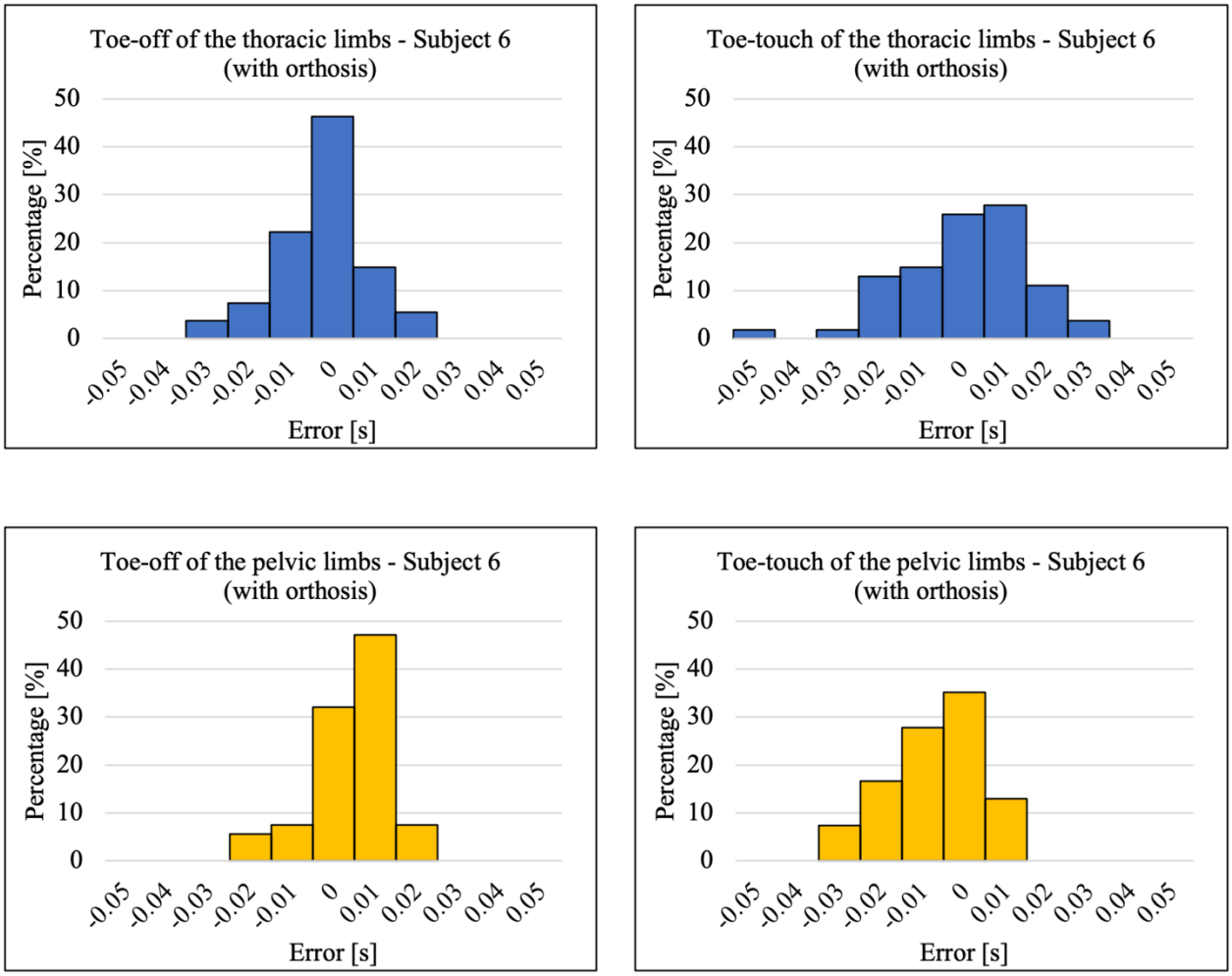

Figure 49. Error distributions (Subject 6 with orthosis). The X-axis indicates the difference between the time values obtained with the two measurement systems.

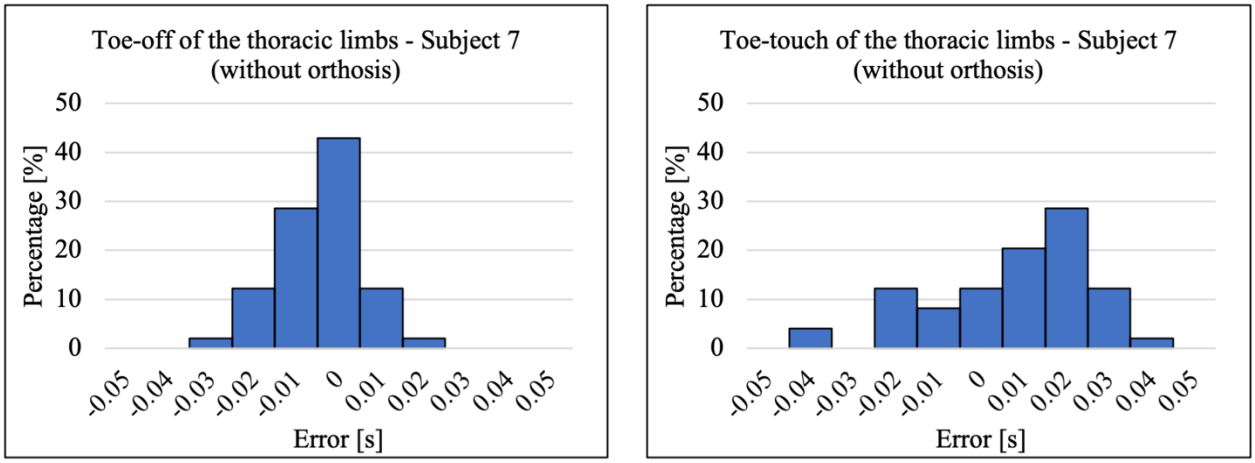

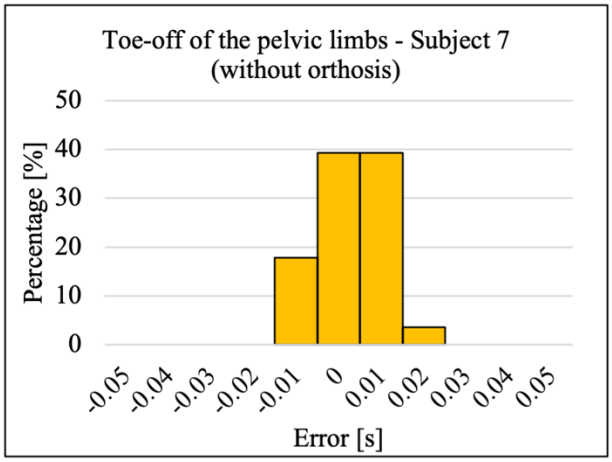

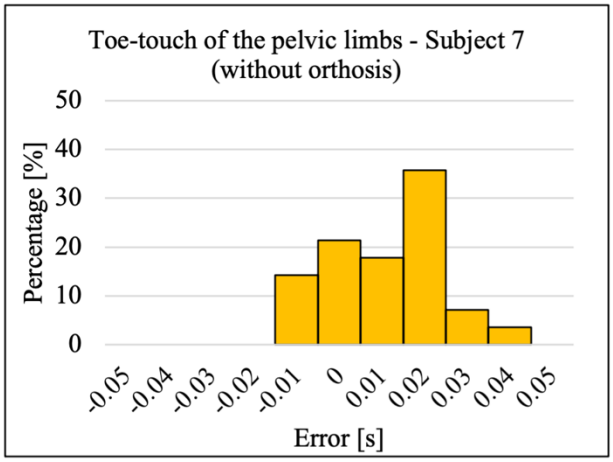

Figure 50. Error distributions (Subject 7 without orthosis). The X-axis indicates the difference between the time values obtained with the two measurement systems.

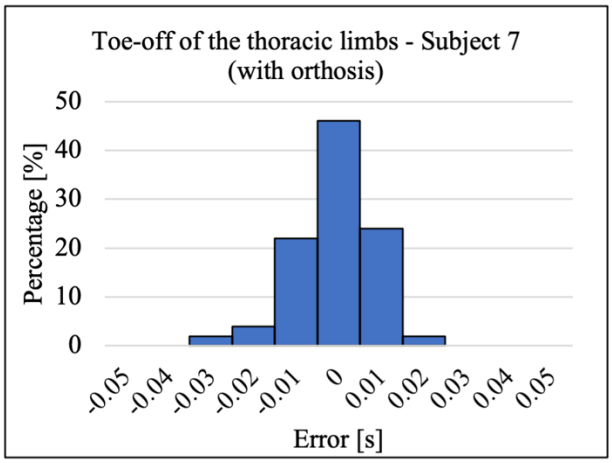

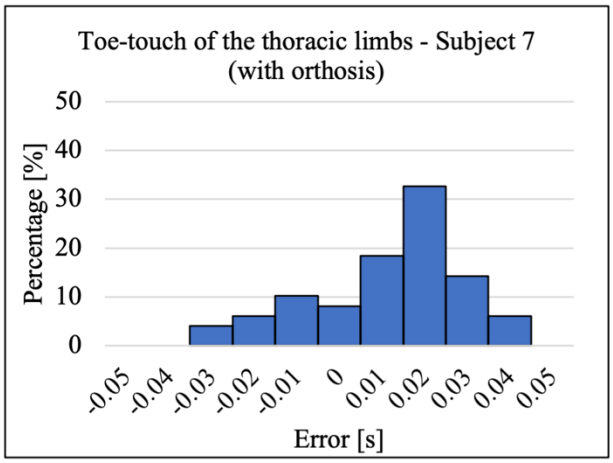

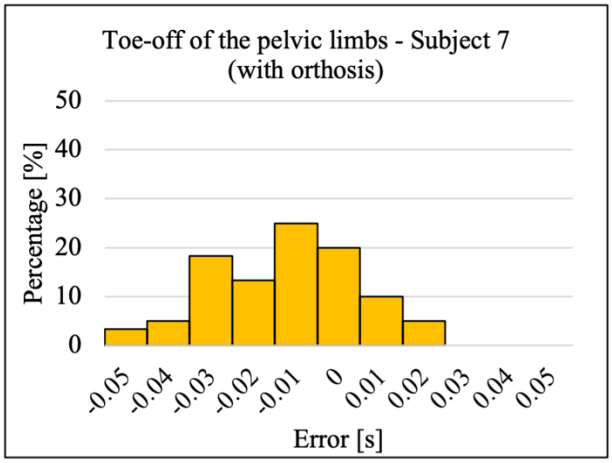

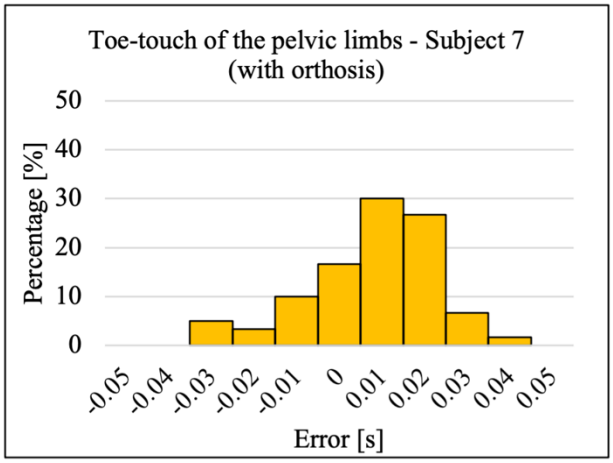

Figure 51. Error distributions (Subject 7 with orthosis). The X-axis indicates the difference between the time values obtained with the two measurement systems.

5.2.3 Swing time and stance time percentages

After estimating the stance time and swing time percentages over the gait cycle, their ratio was calculated (St/Sw). Two symmetry indices were created both to compare dogs with and without musculoskeletal diseases and to assess the reliability of orthoses. *Index 1* is the ratio of the right thoracic limb St/Sw to the left thoracic limb St/Sw $\left(Index\ 1 = \frac{(St/Sw)_{RT}}{(St/Sw)_{LT}}\right)$, while *Index 2* is obtained with the same procedure but considering the pelvic limbs $\left(Index\ 2 = \frac{(St/Sw)_{RP}}{(St/Sw)_{LP}}\right)$. Table 14 displays the St/Sw and the indices for each subject, while the rest of the results are reported in APPENDIX B.

	St/Sw RT	St/Sw LT	St/Sw RP	St/Sw LP	Index 1	Index 2
Subj 1						
1	3.72	3.46	3.26	3.98	1.07	0.82
2	3.12	2.89	2.79	2.98	1.08	0.93
3	2.38	2.69	2.73	2.86	0.88	0.95
Subj 2						
1	5.45	4.46	4.10	3.81	1.22	1.08
2	3.72	3.55	3.39	3.76	1.05	0.90
Subj 3						
1	3.18	3.76	2.61	4.95	0.85	0.53
2	3.24	3.00	2.94	3.26	1.08	0.90
3	2.86	2.55	2.60	2.88	1.12	0.90
Subj 4						
1	3.88	4.13	4.59	4.46	0.94	1.03
2	2.77	3.33	4.03	3.48	0.83	1.16
3	2.60	2.97	3.59	3.61	0.87	0.99
Subj 5						
1	2.56	3.12	3.72	4.18	0.82	0.89
2	2.92	3.07	3.13	2.73	0.95	1.15
3	3.02	2.62	3.17	2.76	1.15	1.15
Subj 6 (without orthosis)						
1	4.26	4.10	4.08	5.10	1.04	0.80
2	4.35	4.41	4.29	4.68	0.99	0.92
Subj 6 (with orthosis)						
1	4.52	3.17	3.15	4.13	1.43	0.76
2	5.13	3.85	3.88	4.56	1.33	0.85
Subj 7 (without orthosis)						
1	3.50	3.65	2.68	5.37	0.96	0.50
2	2.38	2.45	2.68	4.35	0.97	0.62
Subj 7 (with orthosis)						
1	2.64	3.07	2.36	3.69	0.86	0.64
2	2.05	2.77	2.47	3.33	0.74	0.74

Table 14. Ratios between the stance time and swing time percentages, Index 1 and Index 2 for all limbs of each test (R=right, L=left, T=thoracic, P=pelvic).

5.2.4 Accuracy of step detection codes

The accuracy of the two Matlab codes was calculated by comparing the values automatically and manually detected. Table 15 displays the accuracy percentages of both step detection codes for each dog.

Subject	Code 1 (toe-off)	Code 1 (toe-touch)	Code 2 (toe-off)	Code 2 (toe-touch)
1	100%	92.2%	96.7%	98.9%
2	96.7%	58.3%	100%	100%
3	100%	96.7%	98.9%	100%
4	100%	86.7%	98.9%	100%
5	98.9%	86.7%	95.6%	95.6%
6 (without orthosis)	100%	93.3%	100%	100%
6 (with orthosis)	96.7%	95.0%	98.3%	98.3%
7 (without orthosis)	98.3%	70.0%	100%	100%
7 (with orthosis)	98.3%	88.3%	100%	100%
$\bar{x}$	98.8%	85.2%	98.7%	99.2%

Table 15. Accuracy percentages of code 1 (thoracic limb) and code 2 (pelvic limb) for each dog. The last row shows the average values.

5.3 Dog trials: joint angles

A preliminary evaluation of canine joint angles returned by IMU sensors was conducted. As for the step detection, a camera-based system supported by Kinovea was used to obtain a comparison of the results. Two significant graphs of angular values obtained using the two measurement systems are reported in Figure 52 and Figure 53.

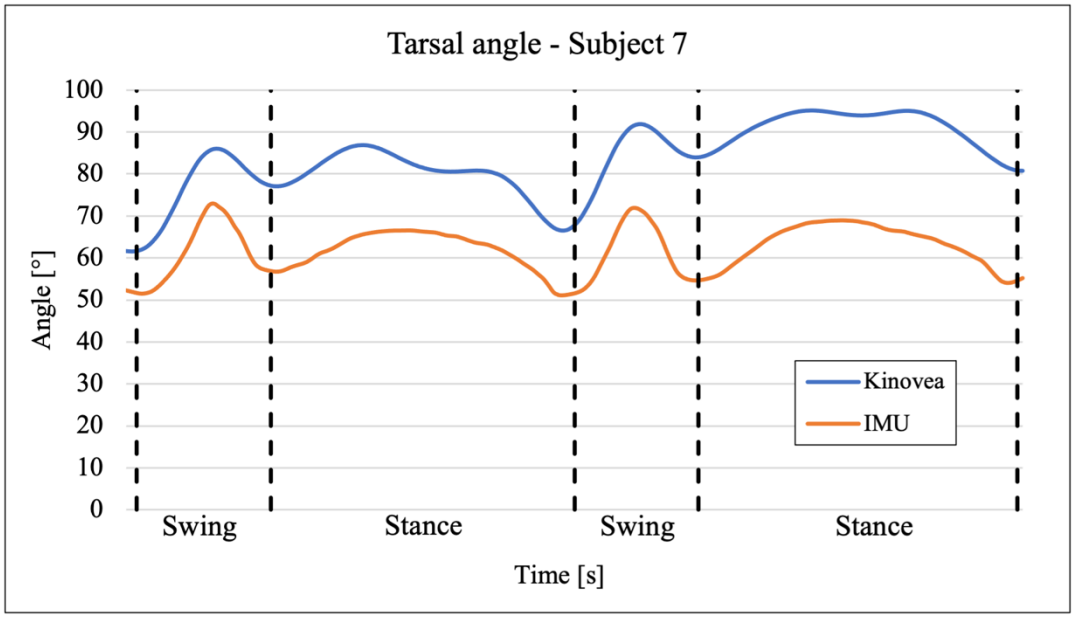

Figure 52. Left tarsal angular values of subject 7 obtained with the IMU sensors (orange line) and the camera-based system (blue line). The values of toe-off and toe-touch are represented as vertical dashed lines.

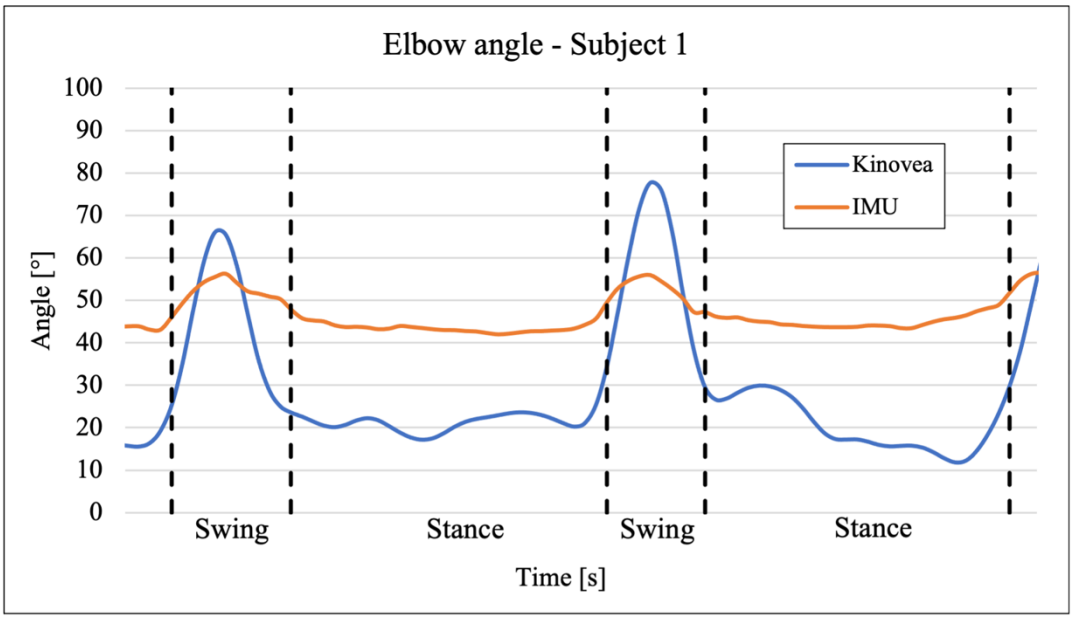

Figure 53. Left elbow angular values of subject 1 obtained with IMU sensors (orange line) and the camera-based system (blue line). The values of toe-off and toe-touch are represented as vertical dashed lines.

CHAPTER 6. DISCUSSION

The discussion was set up following the same structure of the results considering firstly the validation trial and later the dog tests.

6.1 Validation trial

The Pearson's correlation coefficients obtained between the knee angles returned by the IMU sensors and the optoelectronic system prove satisfactory for both subjects. As with other similar studies [58] [59], coefficient values are extremely close to 1 (Table 12), indicating a strong positive relationship between the two measurements.

The accuracy of the sensors is also confirmed by the Bland-Altman plots in Figure 37 and Figure 38. Considering the standard deviation, the two subjects present slightly different values, also affecting the confidence intervals ($CI = bias \pm 1.96\sigma$). However, the intervals include the 0 value in both cases giving an evidence of the reliability of the IMU system. Moreover, the bias obtained as average of the differences are between 0° and 2° for both subjects, providing how IMU sensors do not significantly overestimate or underestimate the results returned by the optoelectronic system.

6.2 Dog trials: step detection

6.2.1 Data interpretation

The thoracic limb was the first to be investigated since a protocol had already been validated by Jenkins et al. [40]. Toe-off of the thoracic limb was the only time instant not requiring the comparison of multiple detection strategies: the instant the paw leaves the ground was identified by a distinguishable peak in the acceleration signal along the axis of the dog's walk. The excellent affinity obtained by Jenkins between the IMU sensors and the camera-based system was confirmed, returning a mean error ± standard deviation of 0.00 ± 0.01 s.

Since the guideline offered by Jenkins for the detection of toe-touch of the thoracic limb was unclear and hardly applicable to the graphs returned by IMU sensors, five other different methods were hypothesized and compared with each other. The effectiveness and efficiency of the investigation strategies can be estimated observing the boxplot in Figure 40. To ensure acceptable results, the method box should be located near the 0 that attests null difference with respect to the

camera-based system. Moreover, the difference between the third and first quartile (IQR) should be as small as possible expressing the dispersion of the data. Considering these criteria, *Method 5* was identified as the most accurate to detect toe-touch of the thoracic limb: a valley in the graph of the jerk signal along the axis of the dog's walk identifies the start of the stance phase. This approach also improved Jenkins' results by reducing the mean error ± standard deviation between the two measurement systems from -0.01 ± 0.03 to 0.00 ± 0.02 s.

Step detection investigation of the pelvic limb could not rely on any previous study as no protocol was found. To detect toe-off, *Method 7* and *Method 8* were compared using the boxplot in Figure 41. Although *Method 8* may seem the most accurate one with the median closer to 0 value and a lower IQR, other aspects must also be considered. The average value ("x" in the graph) returned by *Method 8* is not internal to the IQR but is shifted below close to -0.01, indicating that the values between the first quartile and the minimum are very concentrated at the bottom. Moreover, the acceleration signal along the axis of the dog's walk used in this method was not viable for subjects 3, 4 and 5, as the instants the paw leaves the ground were not clearly visible. For all these reasons the toe-off of the pelvic limb was universally identified as a peak on the graph of acceleration in the vertical direction (*Method 7*).

To detect toe-touch of the pelvic limb, *Method 9* and *Method 10* were also compared. The boxplot in Figure 42 shows how the jerk signal investigated with *Method 10* returns a lower time difference between the two measurement systems, indicating it as the best approach.

Table 16 displays the methods selected to detect toe-off and toe-touch of the thoracic and pelvic limbs.

Method	Limb	Detection	Graph
1	Thoracic	Toe-off	Acceleration signal along the axis of dog's walk
5	Thoracic	Toe-touch	Jerk signal along the axis of dog's walk
7	Pelvic	Toe-off	Acceleration signal along the vertical axis
10	Pelvic	Toe-touch	Jerk signal along the axis of dog's walk

Table 16. Selected methods to detect toe-off and toe-touch of the thoracic and pelvic limbs.

6.2.2 Error distribution

The error distributions of the selected strategies highlight some analogies within the same method and peculiarities related to a single dog.

Method 1 has the lowest variability among the selected strategies with a $\%E_{max\pm0.01}$ between 76% and 95%. E_{max} is 0 for all subjects and its percentage ($\%E_0$) between 28% and 52% highlights the high accuracy in detecting toe-off of the thoracic limb. In contrast, *Method 5* postpones the toe-touch of the thoracic limb for many subjects. A good example is offered by subject 7, showing a E_{max} of 0.02 s both with and without orthosis and a $\%E_0$ between 8% and 12% (Figure 50 and Figure 51). Additionally, a $\%E_{max\pm0.01}$ around 60% indicated a greater error variability than in the previous case.

Considering the pelvic limbs, the method identifying toe-touch (*Method 10*) proved to be more precise and less variable than the one detecting toe-off (*Method 7*). Although *Method 10* sometimes postpones the time instant, for four trials E_{max} is 0 with values of the $\%E_0$ around 33%. Furthermore, a low variability was recorded for all subjects, indicating a good adaptability of the method to any dog. Meanwhile, *Method 7* anticipates or postpones the toe-off depending on the dog tested: E_{max} is -0.02 s for subject 1 (Figure 43) and 2 (Figure 44), while for subject 4 E_{max} is 0.03 s (Figure 46). This variability between subjects negatively influences the evaluation of the reliability of the selected method.

6.2.3 Swing time and stance time percentages

The stance time (St) and swing time (Sw) percentages of the gait cycle were calculated for all limbs of each dog and the results were converted into the ratio St/Sw (Table 14).

As with humans, the gait cycle phase in which the paw maintains contact with the ground depends on the treadmill velocity. In most of the experiments conducted, the increase in velocity caused a reduction in the stance time and consequently in St/Sw. This phenomenon did not always occur due to the variability introduced by the time window selection and the low velocity variation between trials. An example is given by the right thoracic limb of subject 5, where an increase in stance time is recorded as velocity increases. By neglecting these outsiders, the ratio of percentages can be considered indirectly proportional to the velocity set on the treadmill.

In contrast, the stance time and swing time percentages could not be directly used to draw a comparison between healthy and pathological subjects since dogs of different breeds and

anatomical structures were tested. The classifications discussed in Chapter 2.3 could have been used to compare the percentages of dogs belonging to the same group, but this strategy was not suitable for the study. In fact, one of the dogs with motor dysfunctions (subject 7) would have formed a group by itself not allowing a correlation with a healthy one. To conduct a universal analysis not depending on dog breeds, a first symmetry index between the two thoracic limbs (*Index 1*) and a second one between the two pelvic limbs (*Index 2*) were created. Since the ratio St/Sw of right and left limbs should coincide for a healthy dog of any breed, both indices should be close to 1. This statement was confirmed in our study, where the average of *Indices 1* and the average of *Indices 2* of the five healthy dogs are 0.99 and 0.96 respectively.

Specific observations can also be made for the two dogs with musculoskeletal disorders. Subject 6 without orthosis returns indices close to 1, as the absence of a phalanx probably does not affect the dog's gait. In contrast, once the orthosis is applied, a decrease in symmetry between the two thoracic limbs occurs and an *Index 1* of 1.43 and 1.33 is returned. The asymmetry could be connected to the structure of the paw orthosis, which completely envelops the right thoracic limb, raising it from the ground by a few centimeters. This difference in height causes a decrease in stance time of the contralateral limb, which is conditioned to remain in contact with the ground for less time. Although the orthosis improves the support of the limb without phalanx, a more detailed analysis of the consequences should be conducted.

The different motor dysfunction and type of orthosis did not lead to the same conclusions for subject 7. The partial rupture of the Achilles tendon did not allow the dog to walk correctly without orthosis creating a strong asymmetry between the two pelvic limbs: for the two trials an *Index 2* of 0.50 and 0.62 was recorded. In this case the situation enhances with the application of the tarsal joint orthosis which increases the *Index 2* to 0.64 and 0.74 respectively. Nevertheless, the improvement is limited by an increase in asymmetry between the two thoracic limbs. The benefits of the orthosis are indisputable, but some analysis should be conducted to understand if the device can negatively affect the thoracic limbs.

6.2.4 Accuracy of the step detection codes

Toe-off of the thoracic and pelvic limbs is identified with an accuracy greater than 98%, while toe-touch of the pelvic limb is correctly detected more than 99% of the time. The lowest percentage is recorded for toe-touch of the thoracic limb: the time instant identified by the code corresponds to the manually selected one for approximately 85%. The increase in error is connected to subjects 2 and 7, which returned unique and singular graphs due to their different structure and size compared to other dogs. Removing these two subjects from the analysis, the code detects the instant the thoracic paw touches the ground with an accuracy of 92%.

6.3 Dog trials: joint angles

The tarsal angles of subject 7 returned by the IMU sensors and Kinovea (Figure 52) display a similar pattern and range during the gait cycle, but a bias of 15° is identified between the two measurement systems. It could be assumed that the sensors followed the movement of the body segments, but incorrect positioning of the IMUs affected the angular values. A different example is reported in Figure 53, which shows the elbow angle of subject 1. Although the angular variation during the swing phase is recorded by both measurement systems, the angular range obtained with the sensors (15°) is much lower than the one achieved with Kinovea (45°). Moreover, the angular values returned by the IMUs are overestimated during the stance phase. Sensor errors could be related to the specific positioning adopted for the IMUs above the elbow. While the IMUs measuring the tarsal angle of subject 7 were maintained close to their respective center of mass by the circumferential bandage system, this practice was not suitable for the sensor placed between the shoulder and elbow of subject 1. The sensor above the elbow descended close to the joint due to the large muscular mass surrounding the humerus, preventing the detection of movement of the upper part of thoracic limb and measuring a reduced angular displacement.

To ensure a correct evaluation of the cause of errors, other tests must be conducted with the comparison of a validated system. The results obtained from the videos with the support of Kinovea should be considered less reliable than the ones achieved for step detection. To identify the steps of each limb with a single camera, the videos were recorded by imposing a small angulation with respect to the treadmill, which often did not allow the joint angles to be evaluated correctly. Moreover, no markers were used to identify the anatomical landmarks, making the angle

construction using Kinovea inaccurate. The camera-based system offers a first trusted comparison with sensors, but any evaluation must be considered a simple hypothesis.

6.4 Study limitations

This study presented some limitations and for each of them a solution was proposed as possible future development.

The search for canine subjects to be tested turned out to be quite complex due to the COVID-19 pandemic and the experimental set up including a treadmill suitable for dogs limited the possibility of conducting experiments outside the clinical setting. Only 7 dogs without any selections of age, breed or clinical background were found. Since it was not possible to test both a healthy and a pathological dog of the same breed, the evaluation of canine orthoses was limited and only general considerations on the symmetry between limbs were conducted. Future studies should involve a bigger population and be more focused on a specific breed to directly compare kinematic values between healthy and pathological dogs.

Considering the experimental set up, many aspects could have negatively influenced the results. Although the treadmill is indispensable for maintaining a constant velocity, it could be the cause of improper gait. All the dogs tested had never walked on it before and the familiarization time may have been too short. Additionally, an excessively high or low velocity could alter the correct gait, resulting in an irregularity between the limbs. In future studies treadmill adaptation tests should be introduced before starting the trials, allowing a velocity setting based only on the dog's anatomy and size.

The bandage system is another limiting aspect for the results of this study. A slippage of some sensors towards the joint centers was reported during trials, especially with those attached around the humerus and femur, interfering with gait and angular acquisition. The evaluation of joint angles would not have been reliable anyway, as the bandage did not allow the orientation of the sensors to be controlled after placement. The development of a better IMU fixing system should be the purpose of the subsequent studies, involving for example full body suits or specialized "socks" that constrain sensor orientation and positioning.

The sensor design also showed some weaknesses. Although the limited dimension and weight of the sensor were congenial for our tests, the external battery increased the fragility of the IMUs. After a cycle of trials, two of the ten sensors stopped working due to the breakage of the power

cable connecting the sensor to the battery. To solve this problem, new sensors with the battery inside the unit have already been produced and are available for future analyses.

Finally, the comparison between the angular data obtained using IMU sensors and Kinovea exhibited low accuracy. To ensure a correct validation of the experimental set up of the IMU sensors, a comparison with the gold standard should also be conducted on dogs, considering Bertocci's study as a starting point [37].

CHAPTER 7. CONCLUSION

Canine orthoses are artificial devices that provide protected motion within a controlled range, prevent or reduce the severity of an injury, allow lax ligaments and joint capsules to approach normal distensibility, and provide functional stability for an unstable limb segment. These medical devices can be a good solution for many patients that are not good surgical candidates, because of advanced animal age, perceived increased anesthetic risk or circumstances requiring a delay of surgery. Although canine orthoses are becoming more and more widespread, an objective method to evaluate their efficacy has not yet been proposed. Accordingly, the aim of this thesis was to develop a protocol involving Inertial Measurement Units to evaluate the movement of dogs with and without orthoses.

The IMU sensors used in this study were designed and manufactured by the Centre for Biorobotics of Tallin University of Technology (Tallin, Estonia). Since the sensors were prototypes, the system needed to be validated before the dog tests were executed. Consequently, preliminary trials on humans were performed and the external knee angles of two healthy subjects were investigated and compared using the IMU sensors and an optoelectronic system. The Pearson's correlation coefficients prove satisfactory for both subjects since their values are close to 1, indicating a strong positive relationship between the two measurements. The accuracy of the sensors was also confirmed by the Bland-Altman plots, returning biases close to 0 and acceptable confidence intervals.

After successfully completing the validation trials, the IMUs were used to investigate animals in motion. The sensors were tested on five healthy dogs and two suffering from musculoskeletal disorders both with and without orthoses. The protocol involved the use of 10 IMUs, 2 for each thoracic limb and 3 for each pelvic limb, which were placed on dogs with paper tape and cohesive bandages. Moreover, a specific canine rehabilitation treadmill was used to enforce a constant velocity and a standardized walk during the tests. Since the application of IMU sensors is under development in the canine kinematics evaluation field, a high-speed camera-based system was employed as support in the clinical setting to corroborate the data acquired. Actually, an optoelectronic system would have been preferred, but it was unavailable in the dog testing facility and the one in the "Luigi Divieti Laboratory of Posture and Movement Analysis" could not be used due to COVID-19 pandemic.

To evaluate canine kinematics, the analysis focused on step detection. The first task involved the identification of universal strategies to detect toe-off and toe-touch of the thoracic and pelvic limbs using the IMUs. Different methods were hypothesized and compared by searching for the minimum difference between the time instants returned by the sensors and the camera-based system. After selecting the most accurate approaches, two custom functions written in Matlab were developed to automate the detection, and their excellent accuracy (95%) will allow the application also in future studies. Subsequently, the percentages of stance time and swing time were calculated for all subjects and two symmetry indices were created to compare healthy dogs with pathological ones. Only for one of the two subjects with motor dysfunctions an asymmetry was recorded. In this case, the application of the orthosis brought improvements identified by a 30% reduction in the difference between the St/Sw of the pathological limb and the contralateral one. Nevertheless, the orthosis also appeared to cause a decrease in initial symmetry on the other side of the antero-posterior plane. Since the study is strongly conditioned by the limited number of tested subjects and the absence of healthy and pathological dogs belonging to the same breed, further analyses should be conducted to reinforce these claims.

After step detection, a preliminary assessment of the joint angles estimated by the sensors was performed. The graph patterns returned by the IMUs and the camera-based system displayed an acceptable correlation, but the angular range obtained with the sensors was often lower. The problem could be related to the IMU positioning, which requires an improvement of the protocol. Furthermore, a comparison with the gold standard should also be conducted on canine tests, ensuring a correct validation of the experimental set up of the sensors. By optimizing these aspects, the joint angles could be investigated to evaluate the functioning of the orthoses.

In conclusion, this study fulfilled its purpose providing a universal method for assessing the movement of dogs with and without orthoses. The application of IMU sensors could represent an opportunity to obtain a quantitative evaluation of the canine kinematics, highlighting any musculoskeletal pathologies. Starting from the protocol afforded by this research, an investigation into the efficacy and efficiency of canine orthoses could be conducted, certifying the benefits and possible limitations associated with these medical devices.

APPENDIX A

A.1 Synchronization

The following Matlab function was written to synchronize the sensors, exploiting a great acceleration in the vertical direction caused by the hit.

Synchro.m

```
function [Synchro_Data]= Synchro(Raw_Data,n_sensor,n_Data)

for j=1:n_sensor

    % Initialization of the cycle
    M=Raw_Data(1,7+13*(j-1));

    % Time identification of the hit (ts) recognizing with a
    % decreasing of vertical acceleration below percentage
    % threshold of the average of the previous values
    for i=2:length(Raw_Data(:,1))
        M(i)=mean(Raw_Data(1:i,7+13*(j-1)));
        Threshold=0.7;
        if RawDataData(i,7+13*(j-1))<M(i-1)*Threshold
            pos(j)= i;
            break
        end
    end
end

% Identification of the first sensor switched on (Max_pos)
Max_pos=max(pos);

% Inizialisation of the Syncro_Data matrix
Synchro_Data=ones(n_Data-Max_pos,9*n);

% Creation of the Syncro_Data matrix with the time expressed in
% seconds and the accelerometers, gyroscopes and magnatometers
% values

for j=1:n_sensor
    Synchro_Data(:,1+9*(j-1):3+9*(j-1))=Raw_Data(pos(j):pos(j)+
    n_Data-Max_pos-1,(5+13*(j-1):7+13*(j-1)));
    Synchro_Data(:,4+9*(j-1):6+9*(j-1))=Raw_Data(pos(j):pos(j)+
    n_Data-Max_pos-1,(8+13*(j-1):10+13*(j-1)));
    Synchro_Data(:,7+9*(j-1):9+9*(j-1))=Raw_Data(pos(j):pos(j)+
```

```
    n_Data-Max_pos-1,(11+13*(j-1):13+13*(j-1)));
end

T=[0.01:0.01:(v-Max_pos)*0.01]';
Synchro_Data=[T Synchro_Data];
```

A.2 Step detection of the thoracic limbs

The following Matlab codes identified toe-off and toe-touch events of the thoracic limbs with *Method 1* and *Method 5* respectively.

Thoracic_Step.m

```
function[toe_off,toe_touch]=Thoracic_Step(AccX,T1,T2)

% Research of all the peaks on the graph
[PKS,LOCP]=findpeaks(AccX(T1:T2),T1:T2);

toe_off_temp=[];

% Calculating the average of the highest n_peaks to build a
% threshold
n_peaks=15;
max_peaks=maxk(PKS,n_peaks);
threshold=mean(max_peaks);

% Identification of the first toe_off event
for i=5:length(PKS)

    %  The peak must be over half of the threshold
    if PKS(i)>threshold*(0.5)

        % The 70% of the peak must be greater than the 4 previous
        % peaks
        if PKS(i)*0.7>PKS(i-1) && PKS(i)*0.7>PKS(i-2) &&
           PKS(i)*0.7>PKS(i-3) && PKS(i)*0.7>PKS(i-4)

            % Control if the next peak is greater and close to
              the "i" peak
            if PKS(i)<PKS(i+1)
                Mean=mean(AccX(LOCP(i): LOCP(i+1)));
                if PKS(i)<Mean
                    toe_off_temp=[toe_off_temp LOCP(i+1)];
                    LOCP1=i+2;
                else
                    toe_off_temp=[toe_off_temp LOCP(i)];
```

```
                    LOCP1=i+1;
                end
            else
                toe_off_temp=[toe_off_temp LOCP(i)];
                LOCP1=i+1;
            end
            break
        end
    end
end

% Identification of the other toe_off events
for i=LOCP1:length(PKS)
    if PKS(i)>3
        if PKS(i)*0.7>PKS(i-1) && PKS(i)*0.7>PKS(i-2) &&
           PKS(i)*0.7>PKS(i-3) && PKS(i)*0.7>PKS(i-4)
            if LOCP(i)-(toe_off_temp(end))>LOCP(i)-LOCP(i-4)
                if PKS(i)<PKS(i+1)
                    Mean=mean(AccX(LOCP(i)+(T1-1): LOCP(i+1)));
                    if PKS(i)<Mean
                        toe_off_temp=[toe_off_temp LOCP(i+1)];
                    else
                        toe_off_temp=[toe_off_temp LOCP(i)];
                    end
                else
                    toe_off_temp=[toe_off_temp LOCP(i)];
                end
            end
        end
    end
end

% Average time calculation between two toe_off events
Sum=0;
for i=2:length(toe_off_temp)
    Sum=Sum+(toe_off_temp(i)-toe_off_temp(i-1));
end

Mean=Sum/length(toe_off_temp);
toe_off=[toe_off_temp(1)];

% Exclusion of the false toe_off events that identify too short
time window
for i=2:length(toe_off_temp)
    if toe_off_temp(i)-toe_off(end)>Mean*0.6
        toe_off=[toe_off toe_off_temp(i)];
    end
```

```
end
% Identification of the toe_touch within two toe_off events
toe_touch_accx=[];
for i=2:length(toe_off)
    VLS=[];
    LOCV=[];

    % Identification of the valleys
    [VLS,LOCV]=findpeaks(-AccX(toe_off(i-1):toe_off(i)),
    toe_off(i-1):toe_off(i));
    VLS=-VLS;

    % Initialization of the valleys
    if VLS(1)>VLS(2)
        min=VLS(2);
        sec_min=VLS(1);
        min_Loc=LOCV(2);
        sec_min_Loc=LOCV(1);
    else
        min=VLS(1);
        sec_min=VLS(2);
        min_Loc=LOCV(1);
        sec_min_Loc=LOCV(2);
    end

    % Research of the two lowest valleys in the fist 45% of
    % the window
    for n=3:length(VLS)
        if LOCV(n)>toe_off(i-1)+(toe_off(i)-toe_off(i-1))*(0.45)
            break
        end
        if VLS(n)<min
            sec_min=min;
            sec_min_Loc=min_Loc;
            min=VLS(n);
            min_Loc=LOCV(n);
        elseif VLS(n)<sec_min
            sec_min=VLS(n);
            sec_min_Loc=LOCV(n);
        end

    end

    % Identification of the correct valley
    if sec_min>min*0.3
        toe_touch_accx=[toe_touch_accx min_Loc];
    else
```

```
        if min_Loc>sec_min_Loc
            toe_touch_accx=[toe_touch_accx min_Loc];
        else
            toe_touch_accx=[toe_touch_accx sec_min_Loc];
        end
    end
end

% Identification of toe_touch events in the derivative of
% the acceleration
toe_touch=[];
dAccX=diff(AccX);
for i=1:length(toe_touch_accx)
    for k=1:10
       if dAccX(toe_touch_accx(i)-k)<dAccX(toe_touch_accx(i)) &&
          dAccX(toe_touch_accx(i)-k)<dAccX(toe_touch_accx(i)-k-1)
           toe_touch=[toe_touch toe_touch_accx(i)-k];
           break
       end
    end
end
```

Thoracic_Step_Script.m

```
clear all
clc

load ('RightThoracic.mat')
load ('LeftThoracic.mat')

n_sensor=2;  % Number of sensors
tpp=1;  % Possible time exclusion in case of disturbances
A=[length(RightThoracic(1:end,1)),length(LeftThoracic(1:end,1))];
length_1=min(A);
Raw_Data=[RigthThoracic(tpp:length_1,1:13),
LeftThoracic(tpp:length_1,1:13)];
n_Data=length(Raw_Data);
Synchro_Data=Synchro(Raw_Data,n_sensor,n_Data);

% Savitzky-Golay Filtering
Synchro_Data(:,2)=sgolayfilt(Synchro_Data(:,2),3,7);
Synchro_Data(:,11)=sgolayfilt(Synchro_Data(:,11),3,7);

AccXdx=Synchro_Data(:,2);  % Right thoracic limb acceleration X
T1dx=159810;  % Right thoracic limb first time interval
T2dx=161260;  % Right thoracic limb second time interval
```

```
% Alignment of the graph to zero
Sumdx=sum(AccXdx(T1dx:T2dx));
Meandx=Sumdx/length(AccXdx(T1dx:T2dx));
AccXdx(T1dx:T2dx)=AccXdx(T1dx:T2dx)-Meandx;

% Step detection
[inizio_swingdx,inizio_stancedx]=StepAnteriori(AccXdx,T1dx,T2dx);

AccXsx=Synchro_Data(:,11)*(-1);  % Left thoracic limb
                                 % acceleration X
T1sx=159750;  % Left thoracic limb first time interval
T2sx=161340;  % Left thoracic limb second time interval

% Alignment of the graph to zero
Sumsx=sum(AccXsx(T1sx:T2sx));
Meansx=Sumsx/length(AccXsx(T1sx:T2sx));
AccXsx(T1sx:T2sx)=AccXsx(T1sx:T2sx)-Meansx;

% Step detection
[inizio_swingsx,inizio_stancesx]=StepAnteriori(AccXsx,T1sx,T2sx);
```

A.3 Step detection of the pelvic limbs

The following Matlab codes identified toe-off and toe-touch events of the pelvic limbs with *Method 7* and *Method 10* respectively.

Pelvic_Step.m

```
function[toe_touch,toe_off]=Pelvic_Step(AccX,AccY,T1,T2)

% Research of all the valleys (as peaks of the reverse graph)
[VLS,LOCV]=findpeaks(-AccX(T1:T2),T1:T2);

toe_touch_temp1=[];
toe_touch_temp2=[];
toe_touch_temp3=[];
toe_touch_temp4=[];
toe_touch=[];
dAccX=diff(AccX);

% Calculating the average of the highest n_peaks to build a
% threshold
n_peaks=15;
max_peaks=maxk(VLS,n_peaks);
threshold=mean(max_peaks);
```

```
% Identification of the toe_touch events
for i=5:length(VLS)-1

    %  The peak must be over half of the threshold
    if VLS(i)>threshold*(0.5)

        % Control if the next peak is greater and
        % close to the "i" peak
        if VLS(i+1)>VLS(i)*(0.6)
            toe_touch_temp1=[toe_touch_temp1 LOCV(i+1)];
        else
            toe_touch_temp1=[toe_touch_temp1 LOCV(i)];
        end
    end
end

% Neglecting repeating values
for i=1:length(toe_touch_temp1)-1
    if toe_touch_temp1(i)~=toe_touch_temp1(i+1)
        toe_touch_temp2=[toe_touch_temp2 toe_touch_temp1(i)];
    end
end

% Average time calculation between two possible toe_touch events
Sum=0;
for i=2:length(toe_touch_temp2)
    Sum=Sum+(toe_touch_temp2(i)-toe_touch_temp2(i-1));
end

Mean=Sum/length(toe_touch_temp2);

% Exclusion of the false toe_touch events
for i=1:length(toe_touch_temp2)-1
    if toe_touch_temp2(i+1)-toe_touch_temp2(i)>Mean*0.4 ||
       toe_touch_temp2(i)>toe_touch_temp2(i+1)
        toe_touch_temp3=[toe_touch_temp3 toe_touch_temp2(i)];
    end
end

toe_touch_temp4=[toe_touch_temp3(1)];

for i=2:length(toe_touch_temp3)
    if toe_touch_temp3(i)-toe_touch_temp3(i-1)>Mean*0.4
        toe_touch_temp4=[toe_touch_temp4 toe_touch_temp3(i)];
    end
end
```

```
% Calculating the average after the corrections
Sum=0;
for i=2:length(toe_touch_temp4)
    Sum=Sum+(toe_touch_temp4(i)-toe_touch_temp4(i-1));
end

Mean=Sum/length(toe_touch_temp4);

% Identification of the valley not found with the previous cycles
k=1;
m=10;
for i=1:length(toe_touch_temp4)+m
    if k==length(toe_touch_temp4)-1
        break
    end
    Delta1=floor((toe_touch_temp4(k+1)-toe_touch_temp4(k))*0.2);
    if toe_touch_temp4(k+1)-toe_touch_temp4(k)>Mean*1.5
        [Min,Min_loc]=min(AccX(toe_touch_temp4(k)+
        Delta1:toe_touch_temp4(k+1)-Delta1));
        toe_touch_temp4=[toe_touch_temp4(1:k)
        (Min_loc+toe_touch_temp4(k)+Delta1-1)
toe_touch_temp4(k+1:end)];
    else
        k=k+1;
    end
end

% Identification of toe_touch events in the derivative of the
acceleration
for i=1:length(toe_touch_temp4)
    for k=1:10
        if dAccX(toe_touch_temp4(i)-k)<dAccX(toe_touch_temp4(i))
           && dAccX(toe_touch_temp4(i)-
k)<dAccX(toe_touch_temp4(i)-k-1)
            toe_touch=[toe_touch toe_touch_temp4(i)-k];
            break
        end
    end
end

% Identification of the toe_off within of the 60% aand 90% of the
time
% window between two toe_touch events
toe_off=[];

for i=2:length(toe_touch)
```

```
    PKSY=[];
    LOCPY=[];
    Delta2=floor((toe_touch(i)-toe_touch(i-1))*(0.60));
    Delta3=floor((toe_touch(i)-toe_touch(i-1))*(0.90));
    [PKSY,LOCPY]=findpeaks(AccY((toe_touch(i-1)+Delta2):
    (toe_touch(i-1)+Delta3)),(toe_touch(i-1)+Delta2):
    (toe_touch(i-1)+Delta3));
    [Max,Max_loc]=max(PKSY);
    toe_off=[toe_off LOCPY(Max_loc)];
end
```

Pelvic_Step_Script.m

```
clear all
clc

load('RightPelvic.mat')
load('LeftPelvic.mat')

n_sensor=2;  % Number of sensors
tpp=1;  % Possible time exclusion in case of disturbances
A=[length(RightPelvic(1:end,1)),length(LeftPelvic(1:end,1))];
length_1=min(A);
Raw_Data=[RightPelvic(tpp:length_1,1:13),
LeftPelvic(tpp:length_1,1:13)];
n_Data=length(Raw_Data);
Synchro_Data=Synchro(Raw_Data,n_sensor,n_Data);

% Savitzky-Golay Filtering
Synchro_Data(:,2)=sgolayfilt(Synchro_Data(:,2),3,7);
Synchro_Data(:,3)=sgolayfilt(Synchro_Data(:,3),3,7);
Synchro_Data(:,11)=sgolayfilt(Synchro_Data(:,11),3,7);
Synchro_Data(:,12)=sgolayfilt(Synchro_Data(:,12),3,7);

AccXdx=Synchro_Data(:,2);  % Right pelvic limb acceleration X
AccYdx=Synchro_Data(:,3);  % Right pelvic limb acceleration Y
T1dx=151070;  % Right pelvic limb first time interval
T2dx=152530;  % Right pelvic limb second time interval

% Alignment of the graph to zero
SumXdx=sum(AccXdx(T1dx:T2dx));
MeanXdx=SumXdx/length(AccXdx(T1dx:T2dx));
AccXdx(T1dx:T2dx)=AccXdx(T1dx:T2dx)-MeanXdx;

% Alignment of the graph to g
SumYdx=sum(AccYdx(T1dx:T2dx));
MeanYdx=SumYdx/length(AccYdx(T1dx:T2dx));
```

```
AccYdx(T1dx:T2dx)=AccYdx(T1dx:T2dx)-MeanYdx+9.81;
% Step detection
[inizio_stancedx,inizio_swingdx]=StepPosteriori(AccXdx,AccYdx,T1d
x,T2dx);

AccXsx=Synchro_Data(:,11)*(-1);  % Left pelvic limb acceleration
X
AccYsx=Synchro_Data(:,12);  % Left pelvic limb acceleration Y
T1sx=151140;  % Left pelvic limb first time interval
T2sx=152600;  % Left pelvic limb second time interval

% Alignment of the graph to zero
SumXsx=sum(AccXsx(T1sx:T2sx));
MeanXsx=SumXsx/length(AccXsx(T1sx:T2sx));
AccXsx(T1sx:T2sx)=AccXsx(T1sx:T2sx)-MeanXsx;

% Alignment of the graph to g
SumYsx=sum(AccYsx(T1sx:T2sx));
MeanYsx=SumYsx/length(AccYsx(T1sx:T2sx));
AccYsx(T1sx:T2sx)=AccYsx(T1sx:T2sx)-MeanYsx+9.81;

% Step detection
[inizio_stancesx,inizio_swingsx]=StepPosteriori(AccXsx,AccYsx,T1s
x,T2sx);
```

A.4 Angular evaluation

The following Matlab code was written by Cecilia Monoli, allowing the joint angles to be evaluated.

Joint_Angle.m

```
clc
clear all;

load('RightThigh'); % Upper sensor, on the thigh
load('RightShank'); % Lower sensor, on the shank

n_sensor=2;  % Number of sensors
tpp=1;  % Possible time exclusion in case of disturbances
A=[length(RightThigh(1:end,1)),length(RightShank(1:end,1))];
length_1=min(A);
Raw_Data=[RightThigh(tpp:length_1,1:13),
RightShank(tpp:length_1,1:13)];
n_Data=length(Raw_Data);
Synchro_Data=Synchro(Raw_Data,n_sensor,n_Data);
```

```
Thigh = Synchro_Data(:,2:14);
Shank = Synchro_Data(:,15:27);

% Filtering using custom Kalman Filter
r = 100; % how much we have confidence in our signal (low value
         % mean clean signal, high value mean we want to filter
         % it more);
q = 0.1; % how much we trust the new signal after each iteration
         % (low value: we trust the filtered data -- high value:
         % we trust the original data more)

FilteredThigh = Thigh(:,1:4);
FilteredShank = Shank(:,1:4);
for i = 5:13
    FilteredThigh(:,i) = kalmanFilter1(Thigh(:,i), r, q)';
    FilteredShank(:,i) = kalmanFilter1(Shank(:,i), r, q)';
end

Thigh = FilteredThigh;
Shank = FilteredShank;

% Selected time range
range = (150000:155000);

%% Correct magnetic field estimation

% FIRST SENSOR  - SHANK %
% Create gyro matrix
gyroFieldXYZ.raw = [Shank(:,8),Shank(:,9),Shank(:,10)];
gyroFieldXYZ.raw = gyroFieldXYZ.raw(range, :);

% Create acc field vector
accFieldXYZ.raw = [Shank(:,5),Shank(:,6),Shank(:,7)];
accFieldXYZ.raw = accFieldXYZ.raw(range, :);

% Create mag field vector
magFieldXYZ.raw = [Shank(:,11),Shank(:,12),Shank(:,13)];
magFieldXYZ.raw = magFieldXYZ.raw(range, :);

magFieldXYZ.mean = mean(magFieldXYZ.raw);
magFieldXYZ.zero = magFieldXYZ.raw - magFieldXYZ.mean; % remove
mean

% filter data
idxMagOutlier = find(abs(magFieldXYZ.raw) > 1000);
magFieldXYZ.raw(idxMagOutlier) = 0;
```

```
magFieldXYZ.raw = medfilt1(magFieldXYZ.raw,10);
% Calculate hard iron and bias correction data to fit to sphere
[U,c]  = MgnCalibration(magFieldXYZ.zero');
c = c';

% Apply correction to raw mag field vector data
xC = (magFieldXYZ.raw-c)*U;

% Estimate heading based on assumption of a level x-y plane
d = atan2(xC(:,1),xC(:,2)).*(180/pi);

% Apply ecompass fusion (linear accelerometer, magnetometer)
qShank = ecompass(accFieldXYZ.raw,xC);
orientationEuler = eulerd(qShank,'ZXY','frame');

% rotate accelerometer data from sensor body frame to NED
gVectorRotated = rotatepoint(qShank,accFieldXYZ.raw);

% calculate local gravitational vector
gVectorMean = mean(gVectorRotated);

% rotate magnetometer data from sensor body frame to NED
mVectorRotated = rotatepoint(qShank,xC);

% SECOND SENSOR - THIGH %
% Create gyro matrix
gyroFieldXYZ.raw = [Thigh(:,8),Thigh(:,9),Thigh(:,10)];
gyroFieldXYZ.raw = gyroFieldXYZ.raw(range,:);

% Create accel field vector
accFieldXYZ.raw = [Thigh(:,5),Thigh(:,6),Thigh(:,7)];
accFieldXYZ.raw = accFieldXYZ.raw(range,:);

% Create mag field vector
magFieldXYZ.raw = [Thigh(:,11),Thigh(:,12),Thigh(:,13)];
magFieldXYZ.raw = magFieldXYZ.raw(range,:);

magFieldXYZ.mean = mean(magFieldXYZ.raw);
magFieldXYZ.zero = magFieldXYZ.raw - magFieldXYZ.mean;

% filter data
idxMagOutlier = find(abs(magFieldXYZ.raw) > 1000);
magFieldXYZ.raw(idxMagOutlier) = 0;
magFieldXYZ.raw = medfilt1(magFieldXYZ.raw,10);

% Calculate hard iron and bias correction data to fit to sphere
[U,c]  = MgnCalibration(magFieldXYZ.zero');
```

```
c = c';
% Apply correction to raw mag field vector data
xC = (magFieldXYZ.raw-c)*U;

% Estimate heading based on assumption of a level x-y plane
d = atan2(xC(:,1),xC(:,2)).*(180/pi);

% Apply ecompass fusion (linear accelerometer, magnetometer)
qThigh = ecompass(accFieldXYZ.raw,xC);
orientationEuler = eulerd(qThigh,'ZXY','frame');

% rotate accelerometer data from sensor body frame to NED
gVectorRotated = rotatepoint(qThigh,accFieldXYZ.raw);

% calculate local gravitational vector
gVectorMean = mean(gVectorRotated);

% rotate magnetometer data from sensor body frame to NED
mVectorRotated = rotatepoint(qThigh,xC);

qThigh_compact=compact(qThigh);
qShank_compact=compact(qShank);

%% Knee angle estimation Angle

% Vector representing xyz axes
V1 = [1,0,0];
V2 = [0,1,0];
V3 = [0,0,1];

for i=1:min([size(qThigh_compact,1) size(qShank_compact,1)])
    % First sensor - Thigh %

    % Rotate x vector by quaternions
    V1_R_1 = quatrotate(qThigh_compact(i,:),V1);
    % Rotate y vector by quaternions
    V2_R_1 = quatrotate(qThigh_compact(i,:),V2);
    % Rotate z vector by quaternions
    V3_R_1 = quatrotate(qThigh_compact(i,:),V3);

    % Second sensor - Shank%

    V1_R_2 = quatrotate(qShank_compact(i,:),V1);
    V2_R_2 = quatrotate(qShank_compact(i,:),V2);
    V3_R_2 = quatrotate(qShank_compact(i,:),V3);
```

```
ag_x(i)=atan2d(norm(cross(V1_R_1,V1_R_2)),dot(V1_R_1,V1_R_2));

    d = dot(V1_R_1,V1_R_2);
    C = cross(V1_R_1,V1_R_2);

    Vref = [0,0,0.5];
    dir = dot(C,Vref);

    if (dir<0)
     ag_x(i) =355-ag_x(i);
    end


ag_y(i)=atan2d(norm(cross(V2_R_1,V2_R_2)),dot(V2_R_1,V2_R_2));

ag_z(i)=atan2d(norm(cross(V3_R_1,V3_R_2)),dot(V3_R_1,V3_R_2));


end

% Angle of the knee in the 3Dimension
DataAngle = [ag_x' ag_y' ag_z'];

% Filtering using custom Kalman Filter
r = 100; % how much we have confidence in our signal (low value
         % mean clean signal, high value mean we want to filter
         % it more);
q = 0.1; % how much we trust the new signal after each iteration
         % (low value: we trust the filtered data -- high value:
         % we trust the original data more)

FilteredData= kalmanFilter1(DataAngle(:,3), r, q)';
```

APPENDIX B

The average of swing time, stance time and stride time and the respective standard deviations were measured for all limbs of each trial using IMU sensors. Subsequently, the swing time and stance time percentages were calculated to observe how the dog breed, treadmill speed and motor dysfunctions could influence the results. The tables containing all these data are displayed below.

Subject 1					
Limb	**Swing time [s]**	**Stance time [s]**	**Stride time [s]**	**%Swing time**	**%Stance time**
Trial 1					
RT	0.28 ± 0.05	1.05 ± 0.08	1.34 ± 0.08	21.2	78.8
LT	0.30 ± 0.03	1.03 ± 0.08	1.32 ± 0.08	22.4	77.6
RP	0.31 ± 0.06	1.01 ± 0.11	1.32 ± 0.12	23.5	76.5
LP	0.27 ± 0.04	1.07 ± 0.09	1.35 ± 0.08	20.1	79.9
Trial 2					
RT	0.28 ± 0.03	0.87 ± 0.05	1.15 ± 0.06	24.3	75.7
LT	0.29 ± 0.03	0.85 ± 0.06	1.15 ± 0.07	25.7	74.3
RP	0.30 ± 0.05	0.84 ± 0.07	1.14 ± 0.07	26.4	73.6
LP	0.29 ± 0.06	0.86 ± 0.07	1.14 ± 0.06	25.1	74.9
Trial 3					
RT	0.30 ± 0.08	0.71 ± 0.07	1.01 ± 0.11	29.6	70.4
LT	0.27 ± 0.03	0.74 ± 0.15	1.01 ± 0.16	27.1	72.9
RP	0.27 ± 0.03	0.74 ± 0.14	1.01 ± 0.15	26.8	73.2
LP	0.26 ± 0.03	0.75 ± 0.14	1.01 ± 0.14	25.9	74.1

Table 17. Subject 1. Step detection parameters for all limbs of each trial (R=right, L=left, T=thoracic, P=pelvic).

Subject 2					
Limb	**Swing time [s]**	**Stance time [s]**	**Stride time [s]**	**%Swing time**	**%Stance time**
Trial 1					
RT	0.11 ± 0.03	0.61 ± 0.10	0.72 ± 0.11	15.5	84.5
LT	0.13 ± 0.05	0.58 ± 0.13	0.71 ± 0.13	18.3	81.7
RP	0.14 ± 0.02	0.58 ± 0.10	0.72 ± 0.10	19.6	80.4
LP	0.15 ± 0.02	0.57 ± 0.10	0.73 ± 0.10	20.8	79.2
Trial 2					
RT	0.14 ± 0.03	0.52 ± 0.13	0.66 ± 0.14	21.2	78.8
LT	0.14 ± 0.02	0.51 ± 0.15	0.66 ± 0.15	22.0	78.0
RP	0.15 ± 0.02	0.51 ± 0.13	0.66 ± 0.12	22.8	77.2
LP	0.14 ± 0.01	0.54 ± 0.08	0.68 ± 0.09	21.0	79.0

Table 18. Subject 2. Step detection parameters for all limbs of each trial (R=right, L=left, T=thoracic, P=pelvic).

Subject 3					
Limb	**Swing time [s]**	**Stance time [s]**	**Stride time [s]**	**%Swing time**	**%Stance time**
Trial 1					
RT	0.26 ± 0.03	0.83 ± 0.05	1.09 ± 0.06	23.9	76.1
LT	0.23 ± 0.02	0.86 ± 0.04	1.09 ± 0.06	21.0	79.0
RP	0.31 ± 0.04	0.80 ± 0.06	1.10 ± 0.05	27.7	72.3
LP	0.18 ± 0.02	0.91 ± 0.05	1.10 ± 0.05	16.8	83.2
Trial 2					
RT	0.24 ± 0.02	0.78 ± 0.05	1.03 ± 0.05	23.6	76.4
LT	0.26 ± 0.02	0.77 ± 0.07	1.02 ± 0.06	25.0	75.0
RP	0.26 ± 0.04	0.76 ± 0.08	1.02 ± 0.09	25.4	74.6
LP	0.24 ± 0.06	0.78 ± 0.08	1.01 ± 0.08	23.5	76.5
Trial 3					
RT	0.27 ± 0.02	0.77 ± 0.06	1.04 ± 0.06	25.9	74.1
LT	0.29 ± 0.03	0.74 ± 0.10	1.02 ± 0.11	28.2	71.8
RP	0.29 ± 0.06	0.75 ± 0.12	1.04 ± 0.10	27.8	72.2
LP	0.27 ± 0.05	0.78 ± 0.05	1.05 ± 0.08	25.8	74.2

Table 19. Subject 3. Step detection parameters for all limbs of each trial (R=right, L=left, T=thoracic, P=pelvic).

Subject 4					
Limb	**Swing time [s]**	**Stance time [s]**	**Stride time [s]**	**%Swing time**	**%Stance time**
Trial 1					
RT	0.21 ± 0.05	0.80 ± 0.26	1.02 ± 0.24	21.1	78.9
LT	0.20 ± 0.04	0.82 ± 0.17	1.02 ± 0.20	19.5	80.5
RP	0.19 ± 0.03	0.86 ± 0.22	1.05 ± 0.23	17.9	82.1
LP	0.19 ± 0.04	0.86 ± 0.19	1.05 ± 0.20	18.3	81.7
Trial 2					
RT	0.29 ± 0.03	0.80 ± 0.12	1.08 ± 0.11	26.5	73.5
LT	0.25 ± 0.01	0.85 ± 0.11	1.10 ± 0.13	23.0	77.0
RP	0.21 ± 0.02	0.86 ± 0.14	1.07 ± 0.13	19.9	80.1
LP	0.24 ± 0.03	0.83 ± 0.12	1.07 ± 0.12	22.3	77.7
Trial 3					
RT	0.30 ± 0.04	0.79 ± 0.09	1.09 ± 0.10	27.8	72.2
LT	0.27 ± 0.03	0.80 ± 0.07	1.07 ± 0.09	25.2	74.8
RP	0.24 ± 0.03	0.85 ± 0.10	1.09 ± 0.09	21.8	78.2
LP	0.24 ± 0.02	0.86 ± 0.08	1.10 ± 0.08	21.7	78.3

Table 20. Subject 4. Step detection parameters for all limbs of each trial (R=right, L=left, T=thoracic, P=pelvic).

Subject 5					
Limb	**Swing time [s]**	**Stance time [s]**	**Stride time [s]**	**%Swing time**	**%Stance time**
Trial 1					
RT	0.33 ± 0.05	0.84 ± 0.13	1.17 ± 0.13	28.1	71.9
LT	0.28 ± 0.04	0.86 ± 0.11	1.13 ± 0.13	24.3	75.7
RP	0.25 ± 0.07	0.92 ± 0.13	1.17 ± 0.15	21.2	78.8
LP	0.23 ± 0.05	0.95 ± 0.09	1.17 ± 0.11	19.3	80.7
Trial 2					
RT	0.28 ± 0.02	0.81 ± 0.07	1.09 ± 0.07	25.5	74.5
LT	0.27 ± 0.02	0.82 ± 0.05	1.09 ± 0.06	24.6	75.4
RP	0.26 ± 0.04	0.83 ± 0.07	1.09 ± 0.07	24.2	75.8
LP	0.30 ± 0.06	0.81 ± 0.06	1.10 ± 0.08	26.8	73.2
Trial 3					
RT	0.23 ± 0.04	0.70 ± 0.07	0.93 ± 0.10	24.9	75.1
LT	0.25 ± 0.06	0.67 ± 0.06	0.92 ± 0.11	27.6	72.4
RP	0.22 ± 0.06	0.70 ± 0.06	0.92 ± 0.09	24.0	76.0
LP	0.25 ± 0.05	0.68 ± 0.10	0.93 ± 0.11	26.6	73.4

Table 21. Subject 5. Step detection parameters for all limbs of each trial (R=right, L=left, T=thoracic, P=pelvic).

Subject 6 (without orthosis)					
Limb	**Swing time [s]**	**Stance time [s]**	**Stride time [s]**	**%Swing time**	**%Stance time**
Trial 1					
RT	0.18 ± 0.02	0.77 ± 0.08	0.95 ± 0.08	19.0	81.0
LT	0.18 ± 0.01	0.75 ± 0.07	0.94 ± 0.07	19.6	80.4
RP	0.18 ± 0.02	0.75 ± 0.10	0.93 ± 0.11	19.7	80.3
LP	0.16 ± 0.01	0.80 ± 0.09	0.95 ± 0.09	16.4	83.6
Trial 2					
RT	0.19 ± 0.02	0.81 ± 0.07	1.00 ± 0.07	18.7	81.3
LT	0.18 ± 0.02	0.81 ± 0.07	1.00 ± 0.06	18.5	81.5
RP	0.19 ± 0.02	0.82 ± 0.09	1.00 ± 0.09	18.9	81.1
LP	0.18 ± 0.02	0.83 ± 0.07	1.00 ± 0.06	17.6	82.4

Table 22. Subject 6 (without orthosis). Step detection parameters for all limbs of each trial (R=right, L=left, T=thoracic, P=pelvic).

Subject 6 (with orthosis)					
Limb	**Swing time [s]**	**Stance time [s]**	**Stride time [s]**	**%Swing time**	**%Stance time**
Trial 1					
RT	0.18 ± 0.05	0.83 ± 0.10	1.02 ± 0.11	18.1	81.9
LT	0.25 ± 0.03	0.79 ± 0.09	1.04 ± 0.10	24.0	76.0
RP	0.25 ± 0.03	0.77 ± 0.11	1.02 ± 0.11	24.1	75.9
LP	0.20 ± 0.03	0.83 ± 0.11	1.03 ± 0.09	19.5	80.5
Trial 2					
RT	0.18 ± 0.03	0.90 ± 0.10	1.08 ± 0.10	16.3	83.7
LT	0.22 ± 0.03	0.85 ± 0.13	1.07 ± 0.14	20.6	79.4
RP	0.22 ± 0.05	0.86 ± 0.11	1.08 ± 0.13	20.5	79.5
LP	0.19 ± 0.03	0.89 ± 0.09	1.08 ± 0.09	18.0	82.0

Table 23. Subject 6 (with orthosis). Step detection parameters for all limbs of each trial (R=right, L=left, T=thoracic, P=pelvic).

Subject 7 (without orthosis)					
Limb	**Swing time [s]**	**Stance time [s]**	**Stride time [s]**	**%Swing time**	**%Stance time**
Trial 1					
RT	0.31 ± 0.07	1.10 ± 0.35	1.41 ± 0.31	22.2	77.8
LT	0.29 ± 0.06	1.04 ± 0.26	1.33 ± 0.27	21.5	78.5
RP	0.38 ± 0.14	1.03 ± 0.33	1.41 ± 0.31	27.2	72.8
LP	0.22 ± 0.03	1.18 ± 0.34	1.40 ± 0.31	15.7	84.3
Trial 2					
RT	0.37 ± 0.06	0.87 ± 0.05	1.24 ± 0.06	29.6	70.4
LT	0.36 ± 0.03	0.88 ± 0.08	1.24 ± 0.06	29.0	71.0
RP	0.34 ± 0.04	0.91 ± 0.06	1.25 ± 0.07	27.2	72.8
LP	0.23 ± 0.02	1.00 ± 0.06	1.23 ± 0.06	18.7	81.3

Table 24. Subject 7 (without orthosis). Step detection parameters for all limbs of each trial (R=right, L=left, T=thoracic, P=pelvic).

Subject 7 (with orthosis)					
Limb	**Swing time [s]**	**Stance time [s]**	**Stride time [s]**	**%Swing time**	**%Stance time**
Trial 1					
RT	0.36 ± 0.08	0.95 ± 0.11	1.31 ± 0.10	27.5	72.5
LT	0.32 ± 0.05	0.99 ± 0.14	1.31 ± 0.16	24.6	75.4
RP	0.40 ± 0.06	0.93 ± 0.10	1.33 ± 0.12	29.8	70.2
LP	0.29 ± 0.03	1.06 ± 0.11	1.34 ± 0.10	21.3	78.7
Trial 2					
RT	0.41 ± 0.07	0.84 ± 0.07	1.25 ± 0.08	32.8	67.2
LT	0.33 ± 0.05	0.92 ± 0.12	1.25 ± 0.14	26.5	73.5
RP	0.36 ± 0.03	0.89 ± 0.08	1.25 ± 0.08	28.8	71.2
LP	0.29 ± 0.04	0.97 ± 0.09	1.26 ± 0.09	23.1	76.9

Table 25. Subject 7 (with orthosis). Step detection parameters for all limbs of each trial (R=right, L=left, T=thoracic, P=pelvic).

BIBLIOGRAPHY

[1] C. Girardi and P. Mussa, *250 anni dalla fondazione della scuola di veterinaria di Torino*. 2019.

[2] Jobbydoo, “Professione Veterinario: Mansioni, Formazione e Competenze per Lavorare con gli Animali,” 2020. .

[3] Ragioneria Generale dello Stato, “Il monitoraggio della spesa sanitaria,” 2019.

[4] J. Hodges, “Animals and values in society,” *Livest. Res. Rural Dev.*, 1999.

[5] Camera di Commercio Cuneo, “Bovini , ovini e caprini Rilevazione quindicinale dal 16 al 31 ottobre 2020,” 2020.

[6] A. De Simone, “Quanto costa un cavallo,” 2017.

[7] PetAdvisor, “Costo cavallo : quanto costa comprarlo e mantenerlo 1 anno?,” 2020.

[8] M. Tognini, “Pet economy: in Italia il mercato legato alla cura degli animali domestici vale più di 2 miliardi di euro,” *Themilaner*, 2020.

[9] C. Zink and J. B. Van Dyke, *Canine Sports Medicine and Rehabilitation*. 2018.

[10] L. D. Deshales, “Upper extremity orthoses,” in *Occupational Therapy for Physical Dysfunction*, 2002, pp. 313–349.

[11] V. Brullo, “Derrick Campana : il ‘ dottor Dolittle ’ delle protesi per animali,” *Close-up Eng.*, 2019.

[12] Veterinary Health Center University of Missouri, “What is Kinematic Analysis?,” 2020. https://vhc.missouri.edu/small-animal-hospital/motion-analysis-laboratory/what-is-kinematic-analysis/.

[13] O. Sofuwa, A. Nieuwboer, K. Desloovere, A. M. Willems, F. Chavret, and I. Jonkers, “Quantitative gait analysis in Parkinson’s disease: Comparison with a healthy control group,” *Arch. Phys. Med. Rehabil.*, vol. 86, no. 5, pp. 1007–1013, 2005, doi: 10.1016/j.apmr.2004.08.012.

[14] K. S. Gibson, J. Woodburn, D. Porter, and S. Telfer, “Functionally optimized orthoses for early rheumatoid arthritis foot disease: A study of mechanisms and patient experience,” *Arthritis Care Res.*, vol. 66, no. 10, pp. 1456–1464, 2014, doi: 10.1002/acr.22060.

[15] M. Zago *et al.*, “Gait evaluation using inertial measurement units in subjects with Parkinson’s disease,” *J. Electromyogr. Kinesiol.*, vol. 42, no. January, pp. 44–48, 2018,

doi: 10.1016/j.jelekin.2018.06.009.

[16] L. F. Carver, “When pets are family, the benefits extend into society,” *Cover.*, 2019.

[17] Russo *et al.*, “Proposta di legge N.3440, Camera dei Deputati,” 2019.

[18] Legambiente, “Animali in città , Legambiente presenta il suo VIII rapporto nazionale,” 2019.

[19] Tamarack, “Veterinary Orthotics & Prosthetics Directory,” 2020. .

[20] “http://www.ortopaw.com/.” .

[21] “https://www.centroessedi.it/.” .

[22] C. Riegger-Krugh, D. L. Millis, and J. P. Weigel, “Canine anatomy|Veterian Key,” 2016. .

[23] A. Calienno, “Razze di cani: quante ne esistono e quali sono?,” 2019. .

[24] Iltuocane.it, “Appiombi del cane : cosa sono e come si definiscono,” 2018.

[25] B. J. Carr, S. O. Canapp, and M. C. Zink, “Quantitative Comparison of the Walk and Trot of Border Collies and Labrador Retrievers, Breeds with Different Performance Requirements,” *PLoS One*, vol. 10, no. 12, pp. 1–9, 2015, doi: 10.1371/journal.pone.0145396.

[26] E. L. Webster, P. E. Hudson, and S. B. Channon, “Comparative functional anatomy of the epaxial musculature of dogs (Canis familiaris) bred for sprinting vs. fighting,” *J. Anat.*, vol. 225, no. 3, pp. 317–327, 2014, doi: 10.1111/joa.12208.

[27] S. S. Sabanci and M. K. Ocal, “Categorization of the pelvic limb standing posture in nine breeds of dogs,” *J. Vet. Med. Ser. C Anat. Histol. Embryol.*, vol. 47, no. 1, pp. 58–63, 2018, doi: 10.1111/ahe.12324.

[28] J. M. Vilar, M. Rubio, J. M. Carrillo, A. M. Domínguez, A. Mitat, and M. Batista, “Biomechanic characteristics of gait of four breeds of dogs with different conformations at walk on a treadmill,” *J. Appl. Anim. Res.*, vol. 44, no. 1, pp. 252–257, 2016, doi: 10.1080/09712119.2015.1031778.

[29] R. Mullis *et al.*, “Validation of complex interventions in a low back pain trial: Selective video analysis cross-referenced to clinical case notes,” *Contemp. Clin. Trials*, vol. 27, pp. 404–412, 2006, doi: 10.1016/j.cct.2006.05.004.

[30] C. Ladha, J. O’Sullivan, Z. Belshaw, and L. Asher, “Gaitkeeper: A system for measuring canine gait,” *Sensors (Switzerland)*, vol. 17, no. 2, pp. 1–17, 2017, doi: 10.3390/s17020309.

[31] A. I. Cuesta-Vargas, A. Galán-Mercant, and J. M. Williams, "The use of inertial sensors system for human motion analysis," *Phys. Ther. Rev.*, 2010.

[32] W. Y. Wong, M. S. Wong, and K. H. Lo, "Clinical applications of sensors for human posture and movement analysis: A review," *Prosthet. Orthot. Int.*, vol. 31, no. 1, pp. 62–75, 2007, doi: 10.1080/03093640600983949.

[33] S. A. Schurr, A. N. Marshall, J. E. Resch, and S. A. Saliba, "Two-dimentional video analysis is comparable to 3D motion capture in lower extremity movement assessment." .

[34] F. Menegoni, L. Vismara, P. Capodaglio, M. Crivellini, and M. Galli, "Kinematics of trunk movements: Protocol design and application in obese females," *J. Appl. Biomater. Biomech.*, vol. 6, no. 3, pp. 178–185, 2008, doi: 10.1177/228080000800600308.

[35] V. Cimolin, M. Galli, G. Albertini, M. Crivellini, J. Romkes, and R. Brunner, "Quantitative analysis of upper limbs during gait: A marker set protocol," *J. Appl. Biomater. Funct. Mater.*, vol. 10, no. 1, pp. 49–55, 2012, doi: 10.5301/JABFM.2012.9277.

[36] A. Ferrari *et al.*, "Quantitative comparison of five current protocols in gait analysis," *Gait Posture*, vol. 28, no. 2, pp. 207–216, 2008, doi: 10.1016/j.gaitpost.2007.11.009.

[37] F. Duerr *et al.*, "Evaluation of inertial measurement units as a novel method for kinematic gait evaluation in dogs," *Vet. Comp. Orthop. Traumatol.*, vol. 29, no. 6, pp. 475–483, 2016, doi: 10.3415/VCOT-16-01-0012.

[38] R. Morrison, J. J. Reilly, V. Penpraze, E. Pendlebury, and P. S. Yam, "A 6-month observational study of changes in objectively measured physical activity during weight loss in dogs," *J. Small Anim. Pract.*, vol. 55, no. 11, pp. 566–570, 2014, doi: 10.1111/jsap.12273.

[39] K. Clark, C. Caraguel, L. Leahey, and R. Béraud, "Evaluation of a novel accelerometer for kinetic gait analysis in dogs," *Can. J. Vet. Res.*, vol. 78, no. 3, pp. 226–232, 2014.

[40] G. J. Jenkins, C. H. Hakim, N. Nora Yang, G. Yao, and D. Duan, "Automatic characterization of stride parameters in canines with a single wearable inertial sensor," *PLoS One*, vol. 13, no. 6, pp. 1–15, 2018, doi: 10.1371/journal.pone.0198893.

[41] B. T. Torres *et al.*, "The effect of marker location variability on noninvasive canine stifle kinematics," *Vet. Surg.*, vol. 40, no. 6, pp. 715–719, 2011, doi: 10.1111/j.1532-950X.2011.00852.x.

[42] S. B. Williams, J. R. Usherwood, K. Jespers, A. J. Channon, and A. M. Wilson,

"Exploring the mechanical basis for acceleration: Pelvic limb locomotor function during accelerations in racing greyhounds (Canis familiaris)," *J. Exp. Biol.*, vol. 212, no. 4, pp. 550–565, 2009, doi: 10.1242/jeb.018093.

[43] G. Bertocci, C. Smalley, N. Brown, K. Bialczak, and D. Carroll, "Aquatic treadmill water level influence on pelvic limb kinematics in cranial cruciate ligament-deficient dogs with surgically stabilised stifles," *J. Small Anim. Pract.*, vol. 59, no. 2, pp. 121–127, 2018, doi: 10.1111/jsap.12770.

[44] A. P. Marsh, J. D. Eggebeen, J. N. Kornegay, C. D. Markert, and M. K. Childers, "Kinematics of gait in Golden Retriever Muscular Dystrophy," *Neuromuscul. Disord.*, vol. 20, no. 1, pp. 16–20, 2010, doi: 10.1016/j.nmd.2009.10.007.

[45] N. S. M. L. Miqueleto, S. C. Rahal, F. S. Agostinho, E. G. M. Siqueira, F. A. P. Araújo, and A. O. El-Warrak, "Kinematic analysis in healthy and hip-dysplastic German Shepherd dogs," *Vet. J.*, vol. 195, no. 2, pp. 210–215, 2013, doi: 10.1016/j.tvjl.2012.06.021.

[46] P. M. Mich, "The Emerging Role of Veterinary Orthotics and Prosthetics (V-OP) in Small Animal Rehabilitation and Pain Management," *Top. Companion Anim. Med.*, vol. 29, pp. 10–19, 2014, doi: 10.1053/j.tcam.2014.04.002.

[47] B. T. Torres, Y. C. Fu, G. S. Sandberg, and S. C. Budsberg, "Pelvic limb kinematics in the dog with and without a stifle orthosis," *Vet. Surg.*, vol. 46, no. 5, pp. 642–652, 2017, doi: 10.1111/vsu.12634.

[48] M. Fusca, F. Negrini, P. Perego, L. Magoni, F. Molteni, and G. Andreoni, "Validation of a wearable IMU system for gait analysis: Protocol and application to a new system," *Appl. Sci.*, vol. 8, no. 7, pp. 1–16, 2018, doi: 10.3390/app8071167.

[49] Bosch, "Small , low power 9-axis sensor."

[50] ORThesys, "Analisi Cinematica del Movimento con Sistemi Optoelettronici." .

[51] D. A. Winter, "Biomechanics and Motor Control of Human Movement: Fourth Edition," *Biomech. Mot. Control Hum. Mov. Fourth Ed.*, pp. 1–370, 2009, doi: 10.1002/9780470549148.

[52] R. B. Davis, S. Õunpuu, D. Tyburski, and J. R. Gage, "A gait analysis data collection and reduction technique," *Hum. Mov. Sci.*, vol. 10, no. 5, pp. 575–587, Oct. 1991, doi: 10.1016/0167-9457(91)90046-Z.

[53] "http://www.fisio4vet.it/." .

[54] University of the West of England, “Pearson’s correlation coefficient.”

[55] Statistics Solution, “Pearson ’ s Correlation Coefficient.” .

[56] N. Ö. Doğan, “Bland-Altman analysis: A paradigm to understand correlation and agreement,” *Turkish J. Emerg. Med.*, vol. 18, no. 4, pp. 139–141, 2018, doi: 10.1016/j.tjem.2018.09.001.

[57] S. McLeod, “What does a box plot tell you?,” *Simply Psychol.*, 2019.

[58] L. S. Vargas-Valencia *et al.*, “Sleeve for Knee Angle Monitoring: An IMU-POF Sensor Fusion System,” *IEEE J. Biomed. Heal. Informatics*, vol. 25, no. 2, pp. 465–474, 2020, doi: 10.1109/jbhi.2020.2988360.

[59] S. A. A. N. Bolink *et al.*, “Validity of an inertial measurement unit to assess pelvic orientation angles during gait, sit-stand transfers and step-up transfers: Comparison with an optoelectronic motion capture system,” *Medical Engineering and Physics*, vol. 38, no. 3. pp. 225–231, 2016, doi: 10.1016/j.medengphy.2015.11.009.